Journal of Materials Chemistry A

ROYAL SOCIETY OF CHEMISTRY

REVIEW

View Article Online
View Journal | View Issue

Cite this: J. Mater. Chem. A, 2026, 14, 14670

Asymmetric fibre supercapacitors for sustainable energy storage in next-generation soft textile wearables

Neeraj Kumar,[a] Nishu Devi,[b] Rashi Gusain,[c] Patryk Wojciak,[a] Safa Polat[a] and Shayan Seyedin *[a]

The rapid advancement of wearable technologies demands the development of flexible, lightweight, and high-performance energy solutions. Fibre supercapacitors (FSCs) have emerged as a promising wearable energy storage system that can be integrated into everyday fabrics, powering other embedded devices. Asymmetric FSCs (AFSCs), made of two electrodes of different kinds, offer superior voltage and energy density compared to the symmetric designs with two electrodes of the same material. This review provides a comprehensive analysis of AFSCs, beginning with their role in advancing energy-autonomous wearable electronics. Various charge storage mechanisms are discussed along with key performance metrics. This is followed by a discussion of relevant fabrication methods and role of colloidal dispersions in the production of electrode fibres with desirable electrochemical properties. Subsequently, it is shown that AFSCs offer more practical solutions for wearable applications by addressing voltage and energy density limitations of symmetric FSCs. The role of electrolytes in ensuring long-term stability and safety in wearable applications is then explained. A thorough analysis of positive and negative electrodes for AFSCs is presented to understand the emerging trends and their impact on wearability and electrochemical performance. The potential of AFSCs is also explored in various wearable technologies for powering health monitors and medical implants to motivate researchers to develop sustainable and biocompatible AFSCs. The emerging impact of machine learning tools in optimising electrode designs and device performance is then highlighted. Finally, the need to address the existing gaps in scalability, stability under deformations, fabric integration, and multifunctional fibre-based systems is explained. This review provides a roadmap to bridge the gap between laboratory-scale prototypes to real-world implementation, positioning AFSCs as sustainable energy fibres within intelligent fabrics for autonomous wearables.

Received 25th December 2025
Accepted 25th February 2026

DOI: 10.1039/d5ta10485h

rsc.li/materials-a

1. Introduction

The recent advances in soft wearable electronics are driven by the rapid evolution of advanced materials, device designs, and manufacturing technologies, which led to the integration of smart functionalities in clothing from sensing and communication to energy storage and harvesting systems.[1–3] However, the development of intelligent, flexible, and body-conformal systems is still limited by the structural and mechanical constraints of conventional electronic components. Conventional rigid electronic devices are inherently unable to withstand the constant bending, twisting, and multidirectional strain associated with human motion or textile deformation because they were designed for planar architectures.[4] This fundamental mismatch between soft body mechanics and hard electronic devices has sparked keen research interest in textile- or fibre-based electronic systems, which can deliver excellent performance while seamlessly integrating into conventional fabrics for everyday wear.[5–7] The development of fibre-based energy storage technologies that can power other fibre-based devices reliably, safely, and sustainably remains one of the most pressing challenges in soft textile-based wearable electronics. Although lithium-ion batteries offer high energy density (up to 600 Wh kg^{-1}),[8] their intrinsic rigidity, limited cycle life (150–1500),[9] slow charge/discharge rates, flammability, and poor mechanical compliance make them unsuitable for wearable applications.[10] In this context, fibre-based supercapacitors (FSCs) have emerged as one of the most promising energy storage solutions for next-generation soft textile-based wearables, offering high power density (0.5–1370 kW kg^{-1} or 0.1–1150 W cm^{-3}),[11,12] fast charge/discharge response, and long-term cycling stability (1000–100 000),[11,13] while maintaining

[a]School of Engineering, Newcastle University, Newcastle upon Tyne, NE1 7RU, UK. E-mail: shayan.seyedin@newcastle.ac.uk
[b]Chemical Sciences Division, Oak Ridge National Laboratory, TN 37831-6110, USA
[c]Hub for Biotechnology in the Built Environment, School of Geography and Natural Sciences, Northumbria University, Newcastle upon Tyne, NE1 8ST, UK

mechanical flexibility, allowing them to be twisted, stretched, and integrated directly into textiles.[14–16]

The early generation of film-based supercapacitors, incorporating flexible electrodes and electrolytes, offered enhanced bendability but suffered from poor breathability, limited moisture permeability, and mechanical mismatch with textiles.[16–19] Power supply systems in smart textiles should be functionally unobtrusive and physically imperceptible, ensuring seamless integration that preserves both user comfort and aesthetic appeal.[20,21] Planner or film-based energy storage systems often compromise wearing comfort, limited conformability and suffer from structural fragility under repeated deformation, which collectively restrict their practical integration into wearable electronics.[22,23] Fibre geometries overcome these limitations by translating energy storage into the very building blocks of fabrics, that benefit from omnidirectional flexibility, large surface area, and compatibility with existing spinning, knitting, and weaving technologies.[24,25] Additionally, FSCs can be continuously produced *via* industrially-viable solution spinning techniques and seamlessly integrated into textiles using conventional textile manufacturing methods (*e.g.*, knitting or weaving) without compromising softness or breathability, making them exceptionally suited for truly wearable and unobtrusive energy storage systems.[6,15,26–28]

FSCs store the charge mainly *via* two mechanisms: (a) electrochemical double-layer capacitance (EDLC), where ultrafast ion adsorption occurs on fibre electrodes, forming a double layer that separates charge without chemical reactions, and (b) pseudocapacitance, which involves charge transfer through reversible faradaic redox reactions at or near the surface of the fibre electrode.[29,30] The advancement of FSCs has been largely driven by continual innovations in fibre

Neeraj Kumar

Dr Neeraj Kumar is a Research Associate at the School of Engineering, Newcastle University, UK. He previously held a Marie Skłodowska-Curie Fellowship at the same institution, where his work centred on the fibre-based supercapacitors for next-generation soft wearable electronics. He obtained his PhD in Chemistry from the University of Johannesburg, South Africa, and subsequently undertook post-doctoral research at Council for Scientific and Industrial Research (CSIR), South Africa. His research expertise spans the synthesis and processing of emerging 2D materials, materials engineering, scalability, electrochemical energy storage systems, solid-state electrolytes, self-powered autonomous devices, biosensing platforms, and environmental remediation technologies.

Nishu Devi

Dr Nishu Devi is a Postdoctoral Research Associate at the Oak Ridge National Laboratory (ORNL), USA. Her present research investigates electrocatalysis for CO_2 capture and electrochemical conversion. She previously worked at Northwestern University, USA, on seawater-based electrochemical carbon sequestration and mineralization technologies. She earned her PhD in Chemistry from the University of Johannesburg, South Africa, where she studied advanced electrode materials for supercapacitor applications. Her research interests include electrochemical energy storage, seawater electrolysis, carbon capture and mineralization, and interfacial electrochemistry.

Rashi Gusain

Dr Rashi Gusain is a Senior Research Assistant at the School of Geography and Natural Sciences, Northumbria University, UK. She has previously worked at the Indian Institute of Technology Madras, Luleå University of Technology, Sweden, and the University of Johannesburg, South Africa. She was also a visiting researcher at CSIR, South Africa. She received her PhD in Chemical Science from CSIR-Indian Institute of Petroleum, India. Her expertise is in 2D materials, ionic liquids, sustainable biopolymer synthesis, CO_2 capture and conversion, tribology, photocatalysis and water purification.

Patryk Wojciak

Patryk Wojciak is a PhD candidate at Newcastle University. His research focuses on soft wearable electronics, including energy harvesting, sensing, and energy storage technologies. His work explores functional materials and composite systems for mechanically compliant electronic devices, with an emphasis on understanding structure–property relationships through experimental characterisation.

electrode materials. Conductive architectures such as carbon nanotube (CNT) yarns,[31,32] graphene-based fibres,[33,34] and activated-carbon fibres (CFs)[35–37] offer high electrical conductivity and mechanical flexibility, serving as lightweight EDLC backbones for FSCs. Pseudocapacitive nanostructures such as transition metal dichalcogenides (TMDs, *e.g.*, MoS_2),[38,39] metal hydroxides (*e.g.*, $Ni(OH)_2$),[40,41] metal oxides (*e.g.*, MnO_2 and Co_3O_4)[42–44] and conducting polymers, such as polyaniline (PANi),[45,46] polypyrrole (PPy),[47,48] and poly(3,4-ethylenedioxythiophene):polystyrene sulfonate (PEDOT:PSS),[49,50] have also been made into fibres or dip-coated on existing yarns (*e.g.*, cotton and nylon). Among emerging materials, two-dimensional (2D) materials such as MXenes ($M_{n+1}X_nT_x$, M: transition metal, X: carbon and/or nitrogen, n: 1–4, and T_x: surface terminations), particularly $Ti_3C_2T_x$, have transformed fibre electrode technology owing to their metallic conductivity (>20 000 S cm^{-1}),[50,51] and hydrophilic surface-active sites (–OH, –O, and –F) which facilitate efficient charge transport and high interfacial contact, resulting in excellent specific capacitance (~1500–2800 F cm^{-3} for $Ti_3C_2T_x$).[52,53] As a fibre electrode for FSCs, $Ti_3C_2T_x$ MXene has delivered a volumetric capacitance of up to ~1300 F cm^{-3}.[54,55] MXene is employed simultaneously as both an active material and a current collector, thereby simplifying device design and improving overall electrochemical efficiency. By integrating MXenes with carbon-based or pseudocapacitive active materials, hybrid fibre electrodes can be developed that achieve a synergistic balance between mechanical robustness and high electrical performance, facilitating stable and high performance asymmetric configurations.[32,55]

Most studies to date have focused on symmetric FSCs, which consist of two identical electrodes. For example, the free-standing symmetric FSCs made of MXene fibre electrodes demonstrated a high specific capacitance (~285 F cm^{-3}) and excellent charge–discharge performance (~95% capacitance retention after 10 000 cycles) but with a limited voltage of 0.6 V.[56] In another example, a graphene-based symmetric FSC showed a high specific capacitance (182 F g^{-1} or 205 mF cm^{-2}) and a high energy density (15.5 Wh kg^{-1} or 17.5 μWh cm^{-2}), but the working voltage remained limited to 0.8 V.[57] Symmetric FSCs offer outstanding rate capability and long cycling stability, but their narrow voltage window (typically ~1 V in aqueous electrolytes) fundamentally constrains their attainable energy density and suitability for practical deployment as most electronic devices require higher voltages (>1.5 V) to operate.[30,56,58] Asymmetric fibre supercapacitors (AFSCs) address this practical limitation by strategically coupling two different electrode materials that effectively use EDLC and pseudocapacitance.[59] This complementary configuration not only balances power and energy trade-offs but also broadens the operational voltage window to 1.2–2.0 V in aqueous or gel electrolytes, resulting in multi-fold enhancement in energy density compared with symmetric FSCs.[32,36] For instance, a recent study reports an AFSC using $Ti_3C_2T_x$ MXene-coated cotton yarn as a negative electrode and reduced graphene oxide (rGO)/MoS_2-coated cotton yarn as a positive electrode, achieving a high areal energy density (~154.5 μWh cm^{-2}) and a voltage of 1.3 V, while demonstrating mechanical robustness and washability for practical smart textiles.[15]

FSCs have matured significantly by further optimising the electrolyte system. Researchers have studied quasi-solid polymer gel electrolytes, including polyvinyl alcohol (PVA)/H_3PO_4, PVA/H_2SO_4, PVA/LiCl and chitosan-based hydrogels, which provide leakage-free operation, superior mechanical compliance, and enhanced user safety, compared to aqueous electrolytes.[15,32,60] The electrolyte system has further been improved by incorporating insulating materials such as hexagonal boron nitride (h-BN) into a gel electrolyte (PVA/H_2SO_4/h-BN), which

Safa Polat

Dr Safa Polat is currently an Associate Professor at the Faculty of Engineering and Natural Sciences, Karabük University, Turkey. He was previously a TÜBİTAK Post-doctoral Fellow at Newcastle University, UK. He received his PhD in Metallurgical and Materials Engineering from Karabük University in 2020. His research interests include supercapacitors, nanocomposites, and materials characterization.

Shayan Seyedin

Dr Shayan Seyedin is a Senior Lecturer (Associate Professor) in Chemical Engineering at Newcastle University, UK. He previously held several research and fellowship positions at Imperial College London, UK, Deakin University, Australia, and Drexel University, USA. He was awarded a PhD in Chemistry from the University of Wollongong, Australia. His research focuses on developing sustainable solutions for energy, healthcare, and wearable technologies through innovations in materials design and scalable fabrication strategies. His work has made pioneering advances in solution-based processing approaches that unlock the potential of 2D materials in multifunctional structures and devices, particularly for energy storage and sensing applications.

has shown to facilitate the proximity of the electrodes and improve device stability.[15] More recently, gel-based water-in-salt electrolytes (WiSE, *e.g.*, PVA/$NaClO_4$)[61,62] and deep eutectic solvent electrolytes (*e.g.*, polyacrylic acid/choline chloride-urea/cellulose nanofibers),[63] have emerged as next-generation electrolyte systems for flexible supercapacitors, expanding the stable voltage window beyond 1.5 V and enhancing energy density (25–60 Wh kg^{-1}) while preserving high ionic mobility even at sub-zero temperatures (−20–80 °C).[61,63]

Fibre properties such as tensile strength, stretchability, breathability, washability, and tactile softness will also need to be considered for FSCs in addition to energy storage performance. The key challenge for FSCs is to achieve mechanical and performance resilience under complex deformations, including compression, twisting, bending, and stretching, while ensuring durability and safety during daily wear and washing. At the same time, their electrochemical performance, device integration, and scalable manufacturing must advance concurrently to meet the increasing energy demands of modern wearable electronics. Advanced FSC design configurations, such as parallel, twisted, and coaxial, enable the mechanical adaptability required for real garments.[64] At the system level, multiple FSCs can be woven and interconnected in series or parallel within a single fabric to meet the working voltage and energy requirements for the operation of electronic devices such as light-emitting diodes (LEDs), sensors, and communication modules, establishing a fully integrated textile-based energy system needed for next-generation soft wearable electronics.[65] However, the integration of FSCs into textiles for practical applications as electronic textiles (E-textiles) remains a challenge. The integration of FSCs into textiles must be achieved through seamless and manufacturing-compatible processes that preserve both the structural integrity and electrochemical performance of the devices, while maintaining the intrinsic flexibility and breathability of the host fabric. Reliable device interconnections are vital for integrating multiple FSCs in series or parallel and coupling them with sensors, displays, and energy harvesters in multifunctional E-textile systems.[4] For instance, a simple and practical integration strategy has recently been demonstrated where FSCs are interconnected *via* conductive rivets that function as button-like connectors, allowing for charging and detachment from the main garment for washing.[15]

Sustainability has also become a key consideration in wearable technologies,[66] driving the adoption of biodegradable substrates (*e.g.*, cotton, silk, and cellulose), eco-friendly electrolytes, and low-energy fabrication methods such as dip-coating and screen printing.[4,66] FSCs produced from natural or regenerated polymers or fibres provide mechanical comfort with a minimal environmental footprint, offering a practical pathway toward circular end-of-life recovery in E-textiles.[14,67] Sustainability should be introduced throughout the device lifecycle, from solvent-free electrode fabrications to eco-friendly binders, reusable interconnects, and recyclable encapsulations, to reduce or eliminate solid waste requiring landfill disposal or incineration.[68,69] Additionally, the biocompatibility of FSCs has garnered considerable attention as these devices are explored as power sources for implantable medical technologies used in clinical disease-state monitoring, remote therapies, and electro-organ interfaces.[70,71] These applications require the development of safe and reliable FSCs using biocompatible electrolyte, electrode, and encapsulation materials.

In the past decade, substantial progress has been made in developing FSCs in the forms of fibres, yarns, and fabrics (Fig. 1a). Several review articles[14,25,60,72] have been published on FSCs, predominantly addressing symmetric device architectures. A number of reports have also summarised the design and fabrication methods of FSCs and multi-system integration for wearable electronics.[64,65,73,74] While electrode materials,[60,75–77] electrolytes,[60] fabrication techniques,[25,78] and energy-

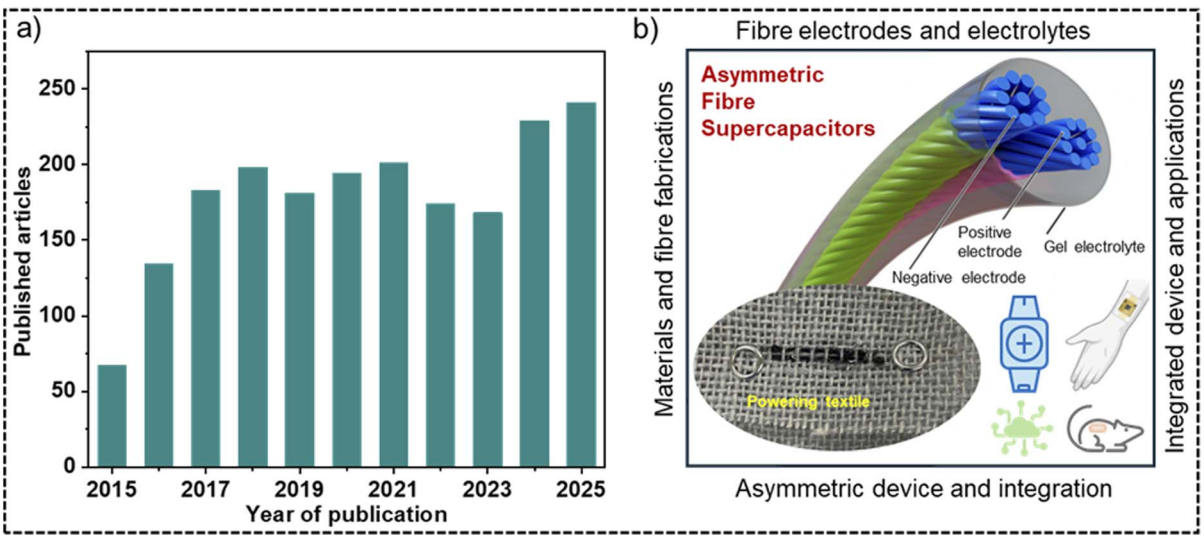

Fig. 1 (a) Total number of annual publications on FSCs (including fibres, yarns, and fabrics) from 2015 to 2025. Data source: ISI Web of Knowledge, accessed on 17/12/2025. (b) Overview of the present review on AFSCs for soft wearable electronics. Created in part with https://BioRender.com.

autonomous systems[16] have been the subject of numerous review articles on FSCs, dedicated reviews on AFSCs for next-generation textile-based wearable electronics are still limited. AFSCs have the potential to provide sufficient energy and power densities, a wide voltage window, and long-term cyclic stability, while being flexible and durable for integration into E-textiles to meet the power demands of soft wearable electronics. This review article focuses mainly on AFSCs to bridge the gap between electrochemical design principles and the integration requirements for soft textile-based wearables (Fig. 1b). By holistically examining key aspects of AFSCs in textile applications, including advanced fibre electrode compositions, next-generation gel electrolytes, material selection under textile-specific constraints, device design evolution, scalable fabrication strategies, standardised testing, and sustainability considerations, this review article guides researchers and industry experts in advancing AFSCs, paving the way for their practical deployment in wearable textiles. This review highlights the latest advancements in AFSCs and outlines key challenges, guiding the future development of wearable energy storage and the broader wearable technology community.

2. FSCs classification and performance metrics

2.1. Classification based on charge storage mechanism

Based on the charge storage mechanism, FSCs can be classified into EDLCs, pseudocapacitors, and hybrid, *i.e.*, a combination of EDLC and pseudocapacitor (Fig. 2). EDLCs store charge electrostatically *via* non-faradaic adsorption/desorption of ions at the interface between a conductive surface and the electrolyte, forming a double layer without redox reactions or ion insertion into the bulk (Fig. 2a and c).[79] Charging and discharging mechanism in EDLC is illustrated in Fig. 2c. The separation of charges across nanometre scale distances results in capacitance values that strongly depend on the fibre electrode's active surface area and the nature of the electrolyte.[80–83] Carbon-based fibres, such as activated carbon, graphene, and CNTs, are widely employed as EDLC electrodes due to their high specific surface area (~100–2500 $m^2\ g^{-1}$) and electrical conductivity (~10^2–10^7 S m^{-1}). The EDLC electrodes typically consist of interconnected pore networks, enabling axial electron transport along the fibre backbone and radial ion access through micropores and mesopores

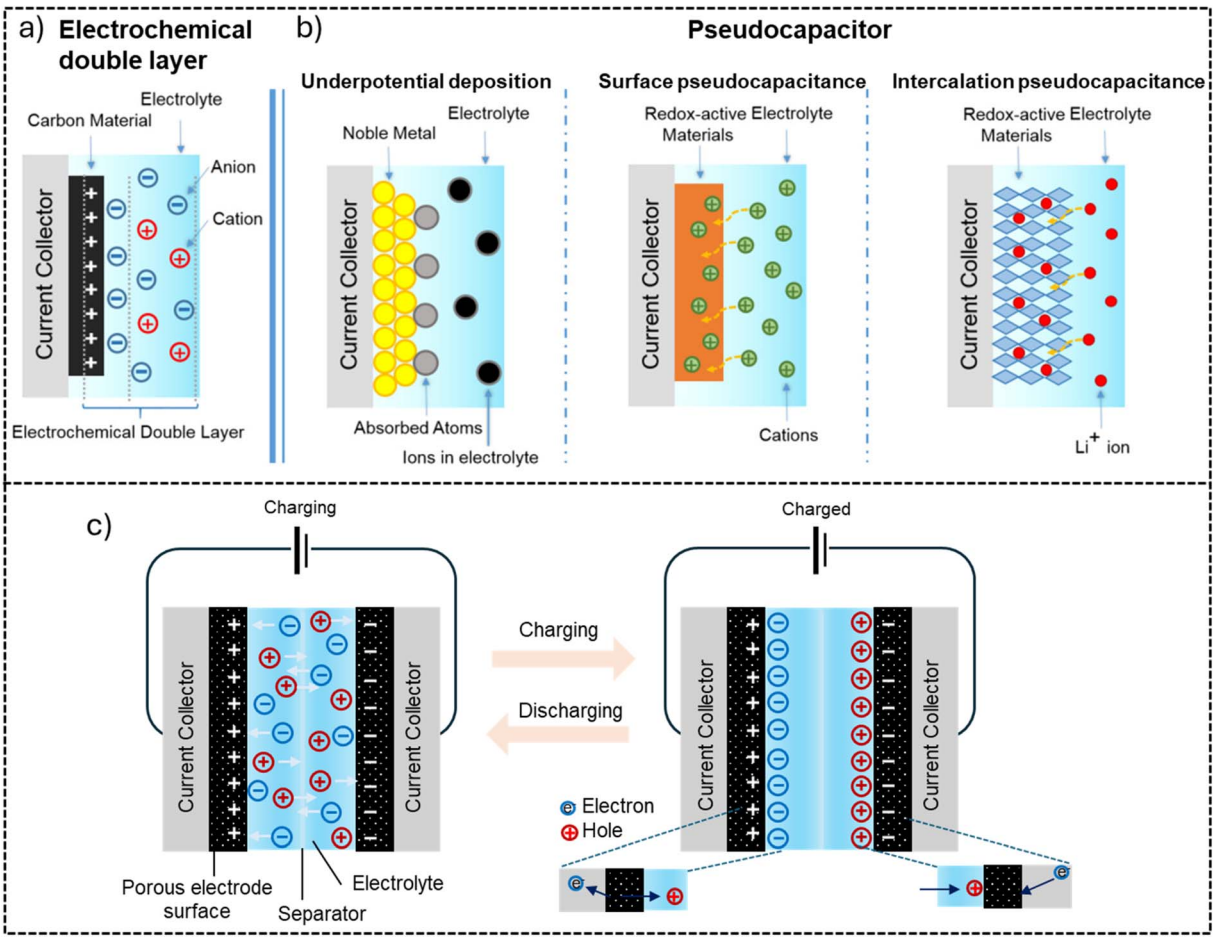

Fig. 2 The charge storage mechanisms in FSCs: (a) EDLC and (b) pseudocapacitance; adapted from ref. 89, Copyright 2014. Royal Society of Chemistry. (c) Charging mechanism of an EDLC: during charging, electrons flow through the external circuit from the negative to the positive electrode, while electrolyte ions migrate in the opposite direction to form electrical double layers at the electrode–electrolyte interfaces. The EDLC reaches a fully charged state once interfacial ion adsorption becomes saturated.

distributed around the circumference.[84–87] Because charge storage is confined only to the fibre electrodes surface and there is no redox reaction taking place, structural integrity of the fibre electrodes is preserved during charge/discharge cycling, enabling a stable operation for a long cycle life. The performance of EDLCs depends on factors such as the ionophilicity of the electrode surface, the molar concentration of electrolyte additives, and the thickness of the electrodes and separator, all of which influence ion accessibility and transport within the device.[88]

In contrast to EDLC systems, pseudocapacitors store charge electrochemically *via* fast, reversible faradaic reactions confined to the surface or near-surface region of the electrodes.[90] Based on the charge storage mechanisms, different types of pseudocapacitive fibre electrodes can be developed such as underpotential deposition, surface redox pseudocapacitor, and ion intercalation pseudocapacitor (Fig. 2b).[59] These fibre electrodes can be made using TMDs such as MoS_2,[38,39] metal hydroxides such as $Ni(OH)_2$,[40,41] metal oxides such as MnO_2 and Co_3O_4,[42–44] conducting polymers such as PANi,[45,46] PPy,[47,48] PEDOT:PSS[49,50] and emerging 2D materials such as MXenes,[50,51] metal organic frameworks (MOFs) or covalent organic frameworks (COFs) with redox-active cites.[91,92] The charge-storage capacity of pseudocapacitive fibres is governed primarily by the density and electrochemical accessibility of redox-active sites rather than by surface area alone. Although pseudocapacitive fibres exhibit rapid charge/discharge kinetics, repeated cycling can lead to partial loss or deactivation of redox-active sites, resulting in compromised electrochemical stability over extended operation.[93,94]

To address these issues, recent studies focus on developing hybrid electrode fibres that combine redox-active materials with conductive substrates, optimizing nanostructure morphology, and maintaining stable operating voltage windows to prevent irreversible side reactions. Hybrid FSCs combine the characteristics of EDLCs and pseudocapacitors, integrating the high-power density and rapid charge/discharge capability of EDLCs with the high energy density provided by faradaic surface redox reactions in pseudocapacitors.[95] These hybrid electrodes promote efficient charge transfer and mitigate the structural degradation commonly observed in pseudocapacitive materials.[96] Hybrid FSC continue to show great promise as next generation energy storage devices that combine the high-power performance of EDLCs with the high-energy capability of pseudocapacitors.

2.2. Classification based on device assembly

FSCs can also be classified based on device assembly, describing the spatial arrangement and mechanical integration of positive and negative fibre electrodes which can be symmetric or asymmetric configuration. Symmetric fibre supercapacitors (SFSCs) use both electrodes made from the same active material, leading to a balanced cell structure.[97] In such devices, both electrodes typically store charge *via* the same mechanism. Because the electrodes are identical, issues such as charge imbalance and potential mismatch are absent, simplifying the device design.[98] However, symmetric supercapacitors typically offer low voltages and energy densities. To expand the operating voltage, organic or ionic liquid electrolytes may be used, but these often suffer from lower electrical conductivities, much lower specific capacitances, higher costs, and potential safety issues compared to aqueous electrolytes.[99] In contrast, asymmetric fibre supercapacitors (AFSCs) use two different type of electrode materials with complementary voltage windows allowing for extended cell voltage and enhanced energy density.[100]

2.3. Performance metrics

The performance of FSCs is primarily determined by key performance metrics such as specific capacitance, operating voltage, energy density, power density, equivalent series resistance (ESR), rate capability, and cyclic stability which collectively define the ability of the FSCs to store and deliver electrical energy efficiently while also providing insights into the electrochemical behaviour, charge storage mechanism, and charge transport kinetics.[65,101]

2.3.1. Specific capacitance. Specific capacitance (C_s) of an electrode (or an FSC device), defined as capacitance per unit mass, volume, area, or length, indicates the intrinsic charge storage capability of the electrode (or the FSC device).[102–104] The capacitance of the cell can be calculated from cyclic voltammetry (CV) or galvanostatic charge/discharge (GCD) measurements, using eqn (1) and (2), respectively.

$$C = \frac{1}{2\nu\Delta V}\int_{V_1}^{V_2} I(V)\mathrm{d}V \quad (1)$$

$$C = \frac{I\Delta t}{\Delta V} \quad (2)$$

Here, C is capacitance (F), ν is scan rate (V s^{-1}), ΔV is potential (or voltage) window (V), I is current (A), Δt is the discharge time (s), and V_1 and V_2 are potential (or voltage) limits. In CV-based capacitance calculations from eqn (1), the factor of 1/2 is used when the full CV loop is integrated between voltage V_1 and V_2, which accounts for both charging and discharging contributions. Capacitance is normalized by fibre electrode's active mass (g), volume (cm^3), area (cm^2), or length (cm) to calculate specific capacitances (C_S) including gravimetric capacitance (C_G in F g^{-1}), volumetric capacitance (C_V in F cm^{-3}), areal capacitance (C_A in F cm^{-2}), or linear capacitance (C_L in F cm^{-1}). When reporting, it is important to specify whether these values refer to the fibre electrode alone or to the assembled FSC device, as the latter is typically lower. For instance, C_s for a fibre electrode can be approximately four times that of a symmetric FSC at the same scan rate or current density. Importantly, for FSCs, reporting a single specific capacitance can be insufficient as fibre thickness, mass loading, and packing density strongly influence C_S. For instance, C_A and C_L can change with fibre diameter or thickness; thick coatings often lead to high C_A values while C_G or C_V can remain low. Reporting all specific capacitance values along with active mass loading, fibre dimensions, and measurement methodology (*e.g.*, CV or GCD), enables meaningful comparison, reproducibility, and accurate assessment of the electrode or device performance in wearable and textile applications.

2.3.2. Operating potential or voltage. The operating potential (or voltage) window (ΔV) of an electrode (or FSC) defines the maximum potential (or voltage) range, which can be

applied to the electrode (or across the FSC) without causing electrolyte decomposition or irreversible reactions. Achieving high voltages is desirable because it allows a single FSC device to power electronics directly, avoiding the need to connect multiple FSCs in series. For comparison, an alkaline battery provides ~1.5 V per cell, while a lithium-ion battery provides ~3.5–4 V. Many FSCs using aqueous electrolytes are limited to ~1 V, whereas organic and ionic liquid electrolytes can achieve voltages in the range of ~2.5–3.5 V.[105,106]

2.3.3. Energy density. Energy density (E) in an FSC is the amount of energy stored or delivered per unit mass (Wh kg^{-1}), volume (Wh cm^{-3} or Wh L^{-1}), area (Wh cm^{-2}), or length (Wh cm^{-1}) and indicates how long a device can be powered. E is essential for long-range applications such as an electric vehicle where high mileage is desirable. E can be calculated using eqn (3) and (4) based on CV and GCD measurements, respectively.

$$E = \frac{1}{2} C_S (\Delta V)^2 \quad (3)$$

$$E = i \int_0^{\Delta t} V(t) \mathrm{d}t \quad (4)$$

Here, C_S is specific capacitance (F g^{-1}, F cm^{-3}, F cm^{-2}, or F cm^{-1}), i is current density (A g^{-1}, A cm^{-3}, A cm^{-2}, or A cm^{-1}), V is voltage (V), $\Delta\Delta$ is operating voltage window (V), t is time (s), and Δt is discharge time (s). E is normalised by mass, volume, area, or length of the FSC as gravimetric (Wh kg^{-1}), volumetric (Wh cm^{-3}), areal (Wh cm^{-2}), or linear (Wh cm^{-1}) energy density, respectively, allowing energy storage to be evaluated across different fibre geometries and device configurations. Linear energy density is useful for yarn-based systems because total energy can be scaled by twisting or weaving multiple fibres; however, values reported per unit length are strongly influenced by fibre diameter and active layer thickness. Areal energy density becomes relevant once fibres are assembled into woven or knitted textiles, as it reflects energy storage per unit fabric footprint, but it depends on yarn packing density and textile architecture. Gravimetric and volumetric energy densities are more appropriate for comparing FSCs of different thicknesses, as they account for three-dimensional packing, yet remain sensitive to porosity and inactive volume or components. To enable meaningful comparison and realistic scaling of FSCs, researchers should report energy density using multiple normalizations, specifically gravimetric and volumetric and also provide the associated geometric parameters, including fibre diameter, active layer thickness, mass loading, and packing density.

2.3.4. Power density. Power density (P) of an FSC represents the amount of power delivered per unit mass (W kg^{-1}), volume (W cm^{-3} or W L^{-1}), area (W cm^{-2}), or length (W cm^{-1}) of the device. P in an FSC defines how quickly the stored energy is delivered to an external load and is essential for applications that require bursts of energy, such as starting a car engine. P can be calculated using eqn (5), where E is energy density and Δt is discharge time (s).

$$P = \frac{E}{\Delta t} \quad (5)$$

A low internal resistance is essential to achieve high power density in FSCs.[101,107] P varies substantially based on FSC's type with EDLC devices typically showing high P (10–15 kW kg^{-1}) due to the rapid ion adsorption/desorption processes at the electrode–electrolyte interface,[108] while pseudocapacitors achieve relatively lower P (1–5 kW kg^{-1}) because of the slow kinetics of surface redox reactions. Like capacitance and energy density, researchers should report gravimetric and volumetric power density values of FSCs, along with areal and linear.

2.3.5. Equivalent series resistance. The equivalent series resistance (ESR, Ω) in FSCs directly influences the device's power delivery, voltage drop, and overall efficiency. ESR arises from the intrinsic resistance of the fibre electrodes, the electrolyte, the separator, and contact resistances within the device. A low ESR is essential to ensure rapid charge/discharge capability and minimize ohmic (IR) losses, particularly in wearable electronics where high currents may be drawn intermittently. For FSCs, ESR should be reported with respect to the fibre geometry (length, area, or volume) to enable meaningful comparisons and practical device scaling. ESR can be measured either using GCD or electrochemical impedance spectroscopy (EIS).[65,109,110] Failure to report ESR can lead to misleading claims of high-power density, as power output is inversely proportional to ESR. Furthermore, ESR depends on device-level factors, including fibre packing density, electrolyte ion mobility, and contact resistance between active material and current collector. Therefore, consistent reporting of ESR with clear normalization, is essential for reproducibility, practical device design, and accurate assessment of FSCs in wearable and textile applications.

2.3.6. Rate capability. The rate capability of an FSC reflects how effectively it can maintain its energy storage performance under different rates of charge/discharge cycling. It is commonly evaluated by measuring capacitance retention as a function of current density (from GCD) or scan rate (from CV). It reveals the true efficiency of ion and electron transport within the device. When an FSC operates at higher current densities or higher scan rates, ions move rapidly through the electrolyte and penetrate in the porous electrode, thus materials with short diffusion paths and high conductivity exhibit superior rate performance, however ionic size and conductivity also play important roles in deciding overall rate capability.[108] At high rates, ions have less time to migrate through the electrolyte and access electrochemically active sites within the electrode. As the rate increases, ion transport becomes incomplete, leading to reduced charge storage. Therefore, at high rates, limitations arise from finite ion mobility, ion size relative to pore dimensions, and restricted ion diffusion along both radial (into the active layer) and axial (along the fibre length) directions. As a result, only a fraction of the available surface or redox-active sites contributes to charge storage under fast cycling conditions. Graphene-based fibres maintained high-rate stability due to their continuous conductive pathways and efficient electron transport. For instance, FSCs fabricated from 40 wt% holey graphene/graphene fibres showed ultrahigh rate capability, retaining 96, 91, and 87% of capacitance at current density of 0.5, 1.0, and 2.0 A cm^{-3}, respectively, and 67% even at ultrahigh current density of 10.0 A cm^{-3}.[111]

2.3.7. Cyclic stability. The cyclic stability of an FSC represents its ability to maintain consistent performance over many charge/discharge cycles. While many laboratory FSCs achieve impressive specific capacitances and energy densities, their practical application for wearable systems ultimately depends on how well those properties are maintained after extended operation. For wearable or textile-based systems, which experience continuous bending, twisting, stretching, and exposure to various environmental conditions, cyclic stability should also include electrochemical retention studies under repeated deformation.[108,112] For instance, a study demonstrated rGO/$Ti_3C_2T_x$ MXene fibres exhibiting ~100% capacitance retention over 20 000 charge/discharge cycles at a current density of 5 A cm^{-3} and a voltage of 0.8 V, underscoring their suitability for textile applications.[113]

3. Electrode fibre fabrication methods

Electrode fibres are produced using several processing strategies that differ in how they integrate active material formulations into fibre-shaped structures. Methods such as coating, solution spinning, electrospinning, and 3D printing are commonly used for fabricating fibre electrodes. Active material formulations vary greatly in terms of their rheological properties and dispersion stabilities leading to fibres with distinct structural and functional characteristics. This section outlines these fabrication routes and highlights how material properties dictate method selection and resulting fibre performance.

3.1. Coating

Coating provides a straightforward route to fabricate fibre electrodes, often using natural fibres such as silk, cotton, or linen as substrates, which already possess mechanical robustness compatible with textile integration (Fig. 3a).[114] Coating strategies have been demonstrated across all structural levels of textile architectures. At the fibre level, dip-coating and electrodeposition have been used to deposit active material layers such as CNT and MnO_2 onto cellulose fibres.[115] At the yarn level, twisted bundles have been functionalised through dip- or spray-coating, including MXene-coated cotton, linen, and bamboo yarns,[15,116] as well as CNT-coated cellulose yarns.[117] At the fabric level, large-area approaches such as spraying, blade-coating, and printing are used to functionalise woven and knitted textiles, enabling cotton fabrics coated with active materials

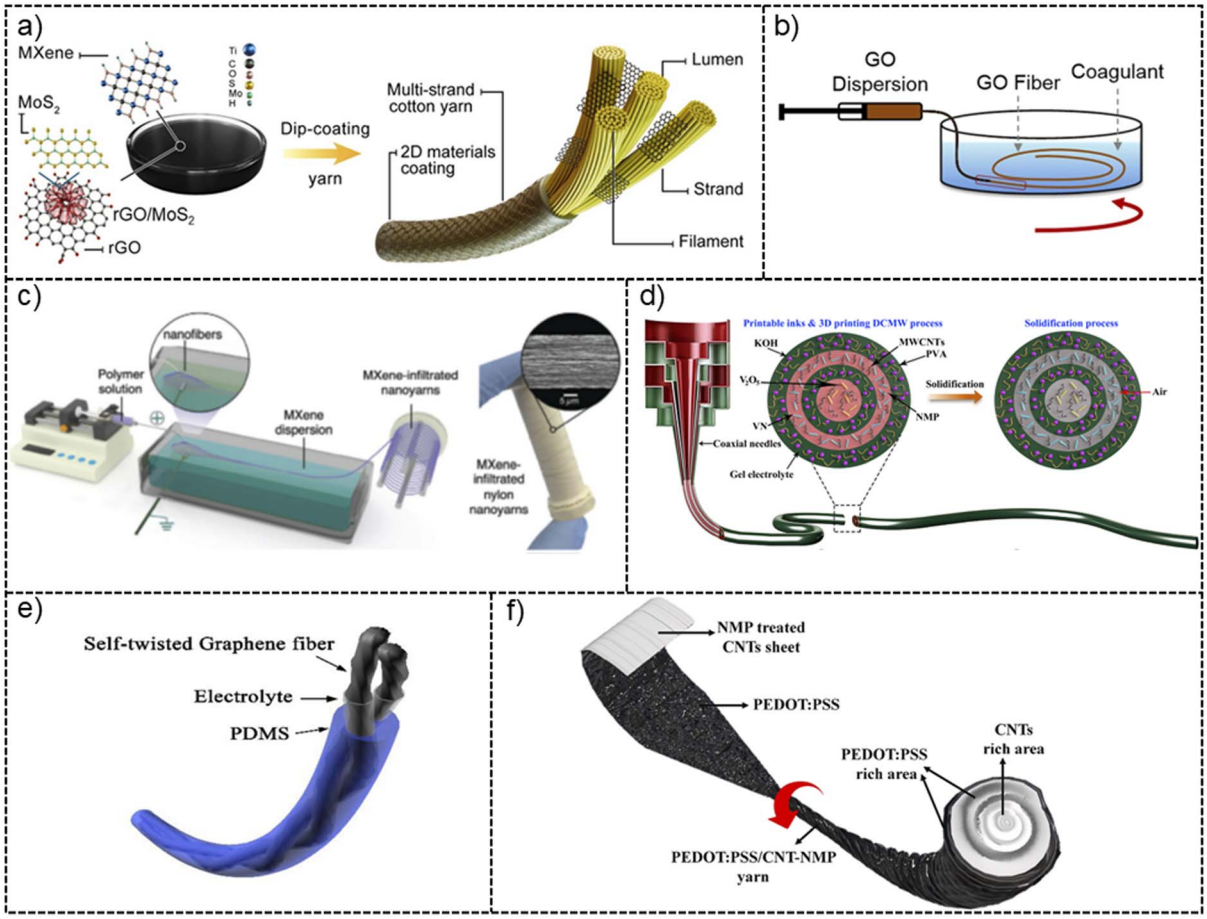

Fig. 3 Schematic illustrations of various fibre electrode fabrication techniques and FSC assembly: (a) dip coating; adapted from ref. 15 Copyright 2025, Wiley-VCH GmbH. (b) Wet-spinning; adapted from ref. 120 Copyright 2015, Springer. (c) Electrospinning; adapted from ref. 121 Copyright 2020, Wiley-VCH GmbH. (d) Multi-nozzle 3D printing; adapted from ref. 28 Copyright 2021, Science. (e) Twisted fibre; adapted from ref. 122 Copyright 2019, Elsevier. (f) Biscrolled fibre; adapted from ref. 123 Copyright 2024, Elsevier.

such as graphene and CNT.[118,119] However, adhesion between the active material and the substrate is often poor, requiring several dip–dry cycles to achieve sufficient loading and electrochemical performance.[15]

Screen printing offers an alternative approach to dip-coating, where a mask or resist (stencil) is used to pattern the surface, allowing active material to be selectively deposited.[124] The screen printing method can achieve a higher active material mass loading compared to dip-coating in a single step, *e.g.*, 4 mg cm^{-2} *vs.* 0.42 mg cm^{-2} for dip-coated cellulose-based textiles.[119] Screen printing also allows for specialised patterns, but it typically coats only a single side of the fabric. Moreover, screen printing is rarely applied at the level of individual fibres and is typically used to deposit active material layers over large fabric areas or to build performance through stacked printed layers.[102,119,124] Coated structures have the tendency to become brittle and mechanical deformations can cause the active material to crumble and break the conductive network.[125] While coating offers a simple way to convert existing fibres into electrodes, it is limited by the mechanical stability of the active layer and by the area-dependent nature of energy storage.

3.2. Solution spinning

Solution spinning involves extruding a highly viscous solution or stable colloidal dispersion into air (dry spinning) or a coagulation bath (wet spinning), where solidification can occur through several distinct mechanisms depending on the chemistry of the spinning formulation (called dope). In standard dry and wet spinning processes, solidification usually happens *via* solvent extraction. For dry spinning this involves the evaporation of solvent in hot air whereas for wet spinning the solvent within the jet-stream diffuses into the non-solvent coagulation bath to drive precipitation. When systems include dispersed active materials like CNTs, graphene, or MXenes, fibre formation can also occur by destabilizing the dispersion. Here, changes in ionic strength or pH can collapse the colloidal stability of that dispersion. As a result, the network locks into place as a continuous fibre. Certain formulations can be spun *via* cross-linking, an approach often used when the active material phase alone cannot form a self-supporting fibre. When spinning formulation is composed of charged species, polyelectrolyte complexation offers a viable route for fibre fabrication. Here, oppositely charged species rapidly associate to form a solid fibre upon extrusion of the formulation into a counter-ionic polymer (polyelectrolyte) coagulation bath. Solution spinning enables continuous fibre formation that can be subsequently collected on a winder (Fig. 3b).[126] Various solution spinning methods can be employed depending on the active material/coagulating system, such as volatility, viscosity, and miscibility, which determine the feasibility of using either dry or wet spinning routes.

When the active material can be dispersed in a volatile, easily evaporated solvent, dry spinning can be employed. For instance, GO fibres[127] and MXene fibres[128] were fabricated *via* dry spinning, though fast evaporation introduced voids, leading to low mechanical properties. Wet spinning is a well-established technique and has demonstrated considerable versatility, enabling the production of a variety of functional fibres, including GO,[126] MXene,[54] PEDOT:PSS,[49] MXene/GO,[113] MXene/PEDOT:PSS,[56] carbon black (CB)/CNT/MnO_2,[129] solution spinning offers significant potential for continuous fibre production. This approach is used, for example, in the manufacture of viscose rayon and polyacrylonitrile fibres,[130,131] which serve as precursors for carbon fibre production. Wet spinning has also been demonstrated as a scalable technology for active material fibre production. Notably, wet spinning of PU/PEDOT:PSS has already achieved kilometre-scale continuous fibre production, underscoring its status as a practically scalable route toward real-world textile energy storage applications.[132,133]

The spinning mechanism plays an important role in controlling fibre morphology and alignment, which in turn directly influences the resulting electrochemical performance. For example, in one study, MXene was wet-spun from a liquid-crystalline (LC) suspension into additive-free fibres.[54] It was shown that the coagulation bath conditions critically control the re-stacking and alignment of sheets, and that these microstructural features directly influence the trade-off between electrical conductivity (enhanced by sheet alignment) and mechanical stability (affected by restacking density). This study illustrates why controlling the spinning formulation (*e.g.*, LC and concentration) and coagulation system (solvent/coagulant pair and mechanism) is essential to tuning final fibre properties. Dry-jet wet spinning can be employed when a continuous jet of solution can be formed in air, however, this is difficult to achieve. Here, the extrudate passes through an air gap before entering the coagulation bath, allowing active materials to align under shear and tension, improving alignment and mechanical strength. For example, in one study, GO fibres were prepared *via* both dry-jet wet spinning and wet spinning methods and found that dry-jet wet spun fibres exhibited uniform morphology and enhanced mechanical properties.[120] Specifically, the dry-jet wet-spun fibres reached a tensile strength of ~135 MPa and a Young's modulus of ~7.9 GPa, compared with ~44 MPa and ~4.1 GPa for fibres produced by conventional wet-spinning under similar conditions. The breaking strain also increased from ~2% to ~6%, leading to a large rise in toughness (~0.5 to ~5.7 MJ m^{-3}). These improvements were attributed to the airgap drawing stage, which promoted greater sheet alignment, denser packing, and reduced internal voids relative to standard wet-spinning.

3.3. Electrospinning

Electrospinning involves the use of an electric field to extrude a viscous solution or colloidal dispersion to achieve sub-micron fibres that can be collected as a mat or nanoyarn[134] and subsequently used as fibre electrodes.[135] Electrospinning is advantageous as the nanofibres produced using electrospinning can achieve high surface areas,[136] which are desirable for FSCs as they promote electrolyte access and EDL formation. The electric field also promotes alignment of charged species, imparting anisotropy that is difficult to achieve with other fabrication methods. For instance, enhancing the alignment of carbon nanofibres created more efficient ion transport pathways, resulting in a ~35.5% increase in capacitance compared to randomly oriented nanofibres.[137]

Previous studies have demonstrated bath-electrospinning of MXene/polyurethane and MXene/nylon composite formulations to produce continuous nanofibres and nanoyarns that can be used as electrodes for FSCs (Fig. 3c).[121] For example, MXene/nylon nanoyarns fabricated *via* bath electrospinning delivered a specific capacitance of ~128 F g^{-1},[121] attributed to the high $Ti_3C_2T_X$ loading and continuous fibre alignment, demonstrating that bath electrospinning can produce mechanically robust, conductive MXene-loaded fibres suitable as electrodes. Beyond MXene–polymer systems, electrospinning has also been widely applied to fabricate FSC electrodes from other materials. PAN-derived electrospun carbon nanofibres (CNF) have reported specific capacitances of ~150 F g^{-1}, with carbon/graphene composite nanofibres showing comparable performance at similar mass loadings.[138] MnO_2-coated CNFs reached a specific capacitance of up to ~630 F g^{-1} due to the faradaic redox reactions of MnO_2, which contribute additional pseudocapacitive charge storage beyond the EDLC of the carbon scaffold.[139] Electrospun MXene/CNF composite fibres also report specific capacitances as high as ~460 F g^{-1},[140] which indicates how the incorporation of MXene within aligned carbon nanofibre networks can significantly enhance charge storage performance. The studies show electrospinning can achieve porous fibre electrodes with high surface area and tuneable mechanical properties, in turn demonstrating versatility for FSC electrode fabrication. However, electrospinning requires very high voltages (in the order of 10^4 V),[141] raising safety concerns and limiting energy efficiency.

3.4. 3D printing

3D printing employs a process analogous to solution spinning, where a printable solution or colloidal dispersion (ink) is extruded through a nozzle into a coagulation bath to solidify and form fibre-based structures (Fig. 3d).[28,142,143] The main advantage of 3D printing lies in its programmable deposition, which allows precise control over shape and spatial material placement, enabling customizable designs and facile switching between inks to introduce localized changes in composition for tailored functionality.[144] 3D printing has been used to fabricate FSCs using GO[145] and MXene-based inks,[146] enabling precise control over electrode architecture. Material-dependent performance is evident: direct-ink-writing of GO aerogel fibres has produced mechanically robust, conductive architectures with a specific capacitance of ~183 F g^{-1},[147] however the large pores in the structure limit their volumetric capacitance because the low packing density reduces the amount of electroactive material per unit volume. MXene-based printed inks achieve specific capacitances up to ~240 F g^{-1},[148] and excellent rate performance due to the high conductivity and surface accessibility of the printed $Ti_3C_2T_x$ networks. These works demonstrate that 3D printing can generate architected, high-surface-area fibre electrodes directly relevant to scalable FSC fabrication.

Although the ink is extruded as a fibre in 3D printing, it is typically deposited layer-by-layer,[149] typically yielding a mesh-like structure rather than a continuous fibre suitable for spool collection and textile integration. Due to this layered deposition and its ability to precisely control geometry, 3D printing is more suitable for electronic skins and skin-mountable electronics, where structural patterning and surface conformity are more critical than fibre continuity. 3D-printed FSCs are generally limited in scale, with most studies producing fibres approaching ~1 m,[28,150] the feasibility of 3D printing as a scalable, continuous manufacturing route for knittable textile fibres remains to be determined. A challenge for this technique is reproducibility, as the extrusion pressure must be precisely matched to the ink's viscosity and concentration, which becomes difficult when batch-to-batch variations occur.[151] This reproducibility concern complicates efforts to scale the process, since maintaining consistent fibre quality over long printing runs becomes increasingly challenging.

3.5. Other electrode fibre assembly methods

Other approaches of electrode fibre production include the use of structural or geometrical manipulation such as twisting, coiling, or scrolling to form fibre or yarn electrodes suitable for subsequent integration into FSCs. One straightforward approach is twisting, in which two or more electrode fibres are wound together to produce a mechanically robust yarn with improved handling and flexibility (Fig. 3e). This has been demonstrated using CNT fibre bundles uniformly coated with a thin layer of PPy to form a core–shell composite electrode.[152] The coated fibres were subsequently twisted into a yarn, producing a flexible electrode that exhibited a specific capacitance of ~350 F g^{-1}, highlighting the effectiveness of twisting for creating high-performance, mechanically resilient electrode yarns. The high gravimetric capacitance reported arises from the pseudocapacitive contribution of PPy combined with efficient electron conduction through the CNT core. The core–shell geometry ensures intimate contact between active material and conductive scaffold, minimizing electrical resistance.

Biscrolling is another technique for electrode fibre assembly, in which layers of active material can be incorporated into fibre electrodes by rolling them around a core or each other (Fig. 3f).[123] Typically, a conductive host is used to support and transport electrons, while guest materials such as metal oxides, conducting polymers, or 2D materials are embedded throughout the scrolling process. This method allows high active-material loading while maintaining mechanical flexibility, producing a continuous yarn electrode suitable for integration into flexible FSCs. One study produced CNT/MnO_2 biscrolled yarns with a specific capacitance of ~166 F g^{-1}, this method was advantageous in imparting elastic stretchability (30%) due to over-twisting to produce yarn coiling.[153]

Thermal drawing has recently emerged as a promising strategy for the continuous fabrication of structured electrode fibres and yarns.[112] In this approach, macroscopic preforms composed of electrode materials can be drawn into microscale fibres while preserving internal structure and alignment. Although thermal drawing can be applied purely for electrode fabrication, it is often combined with electrolyte and separator integration during the drawing process to produce a fully assembled FSC in a single, continuous step. For instance, one

study applied thermal drawing to a preform of porous electrode gels made from a mixture of activated carbon (AC), CB, and poly(vinylidene fluoride) (PVDF). In the reported device, this composite electrode fibre yielded a volumetric capacitance of ~13.6 F cm^{-3} and could be produced continuously up to 100 m in length. It should be noted that this capacitance reflects the performance of the fully integrated device rather than the electrode fibre alone.

4. Intrinsic limitations of symmetric fibre supercapacitors

The performance of FSCs is closely tied to the choice of electrode materials, especially when considering integration into textiles. Symmetric FSCs (SFSCs), which utilize identical materials for both electrodes, are often chosen due to their simple device assembly and fabrication, and uniform mechanical properties along the fibre axis, resulting in consistent performance of the device. However, this architectural simplicity comes at the expense of fundamental performance limitations intrinsic to symmetric designs, such as low operating voltage[154] and low energy density,[155] as outlined in Table 1. These constraints arise from fundamental aspects of electrode–electrolyte interactions, charge storage mechanisms, and materials utilization.

A major limitation of SFSCs lies in their constrained operating voltage range. While the electrolyte sets the theoretical maximum voltage (typically ~1 V in aqueous[156] and 2–3 V in organic/ionic liquid systems[157]), SFSCs can only operate within the narrow, shared stability window of the active material used as both electrodes. This restricts the usable cell voltage well below the electrolyte's decomposition limit (*e.g.*, typically limited to 0.6–0.8 V in aqueous electrolytes).[158–160] Any attempt to extend this range risks triggering unwanted reactions, such as the hydrogen and oxygen evolution reactions in aqueous electrolytes, irreversible oxidation/reduction of the active electrode materials, parasitic faradaic reactions from electrolyte decomposition, or ion depletion/accumulation at the electrodes that drives concentration polarisation and rapid performance loss.[161] For instance, a study showed the use of MnO_2 grown on carbon fibre (MnO_2/CF) electrodes which were assembled into an SFSC using PVA/phosphoric acid (PVA/H_3PO_4) gel electrolyte with a limited voltage of 0.8 V and volumetric energy density of 0.0002 mWh cm^{-3}.[162] As the voltage of this SFSC was limited, three cells were required to be connected in series to achieve a voltage of 2.4 V to power a liquid crystal display (LCD) and light-emitting diode (LED). Maximizing voltage is desirable because energy density scales quadratically with voltage. Even a small increase in voltage translates into large gains in energy output, decreasing the number of cells to be interconnected which in turn simplifies integration into real-world energy systems.

Additionally, the restricted voltage range of SFSCs inherently curtails their energy storage potential. Gravimetric energy density values often remain in the range of ~5–15 Wh kg^{-1} for SFSCs, while volumetric energy densities generally fall in the range of ~1–10 mWh cm^{-3}, insufficient for powering wearable devices for a long period of time.[25,163–166] While increasing thickness or fibre diameter can raise the absolute stored charge, this comes at the cost of flexibility and wearable compatibility. Thus, the key bottleneck in SFSCs is the restricted voltage rather than the charge storage mechanism itself.

Another key limitation in SFSCs is the inherent symmetry of the device. Using the same material on both electrodes forces both sides to operate within the same potential range and often relies on the same charge storage mechanism (*e.g.*, EDLC or pseudocapacitance) on each side, consequently eliminating opportunities for synergistic or complementary electrochemical contributions. The synergistic or complementary effects arise when two different electrode materials are used, in which one material's electrochemical behaviour can enhance or balance the other's, allowing a wider voltage window, improved charge

Table 1 Comparative analysis of SFSCs and AFSCs

Constraint/aspect	Limitations in SFSCs	Advantage in AFSCs	AFSC's implications for textile wearables
Voltage window	Restricted to overlapping stability of identical electrodes	Extended by pairing materials with complementary potentials	Higher operating voltage requires lesser number of cells to be paired
Energy density	Capped due to narrow voltage and identical capacitance of electrodes	Boosted through charge balancing and redox synergy	Higher energy density results in longer operational time
Design flexibility	Constrained by the need for identical materials	Enables tailored selection of positive and negative electrode materials	Facilitates device customization needed for textile integration
Voltage scaling	Requires multiple devices in series to increase voltage	Higher single-cell voltage reduces number of devices in series	Smaller footprint
Electrode optimization	Electrode materials underutilized due to symmetry	Each electrode can be optimized for distinct electrochemical role	Unlocks full capabilities of advanced electrode materials
Integration complexity	Simplified structure with limited tunability	More complex structure allowing for performance-centric design adjustments	More complex with balanced robustness and energy output
Sustainability and scalability	Simple processing and easy to recycle	Resource and process intensive designs	Challenges in large scale manufacturing and end-of-life recycling

distribution, which is absent in symmetric devices as they use identical electrodes.

From a sustainability and materials engineering perspective, to achieve a fixed amount of energy output from any SFSC device, it will need more material due to the limited voltage window and energy density, resulting in low performance and hence low resource efficiency. To accomplish a required energy and voltage output, a large number of cells will be needed in series or parallel, which in turn increases the material and resource demand for producing those additional cells. Also, in the case of pseudocapacitive-based SFSC, high-cost or scarce redox-active materials are required across both electrodes, which increases cost and material usage without much corresponding performance benefit. This inefficiency also affects device footprint and sustainability, which are key considerations for wearable electronics.

5. Asymmetric fibre supercapacitors

AFSCs offer a promising route to overcome the key limitations of the commonly used SFSCs, particularly when high voltage and high energy density are required.[167] By combining two different electrode materials, each optimized for either the positive or negative potential range, AFSCs enable more effective utilization of the full electrochemical stability window of the electrolyte.[168,169] This allows AFSCs to achieve operating voltages of 1.3–2.0 V in aqueous electrolytes, surpassing the SFSCs (limited to ~1.0 V).[167,170,171] The resulting increase in operating voltage subsequently leads to a substantial enhancement in energy density. In addition, AFSCs allow the option for one electrode to prioritize mechanical robustness while the other can maximize electrochemical performance, enabling a tuneable balance that symmetric systems cannot achieve, where both electrodes share identical mechanical and electrochemical behaviour. This makes AFSCs[170] highly attractive for soft textile wearables, where compact, lightweight, and high-performance energy storage solutions are crucial.[73] Table 2 provides a comparison of different AFSCs reported in the literature.

5.1. Positive, negative electrodes and charge balancing

The ability to decouple the electrodes in AFSCs allows for the selection of electrode materials tailored to their specific electrochemical roles. The selection of positive and negative electrodes in AFSCs is governed by their potential stability ranges, selected to maximize the overall operating voltage of the device. Electrode materials that are stable at more negative potentials serve as the negative electrode and those stable at more positive potentials act as the positive electrode. Table 2 provides examples of positive and negative electrode materials reported for AFSCs.

For instance, a study developed an AFSC by using FeC_2O_4/FeOOH grown on CNT fibres as the negative electrode and PANi@CNT as the positive electrode.[180] This AFSC showed an operating voltage of 2.0 V, an areal energy density of ~4.07 μWh cm^{-2}, a power density of ~0.42 mW cm^{-2}, and ~97% capacitance retention after 4000 cycles.[180] Another study reported a coaxial AFSC comprising a MoS_2@Fe_2O_3/CNT composite as the negative electrode and a $Ni(OH)_2$@$NiCo_2O_4$/CNT as the positive electrode, achieving an operating voltage of 1.6 V, a specific capacitance of ~373 mF cm^{-2}, and an energy density of 0.13 mWh cm^{-2}.[181] A coaxial AFSC was also developed using an Au-MnO_x@CoNi@CNT fibre as the positive electrode (core) and a holey graphene paper (HGP) as the negative electrode (sheath) wrapped around the core. This AFSC achieved an operating voltage of 1.8 V, a volumetric energy density of ~15.1 mWh cm^{-3}, a power density of ~7.28 W cm^{-3}, and 90% capacitance retention over 10 000 cycles, with charge/discharge rates of up to 10 V s^{-1}.[175] A stretchable FASC was also demonstrated using hierarchically structured MnO_2@-PEDOT:PSS@oxidised CNT fibres (OCNTF) as the positive electrode and flower-like MoS_2@CNTF as the negative electrode.[167] This AFSC exhibited an asymmetric complementary-chemistry synergy, where MnO_2 provided high-capacitance redox storage at positive potentials and MoS_2 provided stable intercalation storage at negative potentials, together enabling a large operating voltage of 1.8 V, a high specific capacitance of ~278.6 mF cm^{-2}, an energy density of 125.37 μWh cm^{-2}, and ~92% of capacitance retention after the devices being stretched at a strain of 100% for 3000 cycles.[167] Another study developed an AFSC by using $Ni(OH)_2$-decorated porous dendritic Ni–Cu film on Cu wire as the positive electrode and binder-free rGO/carbon fibre as the negative electrode.[182] This AFSC showed an areal, volumetric, and gravimetric energy density of ~195 μWh cm^{-2}, ~15.04 mWh cm^{-3}, and ~54.5 Wh kg^{-1}, respectively, together with a high cycling stability (95.7% capacitance retention after 5000 charge/discharge cycles) over a voltage window of 1.6 V.[182] These examples highlight the advantage of AFSCs in achieving high voltage outputs and energy densities compared to their symmetric counterparts, albeit at the cost of increased complexity in electrode pairing and mechanical integration.

When pairing fibre-based electrodes for AFSC, a key requirement to achieve high performance is ensuring that the charges stored on the positive electrode (Q_+) are the same as those of the negative electrode (Q_-). This is commonly known as charge balancing ($Q_+ = Q_-$). As two distinct electrode materials typically differ in usable potential ranges and capacitances, one way to charge balancing is by tuning the mass (or loading) of the active materials such that the charges stored on the electrodes match under the chosen operating conditions. This charge balance is described using eqn (6).

$$C_+V_+M_+ = C_-V_-M_- \quad (6)$$

Here, $C_\pm$, $V_\pm$ and $M_\pm$ represent the specific capacitance, accessible potential window, and the mass (volume, area, or length) of the positive and negative electrodes. The specific capacitance of an AFSC assembled from two different electrodes can then be obtained using eqn (7)–(9).

$$C = \frac{Q}{(M_+ + M_+)V} \quad (7)$$

Table 2 Comparison of various designs of AFSCs reported in the literature[a]

Positive electrode	Negative electrode	Electrolyte	Device architecture	Voltage	Specific capacitance	Energy density	Power density	Cyclic stability	Reference
MnO_2@Ink/ACF	PANi@Ink/ACF	CMC/Na_2SO_4	Twisted	2 V		16 μW h cm^{-1} 102 μW h cm^{-2}	160 μW cm^{-1}		172
rGO/MoS_2-coated yarn	MXene-coated cotton yarn	PVA/H_2SO_4	Parallel	1.3 V	658 mF cm^{-2} 53 F g^{-1}	154.5 μWh cm^{-2} 12.3 Wh kg^{-1}	8147 μW cm^{-2} 650 W kg^{-1}	75.1% 10 000 cycles	15
MnO_2/PEDOT:PSS/CNT	Ordered microporous carbon/CNT	CMC/Na_2SO_4	Twisted	1.8 V		11.3 mWh cm^{-3}	2.1 W cm^{-3}	85% 10 000 cycles	173
CNT@NiO@MnO_x	CNT@Fe_2O_3	PVA/LiCl	Twisted	1.8 V	10.4 F cm^{-3}	4.7 mWh cm^{-3}		95% 2000 cycles	174
Au-MnO_x@CoNi@CNT	HGP	PVA/LiCl	Coaxial	1.8 V		15.1 mW h cm^{-3}	7.3 W cm^{-3}	90% 10 000 cycles	175
GF/$NiCo_2S_4$	GF	PVA/KOH	Parallel	1.5 V		12.3 mWh cm^{-3}	1600 mW cm^{-3}	92% 2000 cycles	176
MnO_2@PEDOT:PSS@OCNTF	MoS_2@CNTF	PVA/LiCl	Coaxial	1.8 V	278.6 mF cm^{-2}	125.4 μWh cm^{-2}	540 μW cm^{-2}	92% 3000 cycles	167
MnO_2–$NiCo_2O_4$	rGO	PVA/LiCl	Parallel	1.6 V	2.1 F cm^{-2}	37.8 mW cm^{-3}	2678.4 mW cm^{-3}	92% 5000 cycles	177
$NiCo_2O_4$@$Ni(OH)_2$/CNTF	VNNW@CNTF	PVA/KOH	Twisted	1.6 V	291.9 mF cm^{-2} 106.1 F cm^{-3}	103.8 μWh cm^{-2} 37.7 mWh cm^{-3}		90% 5000 cycles	178
Co_3O_4@c-fPI@CF	c-fPI@CF	PVA/KOH	Twisted	1.6 V	56 F cm^{-3}	10.0 mWh cm^{-3}	1.2 W cm^{-3}	95% 8000 cycles	179
PANi/CNT	FeC_2O_4/FeOOH/CNT	PVA/KOH	Parallel	2.0 V		4.1 μWh cm^{-2}	0.4 mW cm^{-2}	96.76% 4000 cycles	180
$Ni(OH)_2$@$NiCo_2O_4$/CNTF	MoS_2@Fe_2O_3/CNTF	PVA/KOH	Coaxial	1.6 V	375 mF cm^{-2}	0.1 mWh cm^{-2}	3.2 mW cm^{-2}	83.3% 10 000 cycles	181
$Ni(OH)_2$/Ni–Cu/Cu	rGO/CF	1 M NaOH		1.6 V	12.2 F cm^{-2}	195 μWh cm^{-2} 15.0 mWh cm^{-3}	2.6 mW cm^{-2} 196 mW cm^{-3}	95.7% 5000 cycles	182
CF/CNT/MnO_2	CF/CNT/PP	PVA/LiCl	Twisted	1.7 V	59.7 F g^{-1}	22.3 Wh kg^{-1}		86.1% 5000 cycles	183
ZNCO@$Ni(OH)_2$/CNTF	VN@CNWAs/CNTS	PVA/KOH	Twisted	1.6 V	94.7 F cm^{-3} 573.8 mF cm^{-2}	33.7 mWh cm^{-3} 204.0 μWh cm^{-2}	396 mW cm^{-3}	90.3% 3000 cycles	184
MnO_2@CNT	AC@CNT	PVA/Na_2SO_4	Braiding	1.6 V	61.8 F cm^{-3}	0.02 Wh cm^{-3}	0.444 W cm^{-3}	79.0% 10 000 cycles	185
rGO/MnO_2 hybrid fibre	rGO fibre	PVA/H_3PO_4	Coaxial	1.6 V	24 F cm^{-3}	8.4 mWh cm^{-3}	0.19 W cm^{-3}		186
CNT@ZnO-NWs@MnO_2	CNT	PVA/H_2SO_4	Twisted	1.8 V	31.2 mF cm^{-2}	13.3 μWh cm^{-2}	2.1 mW cm^{-2}	96.7% 1000 cycles	13
CF@CNC(CNT–NiCoOH)	CF@AC	PVA/KOH	Twisted	1.8 V		0.8 mWh cm^{-3}		80% 8000 cycles	187
NiCoBOH@CuY	rGO/CNT@CuY	PVA/KOH	Woven	1.4 V	133 mF cm^{-2}	78.1 μWh cm^{-2}	14 mW cm^{-2}	82.7% 5000 cycles	188
$NiCo_2S_4$@NiF/NiW	N-rGO	PVA/KOH	Parallel	1.4 V	19.6 F cm^{-2}	855.7 mW cm^{-3}	855.7 mW cm^{-3}	92% 1000 cycles	189
RuO_2/CNT yarn	MXene/CNT yarn	PVA/H_2SO_4	Twisted	1.5 V		61.6 mWh cm^{-3}	5428 mW cm^{-3}	~100% 1000 cycles	32
$NiCo_2S_4$@W-MXene/CF	W-MXene/CF	PVA/KOH	Parallel	1.5 V	939.2 mF cm^{-2}	40.7 mWh cm^{-3}	301.5 mW cm^{-3}	85% 10 000 cycles	190

Table 2 (*Contd.*)

Positive electrode	Negative electrode	Electrolyte	Device architecture	Voltage	Specific capacitance	Energy density	Power density	Cyclic stability	Reference
MnO_2/PEDOT:PSS/CNTs	VN@CNWAs/CNTF	PVA/Na_2SO_4	Coaxial	1.8 V	213.5 mF cm^{-2}	96.0 μWh cm^{-2}	270 μW cm^{-2}	96.8% 5000 cycles	191
MXene/PANi fibre	MXene fibre	PVA/H_2SO_4	Twisted	1 V	510 mF cm^{-2}	15.71 μWh cm^{-2}			192
Mn-doped NiCo oxysulfide/NF wire	AC/CF	PVA/KOH	Cable-type hybrid cells	1.6 V		31.5 Wh kg^{-1}	2616.3 W kg^{-1}	82.2% 4000 cycles	193

[a] Ink: commercial pen ink, ACF: activated carbon fibre, PANi: polyaniline, CMC: carboxymethyl cellulose CMC, rGO: reduced graphene oxide, MoS_2: molybdenum sulfide, MXene ($Ti_3C_2T_x$), PVA: poly(vinyl alcohol), PEDOT: PSS: poly(3,4-ethylenedioxythiophene):poly(styrene sulfonate), CNT: carbon nanotube, Au-MnO_x@CoNi@CNT: gold manganese oxide at cobalt nickel at carbon nanotubes, HGP: holey graphene paper, GF: graphene fibre, OCNTF: oxidized carbon nanotube fibre, CNTF: carbon nanotube fibre, VNNW: vanadium nitride nanowires, CNTF: carbon nanotube fibre, c-fPI: carbonized fluorinated polyimide, CF: carbon fibre, FeC_2O_4: iron oxalate, FeOOH: iron oxide hydroxide, PP: polypyrrole, ZNCO@$Ni(OH)_2$/CNTF: zinc–nickel–cobalt oxide at nickel hydroxide nanowire arrays on a carbon nanotube fibre, VN: vanadium nitride, CNWAs: carbon coated nanowire arrays, CNTs: carbon nanotube strip, AC: activated carbon, ZnO-NW: zinc oxide nanowires, NiCoOH: nickel cobalt hydroxide, NiCoBOH@CuY: NiCo bimetallic oxyhydroxide film deposited on Cu-coated yarn, rGO/CNT@CuY: reduced graphene oxide/carbon nanotube hybrid film coated on Cu-coated yarn, $NiCo_2S_4$: nickel cobalt sulfide, NiF: nickel fibre, NiW: nickel wire, $NiCo_2S_4$@NiF/NiW: nickel cobalt sulfide decorated 3D porous Ni film on Ni wire, N-rGO: nitrogen doped reduced graphene oxide, W-MXene/CF: wet-spun MXene/CF, $NiCo_2S_4$@W-MXene/CF: $NiCo_2S_4$ electrodeposited on wet-spun MXene/CF, NF: nickel foam.

$$C = \frac{Q}{\left(\frac{Q}{C_+V_+} + \frac{Q}{C_-V_-}\right)V} \tag{8}$$

$$\frac{1}{C} = \frac{1}{aC_+} + \frac{1}{bC_-} \tag{9}$$

where $V_+ = aV$ and $V_- = bV$, with a and b being the constants related to mass (volume, area or length) of the positive and negative electrodes. Maximum device capacitance is achieved when $aC_+ = bC_-$. This equation implies that charge balances in AFSCs can be achieved by tuning the mass of the active materials based on their specific capacitances. In AFSCs, mass and volume scale naturally with length, offering a more tractable design parameter. Therefore, charge balance in AFSCs can also be achieved by adjusting the electrode lengths (L), as demonstrated in eqn (10).

$$C_+V_+L_+ = C_-V_-L_- \tag{10}$$

This approach allows capacitance matching simply by cutting the electrodes to the appropriate lengths after fabrication, avoiding the intrinsic variability and process complexity associated with modifying material loading during electrode production. A study demonstrated the approach of a length-matching strategy for AFSC by using PANi@Ink/ACF (Ink: commercial pen ink and ACF: activated carbon fibre) as negative electrode and MnO_2@Ink/ACF as positive electrode with nearly equal capacitance per unit length (~108 *vs.* 107 mF cm^{-1}) which delivered ~16 μWh cm^{-1} or ~102 μWh cm^{-2} of areal energy density with a voltage window of 2 V.[172] Given the electrodes had almost the same specific capacitances and operated in similar voltage windows, the same lengths of the electrodes were used to achieve charge balancing in the AFSC. However, it is possible for the electrodes to have different specific capacitances or potential windows. In this case length-matching will lead to charge imbalance which can lead to suboptimal performance.

Another approach for charge balancing in AFSCs is the capacitance matching strategy. A recent study recognized the limitations of the traditional length matching strategy and demonstrated capacitance-matched electrodes as an effective strategy for developing high performance AFSCs.[15] Here, a $Ti_3C_2T_x$ MXene (negative) and rGO/MoS_2 (positive) yarns were used as the electrode and their specific capacitances were tuned to be in the same range. The lengths of the electrodes were subsequently adjusted to ensure precise matching of the capacitances of the electrodes. This approach led to an AFSC with a high device specific capacitance (~53 F g^{-1}), long-term stability over 10 000 cycles, and an energy density of ~12.3 Wh kg^{-1} over a voltage of 1.3 V. Apart from length and capacitance, another study reported charge balancing by using area where they used a V_2O_5/MWCNT (positive) and VN/MWCNT (negative) electrode having different capacitances and voltage windows ($C_+ = 805.6$ mF cm^{-2}, $V_+ = 0.4$ V, $C_- = 671.2$ mF cm^{-2}, and $V_- = 1.0$ V).[28] Charge balancing can also be achieved by optimising the diameters of electrode fibres. In another example, rGO fibres with different diameters were produced,

and linear capacitance was evaluated.[176] AFSC device was fabricated using $NiCo_2S_4$-coated rGO fibres as the positive electrode and rGO fibres as the negative electrode. Here, charge balancing was achieved by selecting the specific diameter rGO fibre whose charge storage capacity closely matched that of the $NiCo_2S_4$-coated rGO fibre electrode. The charge of both rGO fibre and $NiCo_2S_4$-coated rGO fibres was calculated to be 3.75 mC cm^{-1} by using the linear capacitance and the potential window of each electrode. The resulting AFSC exhibited a voltage of 1.5 V, an energy density of ~12.3 mWh cm^{-3}, and 92% capacitance retention over 2000 charge/discharge cycles.

5.2. Device fabrication and interconnection

Device fabrication refers to the process by which individual components of AFSCs, such as positive and negative fibre electrodes and electrolyte together with separator and encapsulation (when necessary) are combined into a single device. AFSC device fabrication commonly involves pairing a positive fibre electrode with a negative fibre electrode in a charge-balanced system, as charge imbalance can lead to underutilization of one electrode or premature failure of the device. This is followed by the application of an electrolyte which is commonly in the form of a gel or a solid such as polyvinyl alcohol (PVA)/H_2SO_4, PVA/KOH, PVA/Na_2SO_4, and PVA/LiCl. Depending on the device structure, a separator material may be placed between the fibre electrodes or carefully added to the electrolyte to prevent the electrical contact between the two fibre electrodes. Separators include electrospun nanofibre membranes such as polyvinylidene fluoride (PVDF), polyacrylonitrile (PAN), textile fabrics (*e.g.*, cotton, polyester, and nylon) and commercial polypropylene (PP) or polyethylene (PE) membranes commonly used in secondary batteries. The electrolyte system can also be modified by incorporating electrically insulating additives such as h-BN, which allow closer electrode proximity while preventing short circuit and maintaining stable operation.[15] For instance, a study used nylon threads as separator which were helically wrapped around each activated-carbon-coated carbon-fibre yarn (AC-CY) electrode to prevent shorting during twisting and to hold the PVA/LiCl gel electrolyte in place. Twisting two nylon-wrapped AC-CY electrodes (two-ply) in a device increased the volumetric capacitance from ~0.74 to ~1.2 mF cm^{-3} compared to a single-ply device, due to higher active material per unit length, while the device volume increased by ~30%.[194]

The method used for device fabrication depends on the preferred device architecture, which mainly includes parallel,[189] twisted,[183] and coaxial[195] configurations, chosen based on the form and fabrication of the fibre electrodes, performance requirements, and intended application. In the parallel assembly, two fibre electrodes are aligned side-by-side with a separator or gel electrolyte layer positioned between them to prevent a short circuit.[196] In a parallel FSC architecture, the positive and negative yarn electrodes are arranged side-by-side and separated using a separator. For instance, an AFSC was developed by placing the positive (rGO/MoS_2) and negative (MXene-coated cotton yarns) electrodes in parallel and subsequently depositing a layer of PVA/H_2SO_4/h-BN as the electrolyte and separator system (Fig. 4a).[15] This configuration prevents electrical shorting while allowing ion transport, ensuring stable operation. This configuration is easy to assemble and allows independent optimization of each electrode but often requires careful control of electrode spacing and uniform electrolyte deposition and there are some setbacks for large scale textile integration. While the parallel device architecture is often used for performance evaluation, it can be adapted for textiles by first integrating the electrode fibres into the fabric and then applying the electrolyte layer separately. Nevertheless, the side-by-side placement of electrodes can make the device susceptible to delamination or short-circuiting under bending, stretching, or compression.

In the twisted architecture, two electrode fibres are first coated with an electrolyte layer and then intertwined to form an AFSC (Fig. 4b).[183] For instance, an AFSC has been made by twisting the positive CF/CNT/MnO_2 and negative CF/CNT/PPy fibres using a PVA/LiCl gel electrolyte. This AFSC operated over a wide voltage window of 1.7 V and achieved a high energy density of 22.8 μWh cm^{-1} with high flexibility (91.6% after 500 bending cycles) and cyclic stability (86.1% after 5000 cycles).[183] Nyquist plot of the AFSC (obtained by EIS) showed resistive behaviour in the high-frequency region, including an equivalent series resistance (R_s) of 12.8 Ω and a charge transfer resistance (R_{ct}) of 7.6 Ω. The R_s represents the ionic resistance of the gel electrolyte and the intrinsic resistance of the electrodes, while R_{ct} originates from faradaic reactions at the electrode surface. These low resistance values indicate the high conductivity of the CF-CNT network, which offers fast electron and ion transport. The EIS therefore confirms the good capacitance performance of the AFSC. Furthermore, the twisted architecture is a scalable approach of AFSC device fabrication and closely mimics the geometry of conventional yarns used in textiles. However, in this configuration, mechanical deformations can cause torsional compression, which can induce localized stress concentration and may damage the electrode fibres or the gel electrolyte layer, often leading to a short-circuit, especially for long AFSCs.

In coaxial assembly, one fibre electrode forms the core, while the other electrode is placed concentrically as a sheath, separated by an electrolyte layer (Fig. 4c).[184] For instance, a study showed the fabrication of coaxial AFSC by coating Au-MnO_x@-CoNi@CNT core positive electrode with a PVA/LiCl gel electrolyte and wrapping it with an HGP negative electrode (sheath), forming a compact core–sheath structure. This AFSC architecture enables an extended voltage window of 1.8 V and a volumetric energy density of 15.1 mWh cm^{-3}.[175] The Nyquist plot shows R_s of 2.5 Ω, displaying the high electrical conductivity of the AFSC device. Additionally, the near-vertical (~90°) slope in the low-frequency region indicates efficient ion diffusion and favourable charge transport at the electrode/electrolyte interface. Coaxial architectures can also be fabricated in a single step using coaxial spinning or wet-spinning strategies, where the core, separator/electrolyte, and sheath are continuously extruded through a multi-channel spinneret to yield an integrated all-in-one AFSC. For instance, when the inner stream of

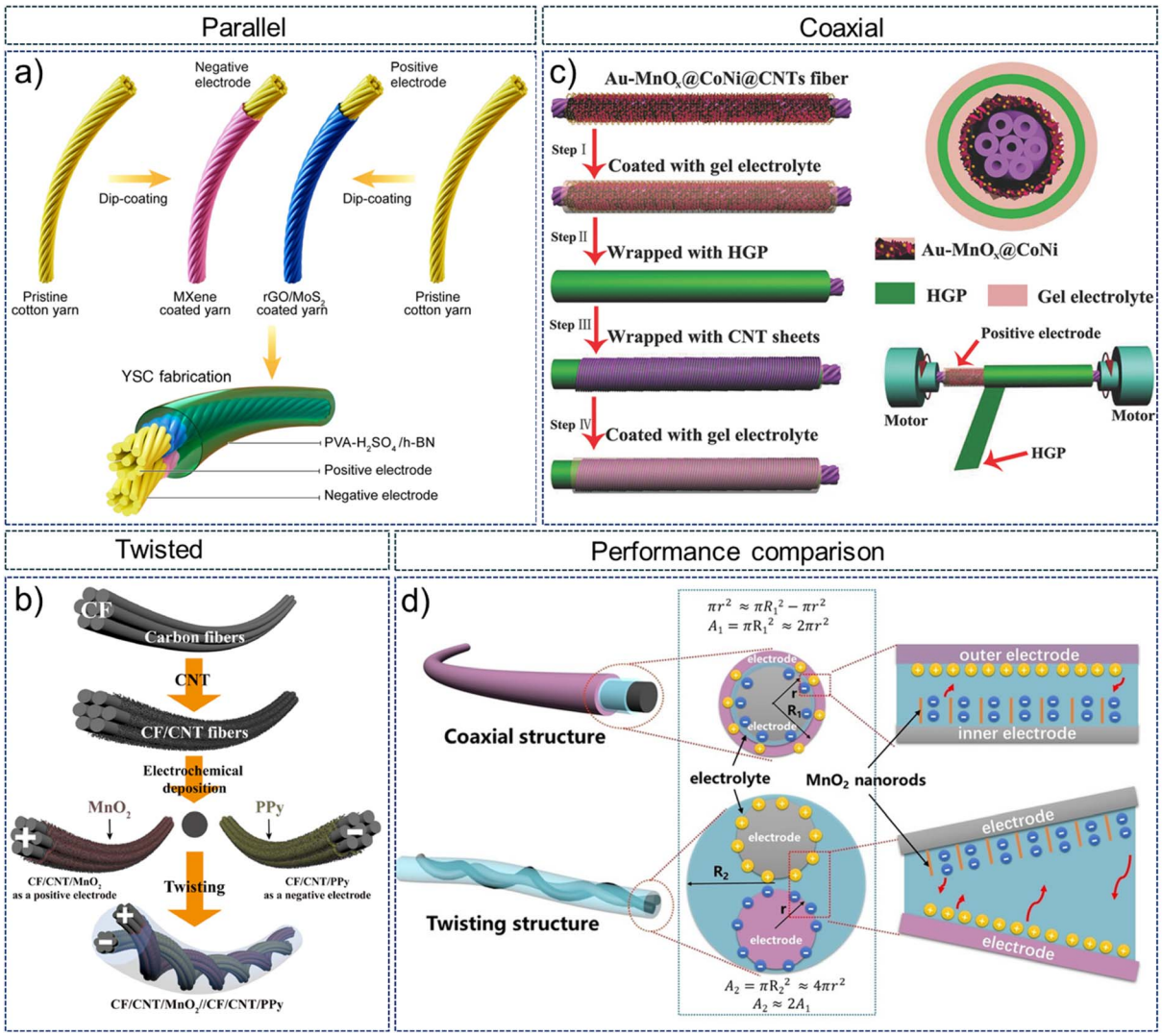

Fig. 4 Device assembly and architecture of AFSCs. (a) Parallel architecture, Adapted from Wiley, Copyright 2025,[15] (b) twisted architecture, Adapted from Elsevier, Copyright 2021,[183] (c) coaxial architecture, Adapted from Wiley, Copyright 2018,[175] and (d) performance comparison of twisted and coaxial architectures, Adapted from Wiley, Copyright 2020.[186]

GO LC and the outer stream of sodium carboxymethyl cellulose (CMC) solution were fed simultaneously through a coaxial spinneret into an ethanol/water (5 : 1) bath containing 5 wt% calcium chloride, this coagulation bath instantly solidified the jet, producing GO/CMC fibres with a well-defined core–sheath architecture.[163] The GO@CMC fibres were chemically reduced by HI to make them conductive (700 S cm^{-1}) for high performance supercapacitor fabrication. The CMC sheath functioned as a fibre-level separator, electrically insulating the electrode while allowing ions to pass through for charge storage. This design offered uniform current distribution and compact geometry, though fabrication is more complex. The coaxial geometry ensures uniform ionic transport, minimizes inter-electrode distance, and typically achieves superior volumetric energy density, rate capability, and cycling stability. However, fabrication requires precise multi-layer coating techniques, and cracks or inhomogeneities in the active layers may lead to performance inconsistency or failure. A study compared the performance of twisted and coaxial architectures using identical rGO/MnO_2 hybrid fibres as the positive electrode, rGO fibre as the negative electrode, and PVA/H_3PO_4 gel electrolyte (Fig. 4d). The coaxial AFSC achieved a higher volumetric performance (~24 F cm^{-3} and ~8.4 mWh cm^{-3}) than the twisted AFSC (~11 F cm^{-3} and ~3.91 mWh cm^{-3}).[186] This difference is primarily rooted in the higher volumetric utilization by compact core–sheath arrangement and a much shorter radial ion-migration distance, which reduces charge-transfer resistance in the case of coaxial architecture.

Encapsulation in a soft polymeric and breathable materials such as polydimethylsiloxane (PDMS)[197] or polylactic acid (PLA)[198] may be used to prevent electrolyte evaporation and leakage, enhance washability, maintain flexibility, and protect the AFSC from degradation caused by sweat and moisture during wear. For instance, a stretchable, waterproof AFSC was

developed by embedding a helix-shaped AFSC made up of stainless steel wires (SW)/MnO_2 as positive electrode and SW/rGO fibre as negative electrode coated with a PVA/LiCl electrolyte and assembled into a helix-like geometry, followed by encapsulation using a bifunctional polymer (Ecoflex, a PLA-based biopolymer), which acted as both an elastic substrate and waterproof encapsulation.[199] The Ecoflex polymer provided complete waterproofing while maintaining flexibility and mechanical stability. This AFSC achieved a voltage of 1.6 V and an energy density of ~2.86 mWh cm^{-3} while retaining over 95% capacitance after 3000 stretching cycles at 400% strain and over 95% capacitance after 10 000 charge/discharge cycles. It also showed stable electrochemical performance when immersed in water for 50 h, demonstrating the role of encapsulation in ensuring waterproofing.[200]

5.2.1. Interconnection and textile integration. Interconnection involves linking multiple AFSC devices as well as embedding them within textiles with other components to create a fully integrated system. A fully functional textile wearable typically comprises diverse components, including sensors, displays, communication modules, energy storage units, and energy harvesters.[201] Establishing effective interconnections among various devices is essential to enable seamless communication and coordinated operation. Multiple AFSCs may also need to be interconnected in series or parallel configurations to form energy networks capable of powering various devices. The method of interconnection is often determined in conjunction with the application requirements. The most common form of interconnection is connecting multiple AFSC units in series to increase the output voltage. For instance, when a voltage of 4.5 V is required, three AFSCs with operating voltages of 1.5 V can be interconnected in series to meet the voltage requirement. Parallel interconnection of AFSCs is also commonly used to increase the overall capacitance when a long operation time is necessary.

A recent study reported a proof-of-concept where automated machine weaving (using an automated loom) was used to integrate various fibre-based devices such as fibre photodetectors (input device), fibre field-effect transistors (electronic driving device), fibre supercapacitors (energy storage device), and fibre quantum dot light-emitting diodes (output device) into textiles, enabling the development of a fully woven E-textile (Fig. 5a).[201] The CFs-based electrodes and PVA/H_3PO_4 electrolyte were used for fabrication of symmetric fibre supercapacitors. The interconnection between fibre electrodes and conductive threads was then established using laser soldering, where a conductive adhesive (silver) was precisely dispensed at junctions followed by rapid curing using a focused infrared laser (Fig. 5b). This method prevented thermal damage and allowed reliable connections for small-diameter fibres. They demonstrated that FSCs can be integrated into textiles *via* automated weaving, with CF inserted along the weft and conductive yarns along the warp directions (Fig. 5c). The use of encapsulation and careful control of the reed speed protected the fibres from

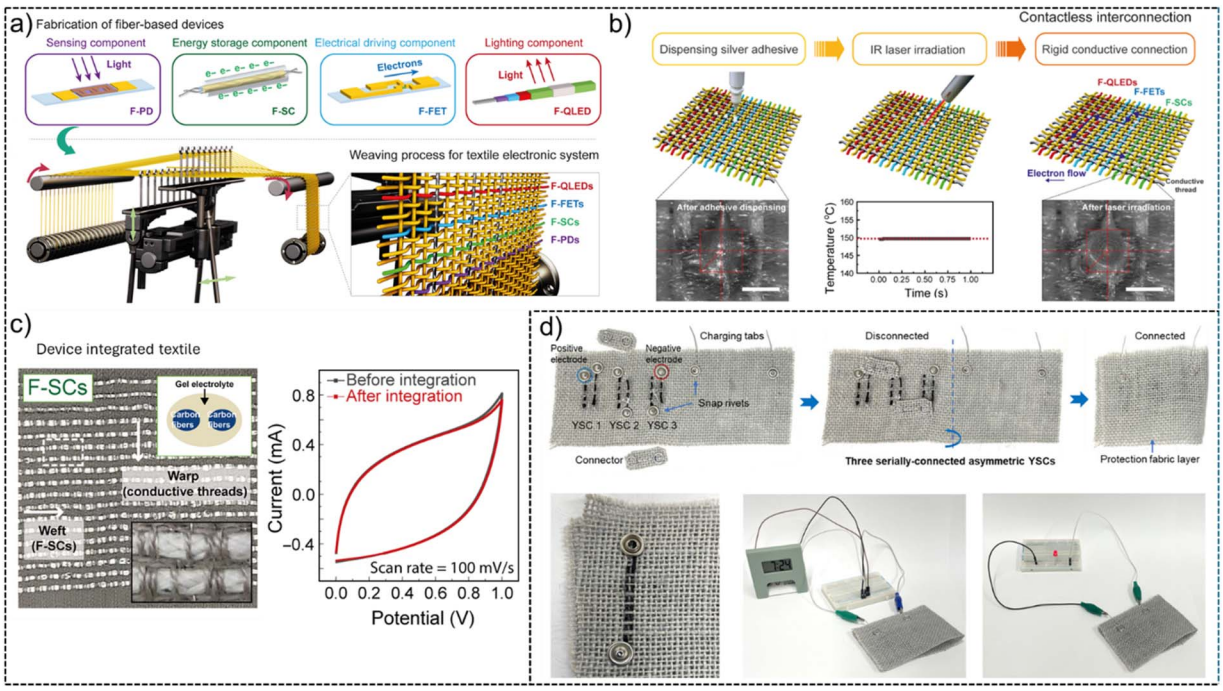

Fig. 5 Interconnection and textile integration. (a) Textile integration of different components, such as fibre photodetector (F-PD) as an input device, fibre supercapacitor (F-SC) as an energy storage device, fibre field-effect transistor (F-FET) as an electronic driving device, and fibre QD light-emitting diode (F-QLED) as output device are shown using a schematic and weaving process. (b) Illustration of contactless integration *via* laser with micrographs at the bottom at a scale bar of 1 mm and a graph in the middle tracking the adhesive temperature over the curing period. (c) Photograph of textile integration of FSC and its performance before and after integration. Images (a–c) adapted from Ref. 201, Copyright 2023, Science. (d) Rietveld interconnection using snap rivets and textile integration *via* sewing, Adapted from ref. 15 Copyright 2025, Wiley.

mechanical stresses applied during weaving, ensuring the performance of FSC is maintained upon integration as shown by unchanged CV profiles of the FSC before and after integration (Fig. 5c). Although this study used SFSCs, it provided a scalable approach for integration of various fibre-based devices into textiles including AFSCs. In another study, an easy and simple method of interconnections and textile integration was demonstrated by using snap rivets (Fig. 5d).[15] Here, individual AFSC units were sewn onto a textile substrate made up of jute fabric and snap rivets, commonly used in clothing such as denim jackets and jeans, were then attached to the yarn electrodes. Snap rivets provided physical anchoring and established metallic conduction pathways. Using this approach, three AFSCs were connected in series which produced a combined working voltage of ~3.9 V and delivered a specific capacitance of ~19 F g^{-1} and an energy density of ~35 Wh kg^{-1}.

Apart from weaving and sewing, studies also reported textile integration *via* knitting, braiding, and embroidery.[125,202] For instance, knitting was used to integrate an AFSC together with fluorinated PDMS-coated triboelectric nanogenerator (TENG) yarns into a textile.[203] The AFSC consisted of NiCo bimetallic oxyhydroxide (NiCoBOH) coated on a Cu coated polyester yarn as the positive electrode, rGO/CNT co-self-assembled on Cu coated polyester yarn as the negative electrode, and PVA/KOH as the quasi-solid electrolyte.[203] This AFSC was integrated into a self-charging cotton fabric *via* knitting and demonstrated a configuration of English letters "BINN" patterned textile, showing an areal energy density of ~78.1 μWh cm^{-2}, a power density of ~14 mW cm^{-2}, an operating voltage of 1.4 V, and ~82.7% retention over 5000 charge/discharge cycles. The TENG yarns were electrically connected to the AFSC *via* a rectifier, enabling the fabric to harvest human motion energy and directly power an electronic watch without external charging. Another study demonstrated the use of braiding to integrate AFSC into wearable textiles.[204] The AFSC was made of AC@CNT fibres as negative electrode, manganese–nickel–cobalt carbonate hydroxide nanoneedle arrays grown on CNT (MnNiCo-CH NNAs@CNT) fibres as the positive, and polyester yarns as the separator and PVA/KOH as the gel electrolyte. The AFSC exhibited an areal energy density of ~46.33 μWh cm^{-2}, a power density of ~9.66 mW cm^{-2}, an operating voltage of ~1.4 V, ~91.6% capacitance retention after 10 000 charge/discharge cycles, and ~90.1% retention after 1500 bending cycles. Two serially connected AFSC devices braided into a flexible watchband powered a commercial digital watch and turned on 65 LEDs with "DHU 70" patterns.

6. Role of electrolyte

The electrolyte serves as the ionic conductor connecting the two electrodes and influences the electrochemical performance, flexibility, and safety of AFSCs. The electrolyte plays a crucial role in governing charge transfer kinetics, internal resistance, energy density, and the long-term durability of the AFSCs. For textile-based wearable systems, the electrolyte in AFSCs needs to demonstrate high mechanical flexibility, environmental stability, and non-toxicity, as these devices undergo continuous deformation and are exposed to air or humidity.[108,205,206] The ideal electrolyte in AFSCs should possess a high ionic conductivity, a wide potential window, a wide operating temperature range, high electrochemical stability, low volatility and flammability, low cost, and environmental friendliness, as well as inertness to device components such as electrodes and separators. Broadly, the common electrolytes used in AFSCs can be categorized as liquid, gel (quasi-solid), and solid-state systems (Table 3).

6.1. Liquid electrolytes

Liquid electrolytes can be classified as either aqueous or organic, depending on the solvent used. Aqueous electrolytes (*e.g.*, H_2SO_4, H_3PO_4, KOH, LiCl, or Na_2SO_4) offer several advantages over other types of electrolytes due to their high ionic conductivities (0.5–1.0 S cm^{-1})[222] and small ionic size, while being inexpensive, making them attractive for AFSCs.[223,224] In AFSCs, aqueous electrolytes have shown excellent power density, rate performance, and capacitance retention. However, the possibility of leakage in liquid electrolytes makes them unfit for wearable applications. Aqueous electrolytes are also restrained by their narrow electrochemical window due to their limited decomposition voltage (1.23 V). Generally, the operational voltage window of FSCs in aqueous systems is limited to 1.0 V due to polarization effects, which restrict the achievable energy density.[225] Additionally, acidic or alkaline electrolytes can be unsuitable for wearable applications as they can cause skin irritation or burns. These can also corrode metal current collectors and degrade electrode materials, reducing the device lifespan.[226] In AFSCs, leakage and evaporation of aqueous electrolytes can compromise safety and performance, although encapsulation within a soft polymer layer can be used to mitigate these risks. Aqueous electrolytes remain the most popular systems for electrode testing and early stage AFSC prototypes. Recently, a new class of aqueous electrolytes, WiSE have been explored in energy storage systems.[227] It helps in breaking the water decomposition challenges at high potential extremes and extends the electrochemical window of supercapacitors by suppressing polarisation reactions.[228] High concentration water-in-salt LiTFSI aqueous electrolyte was shown to extend the electrochemical window of asymmetric supercapacitor to 3 V from −1.5 to +1.5 V.[211] An asymmetric supercapacitor with vanadium nanowire@carbon cloth (VN NWs@CC) as negative electrode and MnO_2 nanosheet based positive electrode with water-in-salt LiTFSI aqueous electrolyte demonstrated an extended electrochemical window combined with a high energy density (~61.5 Wh kg^{-1}). These examples demonstrate the potential of WiSE to combine high safety and high conductivity of aqueous electrolyte systems with an extended voltage range and improved energy density.

Organic electrolytes contain the conductive salts (*e.g.*, $LiClO_4$, $LiPF_6$, tetraethylammonium tetrafluoroborate) in organic or non-aqueous solvents such as (*e.g.*, propylene carbonate, ethylene carbonate, dimethyl carbonate, acetonitrile, and ionic liquids). They offer a wide electrochemical stability window (2.5–3.0 V), which leads to a higher energy

Table 3 Electrolyte systems used in AFSCs[a]

Electrolyte	Type	Operating voltage (V)	Fibre electrode materials	Specific capacitance	Energy density	Power density	Reference
H_3PO_4	Aqueous	2.0	CNT@MnO_2 yarn//CNT yarn	12.5 F g^{-1}	42.0 Wh kg^{-1}	19 250 W kg^{-1}	207
Na_2SO_4	Aqueous	2.0	Na–MnO_2@CFB//PFAC@CFB	32.5 F g^{-1}	18.0 Wh kg^{-1}	5829.1 W kg^{-1}	208
KCl	Aqueous	1.6	Carbon fibres/PEDOT/MnO_2//AC	537 F g^{-1}	49.4 Wh kg^{-1}	224.02 W kg^{-1}	209
KOH	Aqueous	1.2	CF-rGO/Fe_2O_3//CF-MnO_x	50 F g^{-1}	5 Wh kg^{-1}	1437 W kg^{-1}	210
LiTFSI	Aqueous (WiSE)	3	MnO_2@CC//VN-NWs@CC	49.2 F g^{-1}	61.5 Wh kg^{-1}	57.9 W kg^{-1}	211
PVA/LiCl	Gel	1.8	MnO_2@PEDOT:PSS@OCNTF//MoS_2@CNTF	278.6 mF cm^{-2}	125.4 μWh cm^{-2}	540 μW cm^{-2}	167
PVA/KOH	Gel	1.5	rGO fibres/$NiCo_2S_4$//rGO fibres	388 F cm^{-3}	12.3 mWh cm^{-3}	1600 mW cm^{-3}	176
PVA/KOH	Gel	1.6	NiV_2Se_4–Ag//AC	317 mF cm^{-2}	77 Wh kg^{-1}	749 W kg^{-1}	212
PVA/LiCl	Gel	1.8	CNT@NiO@MnO_x//CNT@Fe_2O_3	10.4 F cm^{-3}	4.7 mWh cm^{-3}	27.1 mWh cm^{-3}	174
PVA/LiCl	Gel	1.7	CF/CNT/MnO_2//CF/CNT/PPy	59.7 F g^{-1}	22.3 Wh kg^{-1}	410 W kg^{-1}	183
PVA/H_2SO_4	Gel	1.8	PANi@CNT//PANi/graphene@CNT		160.5 μWh cm^{-2}	13 mW cm^{-2}	213
PVA/H_2SO_4/h-BN	Gel	1.3	MXene-coated yarn//rGO/MoS_2-coated yarn	658 mF cm^{-2}	154.5 μWh cm^{-2}	8146.7 μW cm^{-2}	15
Gelatin/$ZnSO_4$	Gel	1.2	Zn coated yarn//$Ti_3C_2T_x$ MXene coated yarn	214 mF cm^{-2}	42.8 μWh cm^{-2}	0.64 mW cm^{-2}	214
PAANa/Na_2SO_4	Gel	1.6	Nylon/Ag/MnO_2//Nylon/Ag/PPy	181.7 mF cm^{-2}	13.9 μWh cm^{-2}	2902 μW cm^{-2}	215
PVDF-HFP-TEA·BF_4	Gel (organic)	3.5	rGO//MnO_2 embedded CNT yarn	322.4 mF cm^{-2}	43 μW h cm^{-2}	5 mW h cm^{-3}	216
PVA–LiCl	Gel (aqueous)	2.1		171 mF cm^{-2}	30.1 μW h cm^{-2}	3.8 mW h cm^{-3}	
CMC/Na_2SO_4	Gel	2.1	MnO_2/CNT//PI/CNT	59.5 mF cm^{-1}	36.4 μWh cm^{-1}	15.6 mW cm^{-2}	217
PVDF-EMIMBF_4	Gel	2.8	FeC_2O_4/FeOOH-CNT//PANi- CNT fibres	324 mF cm^{-1}	3.1 μWh cm^{-1}	0.97 mW cm^{-2}	180
PVA–$LiClO_4$	Gel	2.2	Fe_2O_3/CFs//MnO_2/CNT-web paper	0.7 F cm^{-3}	0.40 mWh cm^{-3}	0.02 W cm^{-3}	218
PVA/$NaClO_4$	Gel (WiSE)	2.6	Na_xMnO_2 nanosheets//carbon nanofibres	97.2 F g^{-1}	90 Wh kg^{-1}	28.1 kW kg^{-1}	61
PVA/H_2SO_4	Solid	1.6	V_2O_5/rGO/PANi hydrogel//rGO/carbon fibre	209.8 F g^{-1}	29.4 Wh kg^{-1}	2 kW kg^{-1}	219
PVA/Na_2SO_4	Solid	1.5	MoS_2/MWCNTs//PANi/MWCNTs	138.1 F g^{-1}	15.1 Wh kg^{-1}	2217.9 W kg^{-1}	220
PVA/H_3PO_4	Solid	1.6	MoO_3 nanorods/rGO fibres//MnO_2 nanorods/rGO fibres	51.2 F cm^{-3}	18.2 mWh cm^{-3}	76.4 mW cm^{-3}	221

[a] CFB: carbon fibre bundles, PFAC: palmyra fruit waste-derived activated carbon, AC: activated carbon, NW: nanowires, CC: carbon cloth, LiTFSI: lithium bis(trifluoromethane sulfonyl)imide, OCNTF: oxidized carbon nanotube fibres, CNTF: oxidized carbon nanotube fibres, CF: carbon fibres, PAANa: sodium polyacrylate, PI: polyimide, PVDF-EMIMBF_4: polyvinylidene fluoride (PVDF) with the ionic liquid 1-ethyl-3-methylimidazolium tetrafluoroborate, PANi: polyaniline, MWCNTs: multiwalled carbon nanotubes, PVDF-HFP-TEA·BF_4: (PVDF-hexafluoropropylene) gel-based tetraethylammonium tetrafluoroborate (TEA·BF_4) organic electrolyte in propylene carbonate.

density compared to aqueous systems.[108] Organic electrolytes have better compatibility with device components (*e.g.*, electrode materials) as they are less corrosive than aqueous electrolyte systems. For example, an asymmetric supercapacitor was fabricated with $Ti_3C_2T_x$ MXene as the negative electrode and rGO/nickel–cobalt bimetal oxide as the positive electrode, using 1 M $TEABF_4$ in acetonitrile as the electrolyte, which achieved an energy density of ~52.1 Wh kg^{-1}.[229] The disadvantages of organic electrolytes are lower ionic conductivities (10^{-3}–10^{-2} S cm^{-1}), weaker ion dissociation, and higher viscosity compared with aqueous electrolytes, which result in slower ion diffusion as well as flammability or toxicity, posing serious safety concerns for wearable AFSCs. Consequently, there is a need for airtight encapsulation for AFSCs which increases fabrication complexity and cost. Additionally, one of common limitations of using organic electrolytes are their relatively poor performance when used with pseudocapacitive electrodes, which can reduce total energy storage compared to aqueous systems. Organic electrolytes remain attractive where high voltage operation is prioritized, although their use in AFSCs for wearable applications is still limited due to safety concerns.

6.2. Quasi-solid or gel electrolytes

Quasi-solid electrolytes, also known as gel electrolytes, are typically composed of a liquid electrolyte incorporated into a polymer matrix such as poly(vinyl alcohol) (PVA), polyacrylamide (PAM), gelatine, or cellulose.[230,231] These electrolytes combine high ionic conductivity and mobility of liquid electrolytes with mechanical robustness and flexibility of polymeric materials, making them attractive for AFSCs. Gel electrolytes conform well to the irregular surfaces in fibre electrodes, maintaining intimate electrode–electrolyte contact and low interfacial resistance even under bending or twisting deformations, crucial for wearable applications.[232] The polymeric matrix also minimises leakage and evaporation of the liquid electrolyte.[233] Among various quasi-solid electrolytes, PVA/H_2SO_4, PVA/LiCl, PVA/Na_2SO_4, and PVA/KOH are widely used (Table 3), offering ionic conductivities of 10^{-3}–10^{-2} S cm^{-1} while operational voltage remains limited (up to 1.2–2.0 V) due to the aqueous nature of the electrolyte component.[234] Natural polymer gels (*e.g.*, agarose/NaCl and gelatine/H_3PO_4) have also been employed for biocompatible and sustainable FSCs.[235,236] For instance, three dimensional NaCl–agarose gel electrolyte was synthesized featuring oriented interconnected pores, which supports efficient ionic transport while giving mechanical stability needed for FSCs. MnO_2 incorporated thin film-based FSCs achieved a specific capacitance of 286.9 F g^{-1} in NaCl–agarose gel electrolyte and retained 80% of its capacitance at 100 mV s^{-1}.[235] Gel electrolytes are compatible with AFSC device assembly and can be applied using methods like dip-coating, layer-by-layer assembly, and coaxial fibre spinning. Polymer-salt gel electrolytes generally offer a broader and more electrochemically stable operating voltage window than polymer-acid or polymer–alkaline gel electrolytes because neutral salt electrolytes contain far lower concentrations of ions (H^+ and HO^-) than acidic or alkaline systems, which significantly suppress hydrogen and oxygen evolution reactions.[232] For instance, WiSE gel electrolyte can produce a high-voltage device with excellent energy density. An AFSC device fabricated with Na-inserted MnO_2 and N-doped carbon nanofibres using $NaClO_4$-based WiSE/PVA gel systems demonstrated remarkable electrochemical performance, including an operation voltage window of 2.6 V, specific capacitance of ~97.2 F g^{-1}, energy density of ~90 Wh kg^{-1}, power density of ~28.1 kW kg^{-1}, and capacitance retention of ~85.2% over 10 000 charge/discharge cycles.[61] It also exhibits reasonable electrical performance under harsh conditions, such as freezing temperatures and temperatures above 50 °C. One of the main limitations of gel electrolytes is that ionic mobility is strongly affected by the polymer matrix's crosslinking density and water content, making them susceptible to performance degradation from dehydration or freezing.[237] To overcome this, ionic liquid-based gels and hybrid ionogels are gaining traction due to their broader operating voltage windows (~3 V) and enhanced environmental stability.[238] In ionic liquid-based gels, ionic liquids can play dual roles, functioning either as independent electrolytes or as conductive additives incorporated within polymer matrices (*e.g.*, $EMIMBF_4$/PVDF-hexafluoropropylene and PVDF-$EMIMBF_4$).[238,239] This combination leverages the high ionic conductivity of $EMIBF_4$ together with the electrochemical stability and compatibility of PVDF. In another study, a CNT-based AFSC device was assembled using an ionic liquid (3-ethyl 1-methyl imidazolium tetrafluoroborate, $EMIMBF_4$) electrolyte with a polymer (PVDF) and achieved areal energy density of ~3.06 μWh cm^{-2}, and power density of ~0.97 mW cm^{-2}.[177] The liquid electrolyte based on PVDF-$EMIMBF_4$ helped enable ion transport with a high operational window (2.8 V) within the fibre-shaped architecture, which hugely contributed in improving the performance of the device.

6.3. Solid-state electrolytes

Solid electrolytes mainly consist of solid polymer electrolytes, inorganic solid electrolytes, or a combination of inorganic–polymer electrolytes.[240,241] Solid electrolytes have a dual role as a medium for ion transport and as a separator for electrodes. They can address the safety risks associated with liquid or quasi-solid electrolytes such as leakage and thermal instability and offer controllable shapes that simplify the manufacturing process and packaging of wearable AFSCs. Polymers such as PVDF, poly(ethylene oxide) (PEO), poly(methyl methacrylate), polyacrylonitrile, epoxy and polyvinyl chloride with lithium salts (*e.g.*, LiTFSI, lithium bis(fluorosulfonyl)imide, lithium/sodium perchlorate), ionic liquids, inorganic fillers (Al_2O_3 or SiO_2), or MOFs are used to produce a solid electrolyte, where Li salts provide ion transport and fillers enhance ionic conductivity by creating percolation networks and reducing polymer crystallinity.[242–244] However, solid-state electrolytes have shown lower performance in supercapacitors, which can be attributed to lower ionic conductivities (10^{-4} S cm^{-1}) compared to liquid and quasi-solid electrolyte systems[245] as well as high impedance at the solid–solid interface between the electrolyte and electrode, which often leads to poor charge transfer efficiency. To

address this issue, ultrathin electrolyte coatings and composite interlayers are commonly used to enhance adhesion at the electrolyte–electrode interface. Hybrid solid-state electrolyte systems, composed of ionic liquids immobilized in polymer networks, offer a promising route to combine high ionic conductivity with high operating voltages (2.5–3.0 V).[233,237] For instance, an all solid-state AFSC was assembled using a positive electrode made up of MnO_2-coated carbon cloth and a negative electrode made up of rGO-coated carbon cloth with an ionic-liquid (3-butyl 1-methylimidazolium tetrafluoroborate, $BMIMBF_4$)-based polymer solid electrolyte (PVA:BMIMBF4:TBABF$_4$) which showed an ionic conductivity of ~21.7 mS cm^{-1}, comparable to advanced 1-allyl-3-methylimidazolium bis(trifluoromethylsulfonyl)imide/hydroxide/epoxy solid electrolyte (10 mS cm^{-1}).[246,247] This AFSC achieved an operational window of 3 V, a high energy density (~61.2 Wh kg^{-1}), a high power density (~1049 W kg^{-1}), and capacitance retention of ~80% after 3000 charge/discharge cycles. Recent studies on supercapacitors have explored the integration of ionic liquids with epoxy resins (known for high chemical resistance and thermal stability) to enhance the ionic conductivity of thermosetting polymer electrolytes.[248–250] Some other inorganic solid electrolytes such as $Na_3Zr_2Si_2PO_{12}$ (NZSP) dispersed in PEO–$NaCF_3SO_3$ electrolyte membrane,[251] 10NaI-90 [$PEO_{1-x}NZSP_x$],[252] $Li_{1.4}Al_{0.4}Ti_{1.6}(PO_4)_3$ (ref. 253) and $Li_{1.3}Al_{0.3}Ti_{1.7}P_3O_{12}$/$LiMnPO_4$ (ref. 254) have been employed in supercapacitors. Similar solid electrolyte systems can be investigated for AFSCs. Solid-state electrolytes are a promising family of electrolytes for the next generation of AFSCs for wearable applications, where high operating voltage, long-term operation, flexibility, safety, and sustainability are essential.

7. Applications of fibre supercapacitors

Due to their high energy density, long cycle life and flexibility, FSCs are highly promising for next-generation soft wearables. FSCs are used to fabricate energy-autonomous systems by supplying power to flexible sensors and integrated wearables which have applications in health monitoring and internet of things (IoT). They have also found application in biological systems such as implantable devices for minimally invasive tissue integration and long-term energy supply. AFSCs are an emerging class of fibre-based storage devices, and examples of their integration with other fibre technologies are limited. However, the same design principles apply to conventional FSCs, which have been integrated with various fibre-based energy harvesters and sensors. In this section, FSC integration strategies are examined as a basis for future AFSC developments. Such integration eliminates the dependence on external charging sources and allows for self-sustained operation during wear. Energy harvesting is particularly attractive to be paired with FSCs due to the variety of available energy sources, such as mechanical energy from body movements (piezoelectric and triboelectric nanogenerators) and solar energy from ambient light (photovoltaics), which can be converted to electrical energy and stored in FSCs. Integration is generally achieved either by developing a single multifunctional fibre device capable of both harvesting and storing energy or by coupling separate fibre-based harvesting and storage devices within one textile structure. Beyond energy harvesting, FSCs have also been integrated with fibre-based sensing functions, enabling simultaneous energy storage and detection of mechanical and biochemical stimuli. Deformation-induced changes in resistance, capacitance, or electrode–electrolyte interactions allow FSC-based systems to function as strain and pressure sensors, while electrochemically active fibre electrodes enable self-powered biochemical sensing, such as glucose monitoring. These architectures demonstrate that FSCs can operate not only as energy storage components but also as active sensing elements in wearable textile systems.

7.1. Integrated multifunctional energy systems

Integration of energy harvesting, and supercapacitor devices has been demonstrated at the fibre level. One study demonstrated a fibre-based multifunctional energy system which consisted of a photoconversion device on one side and a supercapacitor on the other side.[255] These fibre-based devices shared a common Ti wire core with vertically grown titania nanotubes. The photoconversion device was made by depositing a layer of poly(3-hexylthiophene):phenyl-C_{61}-butyric acid methyl ester (P3HT:PCBM) followed by a PEDOT:PSS layer, and an MWCNT coating on the exterior (Fig. 6a). On the supercapacitor side, a PVA/H_3PO_4 gel electrolyte was applied onto the Ti/TiO_2 wire base serving as one electrode followed by an MWCNT coating (second electrode), forming a coaxial AFSC. Upon exposure to sunlight, excitons generated within the P3HT:PCBM layer separated into electrons and holes. The electrons were injected into and transported along the titania nanotube core, while the holes were carried through the PEDOT:PSS layer to the outer MWCNT electrode. The resulting photovoltage drove charge into the adjacent supercapacitor section, where it was stored. The overall photoconversion and energy storage efficiency increased with MWCNT layer thickness, reaching 0.82% when the coating thickness was increased to 20 μm. This fibre-based multifunctional energy system also exhibited high mechanical flexibility, maintaining its performance after repeated deformation, with the total conversion efficiency decreasing by less than 10% after 1000 bending cycles. However, detailed power output values were not provided. Another study employed a similar shared electrode strategy to produce a fibre-based multifunctional energy system by using a twisted device architecture.[256] Here, a Ti wire with vertically grown titania nanotubes on its surface area was used as the shared electrode. On the photoconversion side, a layer of a ruthenium bipyridine complex dye (N719) was then deposited, followed by a redox electrolyte composed of LiI, I_2, dimethyl-3-*n*-propylimidazolium iodide, and 4-*tert*-butylpyridine in dehydrated acetonitrile. The supercapacitor side consisted of a CNT-coated PVA/H_3PO_4 gel electrolyte and used the Ti based photovoltaic wire as the other electrode (Fig. 6b). The AFSC within this multifunctional energy system was charged to 0.6 V

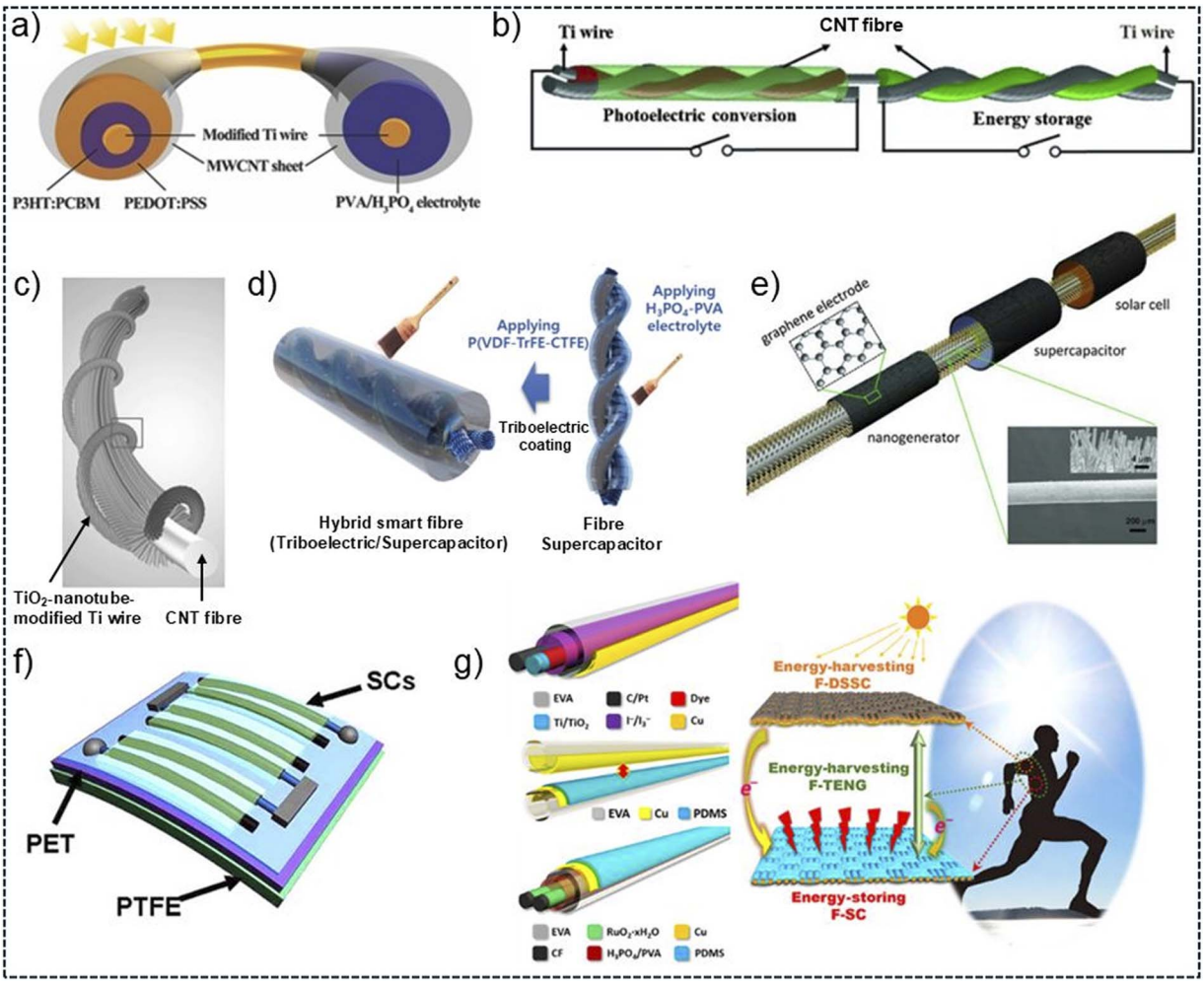

Fig. 6 (a) Schematic of a coaxial solar cell–supercapacitor multifunctional fibre; adapted from ref. 255 Copyright 2014, Wiley-VCH GmbH. (b) Schematic of a twisted solar cell–supercapacitor multifunctional fibre; adapted from ref. 256 Copyright 2012, Wiley-VCH GmbH. (c) Schematic of a wound solar cell–supercapacitor multifunctional fibre; adapted from ref. 257 Copyright 2014, Wiley-VCH GmbH. (d) Schematic of a supercapacitor fibre with an external triboelectric coating; adapted from ref. 258 Copyright 2020, Wiley-VCH GmbH. (e) Schematic of a multifunctional fibre integrating piezoelectric, solar, and supercapacitor components; adapted from ref. 259 Copyright 2011, Wiley-VCH GmbH. (f) Schematic of a triboelectric film integrated with supercapacitor fibres; adapted from ref. 162 Copyright 2022, American Chemical Society. (g) Schematic of a knitted textile comprising solar cell and supercapacitor fibres with triboelectric top and bottom layers; adapted from ref. 260 Copyright 2016, American Association for the Advancement of Science.

within seconds upon illumination of air mass (AM) 1.5 and could subsequently be discharged for about 10 min at a current of 0.1 μA. The operating voltage of the FSC was 0.68 V, where the specific capacitance reached 0.5 mF cm^{-2} and the energy density was reported to be 0.15 μWh cm^{-2}. This twisted configuration showed an overall photoconversion and electrochemical energy storage efficiency of ~1.5%.

A fibre-based multifunctional energy system was also demonstrated by helically winding a PANi/CNT fibre electrode around a Ti wire coated with vertically aligned titania (TiO_2) nanotubes.[257] The Ti/TiO_2-nanotube photoanode core was sensitised with N719 dye and the I_3^-/I^- redox couple was used to facilitate charge transfer between the photoanode and the counter electrode, forming a fibre-shaped dye-sensitised solar cell. The helically wound PANi/CNT fibre served as the counter electrode for the solar cell and simultaneously acted as the outer electrode of the supercapacitor. The inner electrode of the supercapacitor was the Ti/TiO_2 core, coated with the same electrolyte to achieve an AFSC. The AFSC showed an operating voltage of 0.7 V and a specific capacitance of 2.13 mF cm^{-2}. These examples illustrate integration principles, including shared electrodes, coaxial design, and direct coupling of harvesting and storage for future AFSC architectures. Sharing the PANi/CNT fibre allowed the photogenerated current from the dye-sensitised solar cell to be directly fed into the AFSC, achieving harvesting and storage within a single fibre system (Fig. 6c). This fibre-based multifunctional energy system showed a solar-to-electrical conversion efficiency of 6.58% and stable cycling over 5000 charge–discharge cycles.

The integration of a fibre-based triboelectric nanogenerator (TENG) with an FSC within a single continuous fibre has also been demonstrated (Fig. 6d).[258] In this design, unidirectionally

aligned carbon fibres as the electrodes were coated with a layer of PVA/H_3PO_4 gel electrolyte to form the FSC component. The TENG component was achieved using two carbon fibre electrodes that were twisted together followed by encapsulation with a P(VDF-TrFE-CTFE) layer acting as the triboelectric material. Mechanical deformation of the twisted fibre caused periodic contact-separation and surface charge generation within the triboelectric layer, producing an alternating output. This electrical output was rectified and directly fed into the FSC, enabling the harvested energy to be stored. This design enabled the integration of both energy harvesting and storage devices along the entire fibre, rather than being localized in different segments. This fibre-based multifunctional system exhibited great mechanical flexibility with almost 100% capacitance retention after 50 000 charge–discharge cycles and even under repeated bending, knotting, and washing.[258] The PVDF-TrFE encapsulating layer effectively minimized electrolyte leakage when washing for 2 h at 800 rpm. However, power density and energy conversion efficiency were not reported.

Another study demonstrated a fibre-based multifunctional energy system by combining two energy harvesting devices, *i.e.*, photoconversion and piezoelectric, with an FSC for energy storage along separate segments of the fibre.[259] The fibre core consisted of polymethyl methacrylate (PMMA) with vertically grown zinc oxide nanowires (ZnO NWs). For the piezoelectric segment, a graphene layer was coated as the electrode onto the ZnO NWs layer acting as the piezoelectric material. The photoconversion segment was produced by first coating the ZnO nanowires with an N719 dye, followed by a graphene counter electrode, forming a fibre-shaped dye-sensitised solar cell. The FSC segment consisted of a PVA/H_3PO_4 gel electrolyte layer deposited on the PMMA/ZnO fibre and surrounded by an outer graphene electrode layer (Fig. 6e). Although the overall device was presented in separate functional sections, the authors demonstrated integrated operation by simultaneously harvesting light and mechanical deformation. Under illumination, the photoconversion segment generated an output voltage of ~0.7 V, while the piezoelectric ZnO NW segment produced voltage peaks of ~0.12 V under bending. These outputs were collectively directed into the FSC, which exhibited a specific capacitance of ~1.8 mF cm^{-1} and could be charged by the combined harvesting modes. The key outcome of this work was the demonstration of multimodal energy harvesting—photovoltaic and piezoelectric—feeding a FSC energy-storage unit, even though the efficiencies and power densities of the fully integrated system were not quantified.

FSCs have also been interconnected with energy harvesting units to form an integrated film- or textile-based multifunctional energy system. One study demonstrated a film-based TENG composed of a laminate structure of poly(ethylene terephthalate) (PET) and polytetrafluoroethylene (PTFE) as the triboelectric transduction layers and coaxial FSCs made of carbon fibre (core) and MnO_2 (shell) electrodes with a PVA/H_3PO_4 electrolyte attached on the PET surface (Fig. 6f).[162] Three FSCs were electrically connected in series after being mounted on the triboelectric surface. The specific capacitance of the FSC was ~2.5 F cm^{-3} and the energy density reached ~0.22 mWh cm^{-3}. A single FSC showed a voltage of 0.75 V, whereas the serial arrangement of three FSCs reached 2.4 V within 5 s of hand-driven operation, sufficient to power a liquid-crystal display.

Another study integrated fibre-shaped solar cells and fibre-based TENGs as the harvesting units and FSCs as the energy storage components into a fibre-based multifunctional energy system (Fig. 6g).[260] The fibre-shaped solar cells consisted of a Ti wire photoanode coated with vertically aligned TiO_2 nanotubes sensitised with an N719 dye, followed by a Pt-coated counter electrode. Here, transparent, flexible ethylene vinyl acetate (EVA) tubing was used as the structural backbone of the self-charging power textile. The underside of the solar-cell fibres was further coated with a triboelectric material, polydimethylsiloxane (PDMS), to form the TENG interface. In parallel, the FSCs were made by using two CNT fibre electrodes and a PVA/H_3PO_4 gel electrolyte coating layer followed by further coating of a PDMS triboelectric layer on their upper surface. The solar-cell fibres and FSC fibres were subsequently knitted into two separate textile layers and then overlaid, positioning the complementary ethylene vinyl acetate (EVA)-coated face to be in contact with PDMS for triboelectric charge generation. This configuration enabled simultaneous harvesting of solar energy from the upper textile and mechanical energy from frictional contact between the PDMS and EVA layers, while all harvested energy was routed into the textile FSC for storage. The textile FSC had an operating voltage of 0.7 V, specific capacitance of ~1.9 mF cm^{-1} and energy density of ~1.37 mJ cm^{-1} (~0.38 μWh cm^{-1}). The integrated system achieved a solar power conversion efficiency of 5.64% and the TENG generated an output of ~28 V under hand tapping. Demonstrations included powering an array of LEDs using the combined solar–triboelectric harvesting energy stored in the FSC layer. This work illustrated a viable strategy for achieving multifunctional, self-powered energy textiles through layered integration of various fibre-based devices.

7.2. Integrated sensing systems

FSCs are integrated with sensors into fibre-based multifunctional self-powered sensing systems that could track the wearer's health and activity while simultaneously powering the sensing function. Integration is achieved at a fibre or textile level. In a recent study, the combination of the electrodes of FSCs and the conductive layer of strain sensors in the same fibre was investigated to achieve dual functions of energy storage and strain sensing.[261] Coaxial wet-spinning was used to produce fibres consisting of a PEDOT/SWCNTs conductive core blended with PPy and a stretchable PU sheath, demonstrating both high stretchability and robust electrochemical performance. The strain sensing performance came from piezoresistive changes in the conductive network of PEDOT and PU under mechanical deformation, where stretching altered contacts in the PEDOT/SWCNT/PPy network and produced measurable resistance changes without disrupting the fundamental electrochemical charge storage pathways. The electrochemical performance of PU/PPy@PEDOT/SWCNT fibres was measured in three

electrode systems using saturated KCl solution as an electrolyte with 0.8 V potential window. The as-prepared fibres demonstrated a specific capacitance of ~760 F g^{-1}, a stretchability of up to ~375%, and a stable gauge factor of ~76.5 in the 50% strain range which was stable for 4000 cycles, suitable for human motion detection, illustrating the dual strain sensing and energy storage capability of the integrated fibre structure. However, the use of aqueous electrolyte suggests room for improvement in terms of real-world applicability. Another work built upon this study by developing a multifunctional supercapacitor and strain sensor which utilised PVA/H_3PO_4 as part of the design. This study explored the use of hierarchical conductive networks, such as CNT/MXene/PU hybrid fibres.[262] Here, a stretchable, porous conductive network was developed by wet-spinning PU with CNTs and MXene nanosheets, where the PU acted as an elastic polymer scaffold and the CNTs/MXene formed an interconnected electron-conductive porous framework throughout the fibre. This hierarchical conductive architecture combined the electroactive properties of MXene and CNT and the elasticity of the PU polymer matrix, resulting in a device which exhibited a specific capacitance of ~3.9 F cm^{-3}, with an operating voltage of 0.8 V and an energy density of ~1.16 mWh cm^{-3}. The device also showed ~95% capacitance retention after being strained to 50% for 50 cycles.

Pressure or deformation sensing functionalities have also been integrated with FSCs by leveraging the electrode–electrolyte interactions during mechanical deformations. For instance, stretchable, knittable coiled type FSCs were fabricated using elastomeric electrodes produced by coiling a nylon sewing thread followed by helically wrapping with CNT aerogel sheet ribbons and electrochemically depositing MnO_2 nanofibres.[263] These MnO_2/CNT/nylon fibre electrodes offered synergic charge storage mechanism of pseudocapacitive MnO_2 and EDLC behaviour of CNT. A gel electrode (PVA–LiCl) further supported the flexibility and provided an ionic conductive layer on the electrodes. This FSC achieved a voltage window of 1.0 V, a high areal capacitance of ~40.9 mF cm^{-2}, an energy density of ~2.6 μWh cm^{-2}, a power density of ~66.9 μW cm^{-2} and maintained ~85% of its capacitance when stretched by 150% in the fibre direction. When used in a wristband, the FSC retained its electrochemical performance during large strains (50%). In another study, the effective integration of multifunctional components including strain sensor and supercapacitor was demonstrated into one single coaxial fibre.[264] Here, the core of the coaxial fibre was an AFSC made of an MnO_2@-PEDOT:PSS@CNT positive electrode, a PPy@CNT negative electrode, and a PVA–LiCl gel electrolyte, achieving an operating voltage of 1.8 V. The sheath of the coaxial fibre served as high-gauge-factor piezoresistive strain sensor made of a CNT/thermoplastic elastomer composite. This all-in-one integrated coaxial fibre showed a relatively high volumetric energy density of ~1.42 mWh cm^{-3} and ~85.1% capacitance retention after stretching for 6000 cycles at a strain of 200%. On a single charge, this integrated multifunctional system exhibited self-sustained performance with excellent durability and stability on continuously unloading/loading at 40% strain for 10 000 cycles. Multiple pressure-sensitive FSC can be integrated into textiles and connected in series or parallel to obtain the desired voltage, energy storage performance, and sensitivity. This opens the door to wearable pressure sensing systems that are self-powered and combine tactile sensing with supercapacitors.

FSCs have also been integrated with electrochemical sensors,[265–267] such as biochemical glucose sensors for wearable health monitoring. In these cases, the integrated sensor systems were developed by anchoring the electrochemically active sensing layers onto the conductive flexible electrodes that simultaneously support charge storage. For instance, a flexible patch type self-charging supercapacitor with glucose sensing capability was fabricated to measure biological signals with uninterrupted energy supply.[265] When the microneedle-based glucose sensor penetrated the skin, glucose oxidase (GOx) on its surface reacted with glucose present in the interstitial fluid. The electron produced by glucose oxidation was then used for directly powering the system, initiating charge accumulation by establishing a potential difference across the supercapacitor electrodes. The supercapacitor electrodes were developed by coating indium tin oxide (ITO) on the flat (opposite) side of the PDMS substrate, where the microneedle array was developed, followed by rGO deposition. For the other supercapacitor electrode, ITO was coated on a thin PDMS layer, followed by coating rGO and a layer of a gel electrolyte (PVA/H_3PO_4). The device delivered a specific capacitance of ~800 mF cm^{-3} and a power density of ~0.62 mW cm^{-2}. This is an example of a self-powered biosensor where the output power is directly proportional to the concentration of the blood glucose. However, the use of the GOx enzyme raises the question of long-term and environmental stability. To overcome this issue, non-enzymatic fibre architectures were developed that relied on electrocatalytic metal oxides integrated directly onto conductive fibres. For instance, CF-based electrodes coated with $NiCoO_2$ nanosheets and encapsulated within a nitrogen-doped carbon layer (CF/$NiCoO_2$/N–C) were developed using an electrochemical deposition method, which demonstrated an integrated FSC for stretchable, enzyme-free glucose-sensing.[267] Here, the CF/$NiCoO_2$/N–C material had two functions by acting as a supercapacitor and an electrocatalyst for an enzyme-free biosensor. In this design, the CF served as the flexible current collector, while the $NiCoO_2$ nanosheets provided redox-active sites for glucose oxidation, and the N-doped carbon coating enhanced electrical conductivity and provided structural support under deformation. Glucose sensing in this system came from the direct electrooxidation of glucose at the Ni^{2+}/Ni^{3+} and Co^{2+}/Co^{3+} redox couples. The fibre electrodes simultaneously exhibited supercapacitor behaviour, supported by the high surface area of the $NiCoO_2$ nanosheets and the conductive carbon framework. The CF/$NiCoO_2$/N–C fibres showed a specific capacitance of ~644 mF cm^{-2} and ~94% capacitance retention after 10 000 bending cycles. The device showed a high glucose sensitivity and a fast response time. This method presented an important step toward robust, self-powered biochemical sensing textiles by eliminating enzyme degradation as a primary failure pathway while maintaining the sensing accuracy and energy storage performance. These studies emphasize that FSCs can act as an efficient energy storage unit when paired with sensors with

diverse sensing mechanisms including resistive or capacitance strain or pressure sensors and electrochemical biosensors, providing practical routes toward self-powered wearable systems.

7.3. Integrated biological systems

FSCs can be seamlessly woven or implanted into biological systems and function as compact, flexible power sources for bioelectronics. They offer minimal invasiveness and adaptability to dynamic tissues as well as ensuring long term integration without mechanical failure or triggering strong immune responses. FSCs have been investigated for powering implantable devices that stimulate or monitor biological processes including neural activity or vital signs within living organisms.[27,268] In one study, an FSC was developed that was capable of self-charging *via* biological reactions in order to address the need for sustained and stable current in nerve stimulation experiments in rats.[269] Different fibres responsible for energy generation and energy storage were assembled in a multi-strand twisted architecture (Fig. 7a). In this system, energy generation though glucose/oxygen biofuel cells occurred *via* biochemical oxidation and reduction reactions of naturally occurring glucose on GOx/tetrathiafulvalene (TTF)-functionalized CNT fibres and Pt/C-coated CNT fibres. By twisting GOx/TTF/CNT (positive electrode) and Pt/C/CNT fibres (negative electrode) with PANi/CNT fibre, FSCs were fabricated to store generated energy from biofuel cells. The electrochemical performance of the FSC was first investigated *in vitro* in phosphate-buffered saline (PBS) and 4 mM glucose, representing physiological conditions. The FSC exhibited a specific capacitance of ~123 mF cm^{-2} at 1 mA cm^{-2} with voltage of 0.6 V and 95.8% capacitance retention after 10 000 cycles. To investigate the behaviour of the FSC under *in vivo* conditions, the device was subcutaneously implanted in rats, and its terminals were positioned around the sciatic nerve. In this configuration, the FSC operated by utilising naturally occurring glucose in the body and was able to deliver reproducible pulse currents of ~150 μA. As a result of applying these currents to the nerve, a muscle force of ~3 mN was produced, accompanied by an observed hind-limb movement of ~10°. These results clearly demonstrated that the FSC was capable of delivering sufficient power for nerve stimulation under *in vivo* conditions.

In another study, the behaviour of a biocompatible FSC in driving an implantable biomedical load under *in vivo* conditions was investigated.[27] For this purpose, an FSC was developed in which the electrode, electrolyte, current collector, and encapsulation components were fully integrated into a single fibre structure (Fig. 7b). Here, the FSC was fabricated using a thermal drawing process (TDP) and was composed of two PVA-based hydrogel electrodes containing activated carbon (AC) and CB, separated by a NaCl-containing PVA/polyethylene glycol/sodium borate-based hydrogel electrolyte. The electrochemical performance of the FSC was first evaluated *in vitro* within a voltage of 0.8 V. The highest specific capacitance of ~268 mF cm^{-2} was obtained with an energy density of ~29.8 μWh cm^{-2} and a power density of ~8.48 mW cm^{-2}. The FSC retained ~99.3% of its capacitance after 2000 charge–discharge cycles and maintained ~92% of its initial capacitance after 20 weeks of storage in PBS. To evaluate the functionality of the FSC in a living organism, this device was implanted subcutaneously in mice and connected to neural tissue. A micro-LED was also connected to the system and positioned to enable optogenetic stimulation. The activation of the nerve cells was controlled through illumination of the LED powered by the FSC. During these *in vivo* experiments, the FSC provided sufficient current to stimulate both peripheral nerves and brain tissue. Furthermore, more than 99% of the FSC's capacitance was retained after five weeks. Histological analyses revealed no signs of inflammation or damage in the surrounding tissues, demonstrating the strong potential of the FSCs for implantable biomedical applications.

The biocompatibility issues and stability limitations of conventional FSC electrodes used in implantable electronic systems in physiological fluids was also investigated.[270] In this context, an implantable FSC based on biocompatible redox molecules, inspired by cellular energy conversion mechanisms, was developed (Fig. 7c). The FSC was fabricated by biscrolling CNT-based threads into a fibre form. Each CNT fibre contained the redox-active biomolecule nicotinamide adenine dinucleotide (NAD^+) and the redox mediator benzoquinone (BQ) at its interface for facilitating efficient electron transfer. The charge storage mechanism relied on pseudocapacitive behaviour arising from the reversible redox conversions of the NAD^+/NADH pair. Here, BQ was employed to improve the electron transfer kinetics between the NAD^+/NADH redox couple and the CNT conductive network. As both FSC electrodes share the same NAD/BQ/CNT configuration, the device has a symmetric architecture. The electrochemical performance of the FSC was first evaluated *in vitro* in simulated physiological environments. The FSC exhibited a specific capacitance of ~55.73 mF cm^{-2} (at 10 mV s^{-1}) measured using CV and ~52.5 mF cm^{-2} (at 0.8 mA cm^{-2}) measured using GCD. The FSC retained ~69.6% of its capacitance after 10 000 cycles and largely preserved its electrochemical performance under mechanical deformations such as bending and knotting. For *in vivo* performance of the FSC, the fibre electrodes were implanted into the abdominal cavity of rats. After two weeks, ~86.9% of the initial capacitance (measured on the day of implantation) was retained and no histological inflammation developed around the implant. These results highlight the potential of NAD/BQ/CNT FSCs as implantable energy storage devices.

The challenge of simultaneously achieving high capacitance and biocompatibility in implantable FSCs, together with the poor mechanical and electrochemical stability at the electrode–tissue interface, was also addressed.[271] In this context, an AFSC based on hierarchically porous and heterostructured black phosphorus (A-BP)/$Ti_3C_2T_x$ MXene aerogel fibre electrodes was developed (Fig. 7d). Here, A-BP/MXene aerogel fibre was employed as the negative electrode, a rGO fibre served as the positive electrode, and an acidic silk fibroin/polyacrylamide (SF/PAM) hydrogel electrolyte was used as the electrolyte, forming an AFSC device architecture. The electrochemical performance of this AFSC system was first evaluated *in vitro* in 1 M H_2SO_4

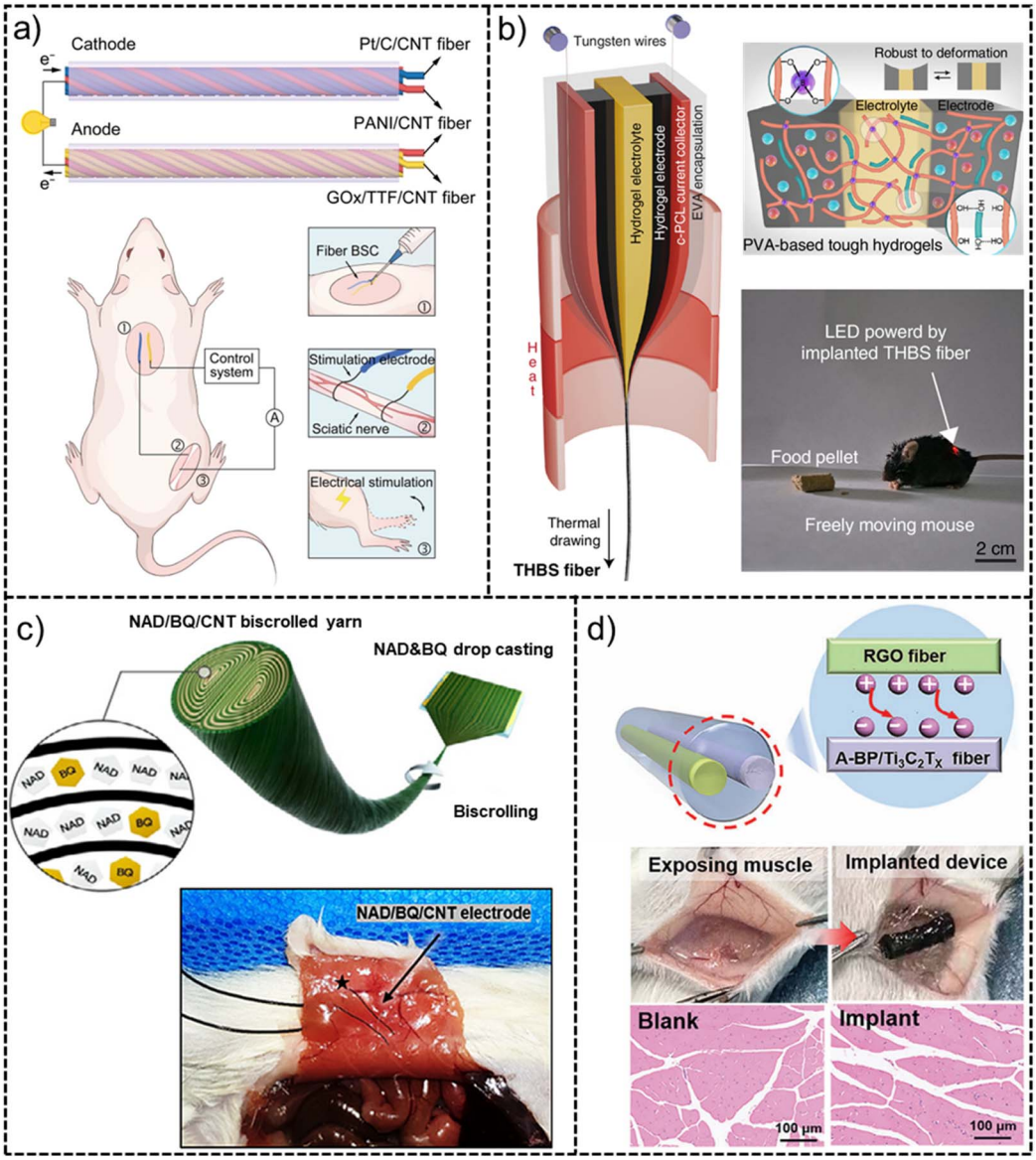

Fig. 7 Implantable fibre supercapacitor systems for *in vivo* applications. (a) Schematic illustration of a biofuel-powered asymmetric fibre biosupercapacitor integrating GOx/TTF–CNT, PANi/CNT, and Pt/C–CNT fibres for self-charging operation and sciatic nerve stimulation in rats; adopted from ref. 269 Copyright 2023, Wiley-VCH GmbH. (b) Fully integrated thermally drawn biocompatible fibre supercapacitor (THBS) architecture and tough hydrogel network composed of PVA, PEG, SB, AC, and CB, providing self-healing capability and robust mechanical strength, and its application in powering an LED for optogenetic stimulation in freely moving mice; adopted from ref. 27 Copyright 2025, Nature. (c) Implantable NAD/BQ/CNT yarn-based symmetric fibre supercapacitor fabricated *via* biscrolling, and its *in vivo* implantation in the abdominal cavity; adopted from ref. 270 Copyright 2021, Wiley-VCH GmbH. (d) Asymmetric solid-state fibre supercapacitor based on BP/$Ti_3C_2T_x$ MXene aerogel and rGO fibres, along with representative implantation and histological evaluation results; adopted from ref. 271 Copyright 2024, Wiley-VCH GmbH.

electrolyte. The specific capacitance of the A-BP/MXene fibre electrode was ~369 F g^{-1} (at 1 A g^{-1}). The AFSC device delivered an operating voltage of 1.0 V and an energy density of ~6.39 Wh kg^{-1} and retained ~85.6% of its initial capacitance after 20 000 charge–discharge cycles. For *in vivo* evaluation, AFSCs were implanted subcutaneously in rats using a PVA/PAA-(*N*-hydroxysuccinimide)-based bioadhesive and histological analyses showed no significant tissue damage around the implant.

8. Machine learning-aided designs and performance prediction

The integration of machine learning (ML) into supercapacitor research has provided a powerful approach for guiding electrode design and accurate prediction of performance metrics reducing the need for the commonly-used and tedious trial and error approaches.[272] ML has been used to predict specific capacitance, energy and power densities, CV and GCD

behaviours, and electrode compositions.[273] The primary motivation for integrating ML methods into FSC research is to reduce the experimental workload and overall testing time and lower the development costs.[274] While the majority of ML studies in the literature have focused on conventional supercapacitors rather than on FSCs, the results obtained are directly relevant as FSCs predominantly use similar electrode materials and performance metrics. For instance, researchers applied interpretable ML such as extreme gradient boosting (XGBoost) to analyse the design parameters that affect hydrogel-based flexible supercapacitors by compiling 232 experimental samples from 41 recent studies.[275] The interactions among 16 key design parameters such as electrolyte formulations, polymer types, and operating conditions were analysed to quantify the importance of various parameters (Fig. 8a). The XGBoost model provided specific capacitance predictions with a coefficient of determination (R^2) of ~0.8. Shapley additive explanations (SHAP) analysis was used to rank the factors. Although ionic conductivity was not identified as the most dominant standalone parameter, it still significantly influences the specific capacitance due to its nonlinear dependence on polymer concentration and electrolyte mass fraction. This suggests that its effect is indirect, arising from coupled variations in ion transport pathways and the distribution of electrolyte within the hydrogel matrix.

The results indicated that synthetic vinyl polymers play a dominant role in determining specific capacitance, whereas conductive polymers (*e.g.*, PANi, PPy and PEDOT) primarily govern cycling stability. The models not only predicted performance but also highlighted the underlying mechanisms such as how increasing conductivity could enhance capacitance up to a threshold beyond which ion crowding would limit further gains.

$Ti_3C_2T_x$ MXene electrodes are commonly employed in AFSCs due to their excellent electrochemical properties. A study focused on evaluating the predictive performance of three ML models for predicting the specific capacitance of $Ti_3C_2T_x$ MXene-based supercapacitors, namely Bayesian ridge regression (BRR), K-nearest neighbours (KNN), and artificial neural networks (ANN) using curated 72 points from the literature.[277] The KNN model achieved an R^2 of ~0.928 with a low root mean square error (RMSE) of ~0.04 F g^{-1} for capacitance. SHAP

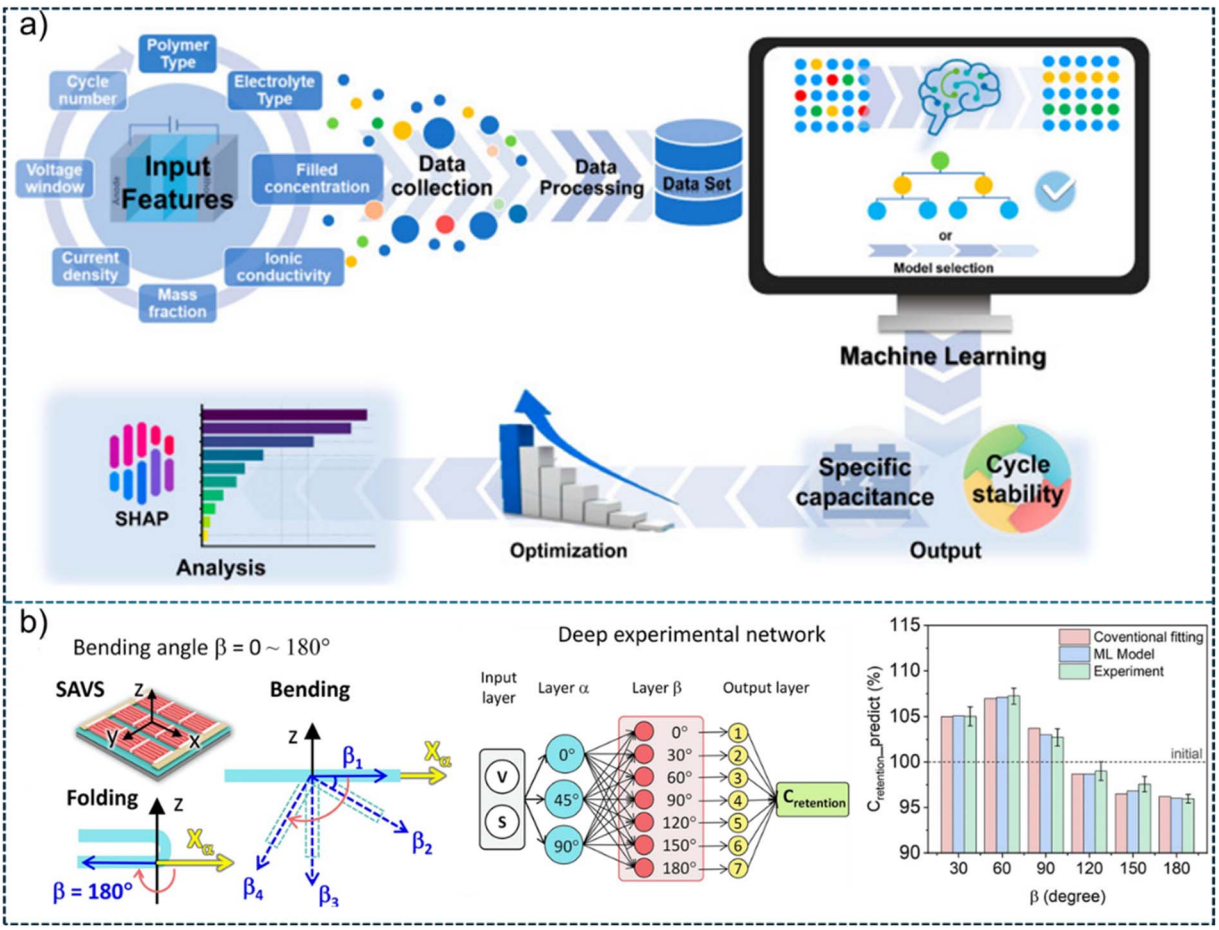

Fig. 8 (a) Workflow of an interpretable machine-learning framework for predicting the performance of hydrogel supercapacitors; adopted from ref. 275 (b) illustration in bending and folding state with bending direction X_α, bending deformation angle β, deep experiment network diagram to collect the experiment data set of capacitance retention and comparison of derived $C_{retention}$ from experiment, machine learning, and conventional fitting; adopted from ref. 276 Copyright 2025, Elsevier.

analysis identified cation mobility, scan rate, and electrolyte concentration as the dominant contributors, revealing non-linear behaviour in which excessive mobility could degrade performance due to ion overcrowding. These findings demonstrated the potential of applying ML approaches to predict the specific capacitance of MXene-based FSCs. In another study, MnO_2 thin-film electrodes with nanofibre morphology were used and their CV behaviours were modelled using a similar ANN-based approach.[278] MnO_2 nanofibres with a three-dimensional interconnected network (0.1–0.5 μm length) were synthesized *via* electrochemical deposition and their CV profiles were obtained in the potential range of 0–1 V (*vs.* saturated calomel reference) which were subsequently used to train a three-layer ANN model (six neurons). The ANN model successfully reproduced the CV curves and showed an excellent agreement between experimental and predicted specific capacitance values, with relative errors in the range of only 0.87–1.28%. For an electrode obtained with 0.1 M $MnSO_4 \cdot H_2O$ precursor, the experimental capacitance ($\sim$392 F g^{-1}) was well matched with predicted capacitance ($\sim$388.6 F g^{-1}), with a relative error of as low as 0.87%, indicating high precision. This study demonstrated that ANN models could achieve high accuracy when reproducing direct electrochemical responses such as CV curves.

In another work, a flexible vertically stacked micro-supercapacitor array (SAVS) was investigated for mechanical flexibility using experimental methods combines with ML techniques under omnidirectional bending and multiple deformation angles.[276] MnO_2 nanospheres electrode-based SAVS showed an impressive specific capacitance of $\sim$509.6 F cm^{-3} ($\sim$1348.9 F g^{-1}) and an energy density of $\sim$8.1 mWh cm^{-3} with $\sim$93.0% capacitance retention after 50 000 cycles, and maintained capacitance under bending test at 90° during 2000 continuous cycles. In the ML model, the voltage window and scan rate were used as input parameters, while the bending angle (α) and bending deformation angle (β) were treated as layer α and layer β, respectively. These parameters were systematically varied to generate a wide range of deformation conditions. A deep experimental data network was then constructed (Fig. 8b). The output layer was comprised of the specific capacitance and capacitance retention, which were calculated from the measured current-density responses. Based on the measured dataset, an ML model was trained to predict capacitance retention across all bending conditions. The predicted minimum capacitance retention of $\sim$95.3% agreed well with the experimental results.

ML also enables rapid screening of large material spaces and guiding iterative improvements by building surrogate models of complex physics and when combined with Bayesian optimization, ML can efficiently identify optimal design conditions.[279] Recently, comparative ML approaches were employed to predict the capacitance of carbon-based supercapacitors based on various electrode features (*e.g.*, surface area and nitrogen doping).[280] These features served as the inputs for training several ML models such as linear regression, support vector regression, decision trees, random forests, deep neural networks, and one-dimensional convolutional neural networks, to predict specific capacitance. 80% of the data was used for training the models and 20% for testing. The convolutional neural network model showed the best performance among all ML models, achieving an R^2 of $\sim$0.941 with mean squared error of $\sim$550.43. SHAP study demonstrated balanced porosity as a key factor, enabling high capacitance while avoiding structural fragility.

9. Sustainability in fibre supercapacitors and life cycle assessment

As textile-based wearable systems continue to evolve, the need for energy storage technologies that not only meet the performance requirements but also address environmental sustainability has increased. Notably, the environmental impact of FSC's disposal and life-cycle assessment should be systematically evaluated to identify sustainable electrode materials, minimize waste, and reduce the overall footprint of FSCs.[281,282] Achieving sustainability in FSCs requires a holistic approach that involves environmentally-friendly and recyclable electrode materials, low-energy fabrication techniques, device architectures that enable component separation for recycling, and textile integration strategies that minimize mixing with conventional fibre materials. At the materials level, biomass-derived and biodegradable components have been used as sustainable alternatives to conventional electrodes.[283–286] Activated carbon from natural sources or biopolymers is increasingly used as an electrode material for FSCs.[283,284] Such electrodes benefit from abundant raw materials, which reduce the reliance on critical metals and use comparatively simpler processing routes, collectively lowering the environmental burdens. Natural fibres such as cotton, silk fibroin, bamboo, and cellulose can serve as lightweight, flexible, and breathable substrates for FSC electrodes.[287–289] Although these fibres are non-conductive in nature but this limitation can be overcome by activating them through coating with conductive materials (*e.g.*, graphene, MXenes, or conducting polymers) so that they function effectively as flexible FSC electrodes.[290] For instance, a type of natural cellulose fibre called Kapok fibre (KF) was used as a low cost template material for the development of KF@MnO_2 and KF@MoS_2/rGO as positive and negative electrodes, respectively in AFSC.[291] The all-solid-state AFSC achieved a maximum energy density of $\sim$63.4 Wh kg^{-1} at a power density of 5 kW kg^{-1}, indicating that natural KFs can serve as effective templates for the design and fabrication of electrode materials for AFSCs.

Minimizing energy consumption during fabrication of AFSCs is also critical to achieve sustainability. Traditional fabrication techniques involve the usage of high temperature, toxic chemicals or energy exhaustive coating processes, which should be replaced by low energy techniques and non-toxic chemicals that can significantly reduce the environmental impact while preserving device performance. Recently, dip-coating cotton yarns with functional materials such as $Ti_3C_2T_x$ MXene and rGO/MoS_2 was produced to fabricate AFSCs with

excellent capacitance and energy density.[15] The AFSC, fabricated using these cotton yarn based electrodes, achieved a remarkable specific capacitance of ~53 F g^{-1}, energy density of ~12.3 Wh kg^{-1}, and power density of ~650 W kg^{-1}. The use of solution processing and template-free methods can reduce waste generation and energy consumption during fabrication process, offering a more sustainable route to AFSC fabrication. It is also important to design AFSCs with recycling and circularity in mind to reduce the environmental impact. Fabricating devices with detachable components or electrodes make disassembly and material recovery easier at the end of their life, which makes a significant impact on life cycle and waste recycling. Recently, the use of riveted connections in AFSC devices allowed the electrode fibres to be detached from the textile for washing or recycling purposes, helping extend the device lifetime and simplifying recycling.[15] Such strategies to disassemble AFSCs from the textile substrate represent an important step toward circular textile-based energy storage systems, where materials can be reused or recycled rather than discarded.

Life cycle assessment (LCA) serves as a quantitative assessment of the environmental impact of AFSC materials and manufacturing routes. LCA measures environmental impact across all stages: raw material extraction, synthesis, fabrication, usage, and disposal, providing insights into energy consumption, greenhouse gas emissions, toxicity, and recyclability.[292] In an LCA study on comparing the environmental life cycle of electrodes made from algae-derived biochar aerogel GO-based electrodes, it has been found that using the biochar-based electrodes could help reduce global warming potential and other environmental damages.[293] This study highlights the benefits of renewable feedstocks and simpler processing routes to lower the environmental footprint of AFSC electrode production. Biochar-based electrodes also showed considerably lower impacts on human health, ecosystems, and resource use than GO-based electrodes as GO synthesis uses energy intensive process, suggesting a greener production pathway for AFSC components. Improving conventional fabrication strategies is essential to minimizing the environmental impact of AFSC production. For MXene-based supercapacitors, an LCA study of MXene synthesis has been carried out.[294] The study revealed that producing 1 kg of MXene at the laboratory scale has a much higher environmental impact than making conventional materials like aluminium or copper foil. This was found to be mainly due to the electricity consumption during the synthesis which accounted for over 70% of the total emissions.[294] In fact, the MXene process was estimated to release ~428 kg of CO_2 per kg, compared with ~23 kg and ~8.75 kg for aluminium and copper, respectively. This suggests that using alternative synthesis routes which include renewable energy and recycling resources could make MXene synthesis significantly more sustainable and have an impact on LCA of MXene-based AFSC. The integration of renewable materials, green electrolytes, and energy-efficient fabrication, combined with LCA-driven design optimization, pave the way toward eco-smart E-textiles for wearable applications.

10. Conclusion and outlook

The rapidly expanding field of flexible and wearable electronics has fuelled the development of FSCs as a compatible energy source to conveniently power the embedded devices. Over the past decade, there have been notable breakthroughs in active materials, electrode fibre development, FSC device architectures, and textile integration. In particular, the progress of

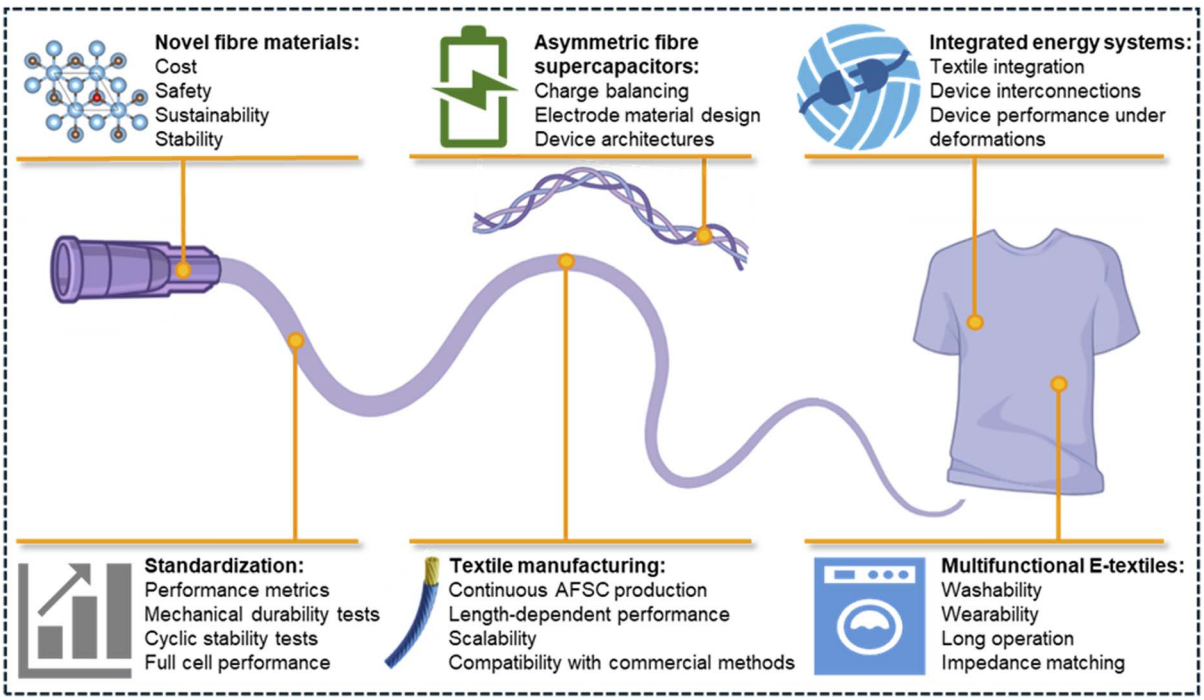

Fig. 9 Challenges and future directions in the development and textile integration of AFSCs. Created in part with https://BioRender.com.

AFSCs has reshaped the field by expanding the range of compatible electrode materials and complementary energy storage mechanisms, consequently achieving higher operating voltages and energy densities than traditional SFSCs. Research on FSCs was initially limited to symmetric FSCs using carbon-based electrode materials such as activated carbon, CNTs, and rGO fibres, which relied on EDLC charge storage mechanism, offering good rate performance and stability with limited operating voltages (~1 V in aqueous electrolytes) and low energy densities (1–5 Wh kg^{-1}).[295] The development of pseudocapacitive materials such as TMOs (*e.g.*, MnO_2), TMDs (*e.g.*, MoS_2), and conductive polymers (*e.g.*, PEDOT:PSS), enabled the emergence of hybrid symmetric FSCs, which offered enhanced energy densities. However, these systems did not achieve significant voltage improvement and often failed to fully exploit the intrinsic potential of the EDLC and pseudocapacitive electrode materials. The paradigm shifts towards AFSCs enabled the strategic combination of EDLC and pseudocapacitive electrodes, which effectively utilised the stable electrochemical potential window of each electrode and led to the expansion of operating voltages (~1.2–2.0 V in aqueous electrolytes) and enhanced energy densities compared to SFSCs. High operating voltages and high energy densities are essential for next-generation wearables. Higher voltage expands the usable energy window while keeping devices compact, and greater energy density enables longer runtime in lightweight, fibre formats that maintain comfort and usability.

Concurrently, the emergence of MXene fibres (*e.g.*, $Ti_3C_2T_x$) combined EDLC and pseudocapacitive surface redox mechanisms with high metallic conductivity, paving the way for the development of advanced AFSCs with unprecedented performance. Due to its high solution processability in diverse solvents, MXene is made into electrode fibres for AFSCs using the commonly used solution spinning method or as by coating on natural (*e.g.*, cotton) or synthetic (*e.g.*, nylon) yarns. MXene-based fibres or yarns typically perform as a negative electrode, and when paired with a complementary positive electrode such as rGO/MoS_2 or RuO_2/CNT fibre or yarn, an AFSC can be developed that combines high operating voltages with exceptional energy and power densities, while maintaining the flexibility, stretchability, and washability required for practical wearable applications. During AFSC device fabrications using parallel, twisted, or coaxial configurations, it is crucial to ensure that both electrodes store equal amounts of charge while operating. It prevents electrode overpotential, side reactions, and premature electrode degradation, resulting in a high-performance device. The practical charge-balancing strategies have also been developed for AFSCs by matching the fibre length or by tuning the capacitance of the asymmetric electrodes to achieve equivalent charge storage.

Electrolyte engineering has also progressed from simple aqueous salts (LiCl, H_2SO_4, Na_2SO_4, Li_2SO_4), organic solvents (*e.g.*, $LiClO_4$ in acetonitrile and propylene carbonate),[296] to advanced systems such as quasi-solid (gel-type), highly concentrated salt systems (*e.g.*, WiSE), and solid systems (*e.g.*, ionic liquid-epoxy solid electrolyte).[37] The organic electrolytes can provide wide voltage windows (~3 V) but raise safety concerns due to flammability and volatility. Quasi-solid electrolytes or gel electrolytes, made with an acid, base, or salts in a polymer gel (*e.g.*, PVA, chitosan, or cellulose) are commonly used in AFSCs to reduce the leakage issue of liquid electrolytes and allow for mechanical flexibility, while issues such as poor washability and sustainability persist.[62] AFSC device using gel electrolyte (PVA/LiCl) is further encapsulated to enhance the washability, showing minimal performance loss even after dipped in stirring water (800 rpm for 8 h).[198] Textile manufacturing methods such as weaving, knitting, braiding, and embroidery techniques have been used to integrate FSCs into fabrics, aiming to minimise impacts on comfort and breathability. AFSCs have been interconnected using textile-compatible approaches such as rivets, which allowed for serial or parallel connections as necessary and detachment of AFSCs for washing purposes. Among the available fabrication configurations, coaxial FSCs deliver superior electrochemical performance and enable modular assembly, supporting straightforward textile integration. Multifunctional energy systems at both fibre and textile levels have also been demonstrated where energy harvesting devices convert mechanical or light energy to electrical energy subsequently stored in AFSCs for powering integrated devices such as LEDs, sensors, or wireless communication devices. To date, most energy harvesting multifunctional fibre systems have focused on photovoltaic integration, with some studies beginning to trial triboelectric and piezoelectric energy harvesting integration which reflects the relative maturity and robustness of these technologies at the fibre level.[260] The emergence of sustainable FSCs is rooted in the development of biodegradable and eco-friendly materials, including carbon-fibre-based hybrid electrodes, natural jute fibre or regenerated cellulose substrates, non-hazardous electrolytes, and green packaging.[67,289,297] Additionally, machine learning has been used to predict the electrochemical performance, such as capacitance and cycling stability, and to optimise electrode (*e.g.*, graphene composites) and electrolyte materials for improvement in flexibility and energy density.[275,298,299] In a flexible supercapacitor, ML is applied to estimate retention rates under mechanical deformation for wearable electronics.[276] Overall, the development of AFSCs accelerates the wearable technology by powering durable e-textiles for on-body health sensing, adaptive computing, and IoT for long duration while promoting sustainable, flexible energy storage in advanced textiles.

10.1. Present challenges

Although AFSCs have achieved significant advancements at the laboratory scale, several intrinsic limitations and practical challenges still hinder their commercial adaptation and integration (Fig. 9). As wearable electronics require lightweight energy storage systems with minimal footprints, AFSCs need to match the energy density of conventional batteries. While AFSCs have significantly advanced over the past decade, their energy densities (~10–50 Wh kg^{-1}) still fall short of the energy density of the commonly-used lithium-ion batteries (100–300 Wh kg^{-1}).[300] The redox-active pseudocapacitive materials that are commonly used

in AFSCs to achieve high energy densities often suffer from relatively low rate capability and cycling stability. To meet the voltage or energy requirements of wearable applications, it is often necessary to connect multiple AFSCs in series or parallel. However, even small voltage imbalances between individual AFSCs can cause overcharging, accelerated degradation, or device failure under high current charge/discharge conditions. As a result, maintaining consistent voltage distribution throughout interconnected AFSCs is essential for device consistency and safety. There is also a challenge of self-discharging in AFSCs, occurring from charge recombination at the porous electrode surface due to the presence or consumption of redox impurities (*e.g.*, surface functional groups), or by the diffusion of ions from the EDL back into the electrolyte. This unwanted loss limits long-term energy retention, reduces energy density, and complicates the integration of the AFSCs for wearable energy autonomous systems.

The impressive performance often reported for fibre electrodes is typically obtained in liquid electrolytes. However, solid or quasi-solid electrolytes, which typically offer lower ionic conductivity and reduced electrochemical stability, are used in practical AFSCs, resulting in a noticeable performance gap. Moreover, quasi-solid systems can dry out or crystallize during prolonged ambient cycling, leading to performance decays. The interface between the fibre electrodes and electrolyte remains susceptible to fatigue under repetitive bending, twisting, or washing. Interfacial engineering (*e.g.*, surface roughening, functionalization, or grafting) is necessary to enhance the adhesion of the electrolyte to fibre electrodes to ensure performance stability of AFSCs during wear. Another challenge in AFSCs is maintaining mechanical durability and flexibility or stretchability while withstanding large deformations, particularly in applications involving high-frequency or high-amplitude dynamic motions. The incorporation of self-healing materials (*e.g.*, self-healing gels) in AFSCs is important to enhance the reliability and lifespan of wearables, facilitating recovery from physical damage, thus decreasing overall maintenance demands.

AFSCs produced so far have been characterised under ideal laboratory conditions and performance metrics have been reported solely based on the mass, volume, area, or mass of the electrodes, ignoring the contributions of other components such as electrolyte, separator, and encapsulating layer. To guarantee accurate comparisons and advance the technology, standardised testing and reporting of AFSC performance at the whole-device level are crucial. Notably, for meaningful comparison, researchers must report specific capacitance, energy density, and power density values based on mass, volume, area, and length, while considering the wide range of AFSCs in terms of electrode materials, electrode form, and device architecture. Moreover, a key challenge in the literature is the ambiguous classification of electrolytes, where polymer gels or quasi-solid systems are often referred to as solid electrolytes. Since these materials still contain liquid components that facilitate ion transport, referring to them as solid electrolytes can be misleading, emphasising the need for clearer definitions to enable reliable comparison of performance across studies. Additionally, unified testing standards are required for reporting washability and mechanical durability, so that AFSC performance can be uniformly assessed and compared consistently across laboratories.

ML has been employed in conventional supercapacitor systems. However, it has not yet been directly applied to the design and performance prediction of AFSCs. The main obstacles in the use of ML predictions for supercapacitors are fragmented and non-standardised datasets, poor transferability across different electrode chemistries and operating conditions, and limited physical interpretability of model outputs.

AFSCs produced to date have largely been limited to small centimetre-scale devices developed in research laboratories, which remain impractical for commercial applications.[301] To enable real-world deployment, it is crucial to investigate how factors such as fibre length, uniformity, and scalability affect electrochemical and mechanical performance, and to develop effective strategies for large-scale fabrication and integration. Industrial scale textile manufacturing methods, such as weaving and knitting, rely on the availability of continuous fibres with suitable mechanical properties that can withstand the tensions applied during the production process. Consequently, it is essential to produce long and continuous AFSCs to enable the transition of the technology from laboratory prototypes to large-scale, textile-integrated AFSCs. Furthermore, obtaining effective energy transfer and voltage compatibility in integrated multifunctional systems requires complex device architectures, highly customized interfaces, and precise impedance matching. As such, the seamless integration of AFSCs with other devices, such as energy harvesters (triboelectric, piezoelectric, and photovoltaic), is still difficult. Nevertheless, successful integration of AFSCs with energy harvesters embedded in textiles produces self-powered systems that enhance the sustainability of wearable electronics.

With an ever-increasing demand for fully-integrated energy storage devices, addressing the environmental impact of AFSCs production is extremely important. Achieving sustainable AFSCs using eco-friendly fabrication routes, green electrodes, non-hazardous binders, and recyclable electrolytes remains challenging, especially when these devices must deliver high performance while ensuring washability, biocompatibility, and mechanical robustness. Because wearable electronics are exposed to harsh conditions such as temperature fluctuations, high humidity, and complex body contour motions, they must be optimized for environmental resilience. In this context, it is crucial to use materials capable of operating under harsh conditions and eco-friendly encapsulation strategies that preserve device performance to broaden the applications of AFSCs, yet this remains difficult to achieve. Practical deployment of AFSCs for wearable applications remains a significant challenge as current AFSCs are yet to satisfy the practical wearability requirements of conventional clothing such as washability, breathability, and mechanical robustness.

10.2. Future directions

The future of AFSCs depends on the advancement of new materials, fibre engineering, intelligent device design and

assembly, scalable production, and incorporation of sustainability and biocompatibility. Emerging systems, including metal–organic frameworks (MOFs), covalent organic frameworks (COFs), and various 2D materials such as borophene, TMDs, and Xenes, present significant potential for advanced electrode fibre development needed for AFSCs. High-performance AFSCs can be achieved by leveraging the redox behaviour in the fibre form factor, adjustable porosity, and structural flexibility of these materials.[302] Further, fibre engineering is required to develop sophisticated AFSC device architectures that seamlessly integrate positive and negative electrodes with an electrolyte (and a separator if necessary), enabling high proximity of the electrodes while preventing a short-circuit. The mechanical flexibility and multifunctional ion pathways in MXene fibres can be improved by integrating MXene with conducting polymers, TMOs, or fibre TMDs. Concurrently, fabrication methods (*e.g.*, microfluidics, dry-jet wet-spinning, 3D printing, and direct-ink writing) offer the design flexibility required to develop intricate fibre architectures, facilitating customized porosity and spatially regulated functionalities. Furthermore, developing scalable, large-scale manufacturing strategies for electrode fibres represents a viable route to address current integration challenges, enabling straightforward textile incorporation and accelerating the commercial adoption of AFSCs. The increased stiffness or lack of flexibility upon textile integration can be overcome by better coating methods, which can prevent stiff layer formation while obtaining optimal active material loading for fibre balanced performance. Insights from traditional textile research such as dyeing chemistries can be used to find solutions for the issue of increased stiffness. Detailed understanding of active material chemistries, their colloidal dispersion properties, and the evolution of the spinning dope at various stages of fibre spinning (*e.g.*, coagulation and drawing) is important to develop a spinning setup that achieves fibres with suitable mechanical, morphological, electrical, and electrochemical properties for AFSCs. The knowledge gained from spinning charged polymers such as biopolymers and silk proteins and high-performance fibres such as carbon and Kevlar® fibre can guide researchers in the development of fibre electrodes that are most suited for AFSCs. Further investigations on incorporating click chemistry and sequential bridging fibre could improve the mechanical strength as well as fibre handling. These can also be employed to introduce a coating layer to improve environmental resilience or new functionality.

The voltage limitation (~1 V) of conventional aqueous electrolytes can be addressed by iono-gel electrolytes based on WiSE, polymer-ionic liquids,[303] deep eutectic solvent,[304,305] and zwitterionic systems,[306] which can be an alternative to organic electrolytes and can extend the voltage window (>2.0 V), while being eco-friendly and flexible. Future performance improvement will benefit from a thorough mechanistic understanding of ion migration within electrode/electrolyte interfaces. Interfacial resistance could be mitigated by introducing a conductive polymer or 2D materials layer at the electrode–electrolyte interface. For practical wearable applications, a biodegradable and biocompatible green electrolyte system with self-healing and moisture-adaptive properties would be highly desirable, offering safe skin contact and a long service life for AFSCs. More research on self-healing materials, for example, hydrogels used as an electrode and electrolyte, can offer an effective solution for performance loss during mechanical deformation. Future research should focus on the development of eco-friendly materials and green manufacturing processes to reduce the dependence on toxic or flammable materials and solvents and allow for the recyclability of AFSCs. Fibre electrodes based on bio-derived materials (*e.g.*, cellulose, alginate, and silk protein) or organic redox-active materials and green electrolytes can help achieve sustainable AFSCs.[307] Additionally, future efforts should aim to standardise terminology and classification criteria to clearly distinguish true solid electrolytes from gel and quasi-solid systems for more consistent evaluation and device design.

Established computational modelling, such as density functional theory and molecular simulations needs to be used to understand the fundamental interactions between the new electrode and electrolyte, charge storage mechanisms, and key performance metrics (*e.g.*, electrical conductivity, specific capacitance, and mechanical strength). Future research on ML should prioritize the inclusion of fibre-specific descriptors (*e.g.*, AFSC device architecture) and fibre-specific metrics such as flexibility, stretchability, and environmental stability under various temperature and humidity conditions into ML models. Explainable AI would be needed to disentangle the relationships between structural, mechanical, and electrochemical parameters. Multi-objective optimization frameworks can help achieve balanced electrochemical performance while ensuring textile compliance.

Future research efforts must be focused on translating laboratory-scale AFSCs into practical energy textile prototypes using commercially-relevant manufacturing approaches. The seamless convergence of energy storage, energy harvesting, sensing, and computation will be critical as E-textiles advance towards self-powered or self-sustainable systems. For instance, photo-rechargeable AFSCs provide an uninterrupted power supply while built-in resistive or capacitive sensing units act as signal transducers, enabling compact, self-powered wearable health and activity tracking. Interconnecting AFSCs with other devices within a textile will be crucial for powering embedded electronics such as IoT devices, sensors, and on-body computing and data communication circuits to demonstrate practical E-textile applications. It is now possible to realize fully integrated fibre-based energy systems in large area textiles for real-world applications. Embedding life-cycle and sustainable thinking through green synthesis, biodegradable substrates, waste fibres and recyclable connectors will be essential to achieving truly sustainable and circular energy textile technologies for the next generation of soft wearable electronics.

AFSCs have the potential to serve as the key energy storage elements in multifunctional soft E-textiles, storing energy generated by the harvesting systems to reliably power embedded sensors for real-time health and activity monitoring, without compromising comfort or design. The applications of such multifunctional E-textiles will be diverse, spanning wearable health monitoring, soft robotics, the IoT, virtual and augmented reality, smart sportswear, and adaptive clothing.

Conflicts of interest

There are no conflicts of interest to declare.

Data availability

No primary research results, software or code have been included and no new data were generated or analysed as part of this review.

Acknowledgements

The authors acknowledge funding from the Engineering and Physical Sciences Research Council in the forms of Northern Net Zero Accelerator Award (EP/Y024052/1), Doctoral Training Programme (EP/W524700/1), Health Technologies Connectivity Award (UKRI828), and Horizon Europe Guarantee Scheme (EP/Y023439/1). ND's contribution is supported by the Centre for Understanding & Controlling Accelerated and Gradual Evolution of Materials for Energy funded by the US Department of Energy (DE-SC0012577). The graphical abstract, Fig. 1 and 9 were created in part using https://BioRender.com (reference number: BC3ATBRC0002).

References

1 R. Wei, H. Li, Z. Chen, Q. Hua, G. Shen and K. Jiang, *npj Flexible Electron.*, 2024, **8**, 83.
2 A. S. S. Abadi, A. Koguciuk, M. Jangas, P. Korycki, K. Tylicka and P. Targos, *Electron. J. Inf. Syst.*, 2025, **7**, 50–71.
3 N. Gupta, H. Cheung, S. Payra, G. Loke, J. Li, Y. Zhao, L. Balachander, E. Son, V. Li, S. Kravitz, S. Lohawala, J. Joannopoulos and Y. Fink, *Nature*, 2025, **639**, 79–86.
4 S. P. Beeby, R. N. Torah, M. Wagih, B. Isaia, S. Black, J. Saunders and K. Yang, *Adv. Mater. Technol.*, 2025, **10**, 2400844.
5 W. Zhang, S. Luan, M. Tian, L. Qu, X. Zhang, T. Fan and J. Miao, *Nanoscale*, 2025, **17**, 22733–22762.
6 K. A. S. Usman, J. Zhang, L. Bi, S. Seyedin, X. Wang, Y. Gogotsi and J. M. Razal, *Adv. Mater.*, 2025, **37**, 2506437.
7 H. Kim, D. Kim, J. Kim, Y. Lee, M. Shin, J. Kim, F. M. Bossuyt, G.-H. Lee, B. Lee, W. R. Taylor and J. Lee, *npj Flexible Electron.*, 2025, **9**, 84.
8 H. Huang, Y. Hu, Y. Hou, X. Wang, Q. Dong, Z. Zhao, M. Ji, W. Zhang, J. Li, J. Xie, H. Guo, X. Han, X. Ouyang and W. Hu, *Nature*, 2025, **644**, 660–667.
9 P. Phogat, S. Dey and M. Wan, *RSC Sustain.*, 2025, **3**, 3266–3306.
10 J. He, L. Cao, J. Cui, G. Fu, R. Jiang, X. Xu and C. Guan, *Adv. Mater.*, 2024, **36**, 2306090.
11 D. Lee, J. Kim, C. W. Kim, J.-G. Kim, S. E. Jung, S. J. Heo, B. W. Im, N. D. Kim, S. G. Kim, Y. Piao and B.-C. Ku, *Composites, Part B*, 2025, **295**, 112179.
12 E. Senokos, M. Rana, M. Vila, J. Fernandez-Cestau, R. D. Costa, R. Marcilla and J. J. Vilatela, *Nanoscale*, 2020, **12**, 16980–16986.
13 Y. Li, X. Yan, X. Zheng, H. Si, M. Li, Y. Liu, Y. Sun, Y. Jiang and Y. Zhang, *J. Mater. Chem. A*, 2016, **4**, 17704–17710.
14 D. Liu, Y. Xue, X. Yang, Y. Shen, P. Zhang, H. Zheng, C. Wang, H. Chen, X. Zheng and T. Zhang, *Interdiscip. Mater.*, 2025, **4**, 377–411.
15 N. Kumar, P. Wojciak and S. Seyedin, *Small Sci.*, 2025, **5**, 2500229.
16 B. Tawiah, R. K. Seidu, B. K. Asinyo and B. Fei, *J. Power Sources*, 2024, **595**, 234069.
17 X. Zang, Q. Chen, P. Li, Y. He, X. Li, M. Zhu, X. Li, K. Wang, M. Zhong, D. Wu and H. Zhu, *Small*, 2014, **10**, 2583–2588.
18 Y. Chao, Y. Han, Z. Chen, D. Chu, Q. Xu, G. Wallace and C. Wang, *Adv. Sci.*, 2024, **11**, 2305558.
19 L. Dong, C. Xu, Y. Li, Z.-H. Huang, F. Kang, Q.-H. Yang and X. Zhao, *J. Mater. Chem. A*, 2016, **4**, 4659–4685.
20 H. Liu, Y. Shi, Y. Pan, Z. Wang and B. Wang, *npj Flexible Electron.*, 2025, **9**, 23.
21 A. S. Ghouri, R. Aslam, M. S. Siddiqui and S. K. Sami, *Front. Mater.*, 2020, **7**, 2020.
22 L. Nyholm, G. Nyström, A. Mihranyan and M. Strømme, *Adv. Mater.*, 2011, **23**, 3751–3769.
23 H. Xiang, Y. Li, Q. Liao, L. Xia, X. Wu, H. Zhou, C. Li and X. Fan, *Energies*, 2024, **17**, 2627.
24 K. Zeng, X. Shi, C. Tang, T. Liu and H. Peng, *Nat. Rev. Mater.*, 2023, **8**, 552–561.
25 P. Teymoory, J. Zhao and C. Shen, *Micromachines*, 2023, **14**, 1249.
26 J. Ahn, S. Padmajan Sasikala, Y. Jeong, J. G. Kim, J.-H. Ha, S. H. Hwang, S. Jeon, J. Choi, B.-H. Kang, J. Ahn, J.-H. Jeong, S. O. Kim and I. Park, *Adv. Fiber Mater.*, 2024, **6**, 1927–1941.
27 S. Jeon, H. Seo, Y. Kim, Y. Choi, Y. Lee, Y. Jung, S. Lee, J. T. Lee and S. Park, *Nat. Commun.*, 2025, **16**, 8207.
28 J. Zhao, H. Lu, Y. Zhang, S. Yu, O. I. Malyi, X. Zhao, L. Wang, H. Wang, J. Peng, X. Li, Y. Zhang, S. Chen, H. Pan, G. Xing, C. Lu, Y. Tang and X. Chen, *Sci. Adv.*, 2021, **7**, eabd6978.
29 P. Simon and Y. Gogotsi, *Nat. Mater.*, 2020, **19**, 1151–1163.
30 D. Chen, K. Jiang, T. Huang and G. Shen, *Adv. Mater.*, 2020, **32**, 1901806.
31 J. Yu, W. Lu, J. P. Smith, K. S. Booksh, L. Meng, Y. Huang, Q. Li, J.-H. Byun, Y. Oh, Y. Yan and T.-W. Chou, *Adv. Energy Mater.*, 2017, **7**, 1600976.
32 Z. Wang, S. Qin, S. Seyedin, J. Zhang, J. Wang, A. Levitt, N. Li, C. Haines, R. Ovalle-Robles, W. Lei, Y. Gogotsi, R. H. Baughman and J. M. Razal, *Small*, 2018, **14**, 1802225.
33 X. Jiang, T. Ding, J. Quan, R. Wang, J. Zhou, Y. Wei, W. Li, M. Li, C. Lan, W. Ma and M. Zhu, *Carbon*, 2025, **238**, 120254.
34 B. T. Ho, T. Lim, M. H. Jeong and J. W. Suk, *ACS Appl. Energy Mater.*, 2021, **4**, 8883–8890.
35 Y. Yang, D. Chen, W. Han, C. Hou, G. Chen, J. Han and X. Zhang, *Adv. Funct. Mater.*, 2025, **35**, 2416249.
36 X. Cao, Y. Liu, Y. Zhong, L. Cui, A. Zhang, J. M. Razal, W. Yang and J. Liu, *J. Mater. Chem. A*, 2020, **8**, 1837–1848.
37 B. Dharmasiri, F. Stojcevski, K. A. S. Usman, S. Alex Qin, J. M. Razal, E. H. Doeven, P. S. Francis, T. U. Connell,

Y. Yin, G. G. Andersson, A. Borkar and L. C. Henderson, *Chem. Eng. J.*, 2023, **455**, 140778.
38 J. T. Carvalho, A. Correia, N. J. A. Cordeiro, J. Coelho, S. A. Lourenço, E. Fortunato, R. Martins and L. Pereira, *npj 2D Mater. Appl.*, 2024, **8**, 20.
39 X. Jian, H. Li, H. Li, Y. Li and Y. Shang, *Carbon*, 2021, **172**, 132–137.
40 P. Shi, R. Chen, L. Hua, L. Li, R. Chen, Y. Gong, C. Yu, J. Zhou, B. Liu, G. Sun and W. Huang, *Adv. Mater.*, 2017, **29**, 1703455.
41 K. Jin, L. Su, Z. Jin, Y. Zhao and Z. Cai, *J. Alloys Compd.*, 2022, **908**, 164616.
42 J. Ren, L. Li, C. Chen, X. Chen, Z. Cai, L. Qiu, Y. Wang, X. Zhu and H. Peng, *Adv. Mater.*, 2013, **25**, 1155–1159.
43 J. H. Kim, C. Choi, J. M. Lee, M. J. de Andrade, R. H. Baughman and S. J. Kim, *Sci. Rep.*, 2018, **8**, 13309.
44 F. Su, X. Lv and M. Miao, *Small*, 2015, **11**, 854–861.
45 Y. Qiu, X. Jia, M. Zhang and H. Li, *Nanomaterials*, 2022, **12**, 3297.
46 J.-G. Kim, D.-M. Lee, J. Y. Jung, M. J. Kim, M.-S. Khil, H. S. Jeong and N. D. Kim, *ACS Appl. Energy Mater.*, 2021, **4**, 1130–1142.
47 J. Zhang, X. Wang, G. Hang, W. Zhang, Z. Zheng, J. Duan and Z. Liu, *Compos. Commun.*, 2024, **45**, 101817.
48 Y.-S. Sung and L.-Y. Lin, *Nanomaterials*, 2020, **10**, 248.
49 J. Zhang, S. Seyedin, S. Qin, P. A. Lynch, Z. Wang, W. Yang, X. Wang and J. M. Razal, *J. Mater. Chem. A*, 2019, **7**, 6401–6410.
50 Y. Liu, B. Weng, J. M. Razal, Q. Xu, C. Zhao, Y. Hou, S. Seyedin, R. Jalili, G. G. Wallace and J. Chen, *Sci. Rep.*, 2015, **5**, 17045.
51 T. S. Mathis, K. Maleski, A. Goad, A. Sarycheva, M. Anayee, A. C. Foucher, K. Hantanasirisakul, C. E. Shuck, E. A. Stach and Y. Gogotsi, *ACS Nano*, 2021, **15**, 6420–6429.
52 C. Yang, Y. Tang, Y. Tian, Y. Luo, M. Faraz Ud Din, X. Yin and W. Que, *Adv. Energy Mater.*, 2018, **8**, 1802087.
53 M. R. Lukatskaya, S. Kota, Z. Lin, M.-Q. Zhao, N. Shpigel, M. D. Levi, J. Halim, P.-L. Taberna, M. W. Barsoum, P. Simon and Y. Gogotsi, *Nat. Energy*, 2017, **2**, 17105.
54 J. Zhang, S. Uzun, S. Seyedin, P. A. Lynch, B. Akuzum, Z. Wang, S. Qin, M. Alhabeb, C. E. Shuck, W. Lei, E. C. Kumbur, W. Yang, X. Wang, G. Dion, J. M. Razal and Y. Gogotsi, *ACS Cent. Sci.*, 2020, **6**, 254–265.
55 L. Pan, H. Wang, J. Zhou, H. Dai, H. Xu, Y. Guo, T. Cheng, L. Yin, T. Zhang, Y. Wang, J. Zhou and G. Sun, *Adv. Funct. Mater.*, 2025, **35**, 2505247.
56 J. Zhang, S. Seyedin, S. Qin, Z. Wang, S. Moradi, F. Yang, P. A. Lynch, W. Yang, J. Liu, X. Wang and J. M. Razal, *Small*, 2019, **15**, 1804732.
57 X. Zhao, B. Zheng, T. Huang and C. Gao, *Nanoscale*, 2015, **7**, 9399–9404.
58 D. Yu, Q. Qian, L. Wei, W. Jiang, K. Goh, J. Wei, J. Zhang and Y. Chen, *Chem. Soc. Rev.*, 2015, **44**, 647–662.
59 Y. Shao, M. F. El-Kady, J. Sun, Y. Li, Q. Zhang, M. Zhu, H. Wang, B. Dunn and R. B. Kaner, *Chem. Rev.*, 2018, **118**, 9233–9280.
60 Y. Xue, Z. Zhang, D. Liu, X. Yang, C. Wang, H. Chen, X. Zheng, Q. Li and T. Zhang, *Energy Storage Mater.*, 2025, **77**, 104222.
61 H. Lee, K. Gong, H. Kang, G. Jung, J. Y. Kim, K. Keum, D. S. Kim, S. Kim, J. W. Kim and J. S. Ha, *J. Alloys Compd.*, 2023, **960**, 170714.
62 Q. Liu, J. Zhou, C. Song, X. Li, Z. Wang, J. Yang, J. Cheng, H. Li and B. Wang, *Energy Storage Mater.*, 2020, **24**, 495–503.
63 L.-H. Xu, Y.-T. He, Y. Xu, S. Sun, J. Liu, J. Yang, J.-L. Wen and T.-Q. Yuan, *Adv. Funct. Mater.*, 2025, **35**, 2501263.
64 T. Zhang, J. Wu, Y. Wang, L. Zhang and F. Ran, *Adv. Energy Mater.*, 2024, **14**, 2303587.
65 A. Inman, T. Parker, Y. Zhang, M. Saraf and Y. Gogotsi, *Adv. Energy Mater.*, 2024, **14**, 2402367.
66 H. H. Shi, Y. Pan, L. Xu, X. Feng, W. Wang, P. Potluri, L. Hu, T. Hasan and Y. Y. S. Huang, *Nat. Mater.*, 2023, **22**, 1294–1303.
67 J. T. Carvalho, I. Cunha, J. Coelho, E. Fortunato, R. Martins and L. Pereira, *ACS Appl. Energy Mater.*, 2022, **5**, 11987–11996.
68 E. Bel Hadj Jrad, F. Soavi and C. Dridi, *J. Energy Storage*, 2024, **88**, 111471.
69 L. Navone, K. Moffitt, K.-A. Hansen, J. Blinco, A. Payne and R. Speight, *Waste Manage.*, 2020, **102**, 149–160.
70 Z. Qian, Y. Yang, L. Wang, J. Wang, Y. Guo, Z. Liu, J. Li, H. Zhang, X. Sun and H. Peng, *Angew Chem. Int. Ed. Engl.*, 2023, **62**, e202303268.
71 S. He, A. Zhang, D. Wang, H. Song, H. Chu, F. Ni, Y. Zhang, P. Chen, B. Zhang, L. Qiu and H. Peng, *Chem. Eng. J.*, 2022, **441**, 136106.
72 F. Meng, Q. Li and L. Zheng, *Energy Storage Mater.*, 2017, **8**, 85–109.
73 A. Grube, M. M. Shaban, L. Hilger, M. D. Firouzjaei, A. A. Shamsabadi, Y. Demirel, M. Elliott, S. Nejati and M. Bavarian, *J. Energy Storage*, 2024, **99**, 113228.
74 S. Newby, W. Mirihanage and A. Fernando, *ACS Omega*, 2023, **8**, 12613–12629.
75 S. Zhai and Y. Chen, *Acc. Mater. Res.*, 2022, **3**, 922–934.
76 M. R. Karim, M. Rahman, C. B. Mukta, C.-H. Choi and W. H. Shin, *J. Energy Storage*, 2025, **121**, 116606.
77 J. Zhang, X. Wang, G. Hang, Y. Wei, H. Wang, S. He and Z. Liu, *ACS Appl. Electron. Mater.*, 2023, **5**, 4704–4725.
78 J. García-Torres, *J. Chem. Educ.*, 2025, **102**, 821–828.
79 S. I. Wong, J. Sunarso, B. T. Wong, H. Lin, A. Yu and B. Jia, *J. Power Sources*, 2018, **396**, 182–206.
80 L. L. Zhang and X. Zhao, *Chem. Soc. Rev.*, 2009, **38**, 2520–2531.
81 R. Kötz and M. Carlen, *Electrochim. Acta*, 2000, **45**, 2483–2498.
82 P. Simon, Y. Gogotsi and B. Dunn, *Science*, 2014, **343**, 1210–1211.
83 A. Afif, S. M. H. Rahman, A. Tasfiah Azad, J. Zaini, M. A. Islan and A. K. Azad, *J. Energy Storage*, 2019, **25**, 100852.
84 Y. Wu and F. Ran, *J. Power Sources*, 2017, **344**, 1–10.
85 X. Mao, T. A. Hatton and G. C. Rutledge, *Curr. Org. Chem.*, 2013, **17**, 1390–1401.

86 P. Forouzandeh, V. Kumaravel and S. C. Pillai, *Catalysts*, 2020, **10**, 969.
87 Y. Wang, L. Zhang, H. Hou, W. Xu, G. Duan, S. He, K. Liu and S. Jiang, *J. Mater. Sci.*, 2021, **56**, 173–200.
88 D. Paolini, L. Antony, G. Seeta Rama Raju, A. Kuzmak, T. Verkholyak and S. Kondrat, *Chemelectrochem*, 2024, **11**, e202400218.
89 V. Augustyn, P. Simon and B. Dunn, *Energy Environ. Sci.*, 2014, **7**, 1597–1614.
90 S. Fleischmann, J. B. Mitchell, R. Wang, C. Zhan, D.-e. Jiang, V. Presser and V. Augustyn, *Chem. Rev.*, 2020, **120**, 6738–6782.
91 J. Wang, S. Dong, B. Ding, Y. Wang, X. Hao, H. Dou, Y. Xia and X. Zhang, *Natl. Sci. Rev.*, 2017, **4**, 71–90.
92 F. Daneshvar, A. Aziz, A. M. Abdelkader, T. Zhang, H.-J. Sue and M. E. Welland, *Nanotechnology*, 2019, **30**, 015401.
93 N. Kumar, S.-B. Kim, S.-Y. Lee and S.-J. Park, *Nanomaterials*, 2022, **12**, 3708.
94 P. Bhojane, *J. Energy Storage*, 2022, **45**, 103654.
95 D. P. Chatterjee and A. K. Nandi, *J. Mater. Chem. A*, 2021, **9**, 15880–15918.
96 N. Parvin, D. Merum, M. Kang, S. W. Joo, J. H. Jung and T. K. Mandal, *J. Mater. Chem. A*, 2025, **13**, 24320–24386.
97 C. Lu and X. Chen, *Acc. Chem. Res.*, 2020, **53**, 1468–1477.
98 J. Cherusseri, D. Pandey and J. Thomas, *Batter. Supercaps*, 2020, **3**, 860–875.
99 D. Zhang, C. Tan, W. Zhang, W. Pan, Q. Wang and L. Li, *Molecules*, 2022, **27**, 716.
100 N. Wu, X. Bai, D. Pan, B. Dong, R. Wei, N. Naik, R. R. Patil and Z. Guo, *Adv. Mater. Interfaces*, 2021, **8**, 2001710.
101 B. E. Conway, *Electrochemical Supercapacitors: Scientific Fundamentals and Technological Applications*, Springer Science & Business Media, 2013.
102 K. Jost, G. Dion and Y. Gogotsi, *J. Mater. Chem. A*, 2014, **2**, 10776–10787.
103 Q. Liu, H. Wang, C. Jiang and Y. Tang, *Energy Storage Mater.*, 2019, **23**, 566–586.
104 R. Kötz and M. Carlen, *Electrochim. Acta*, 2000, **45**, 2483–2498.
105 A. Burke, *J. Power Sources*, 2000, **91**, 37–50.
106 Y. Wang, K. Xue, C. Yan, Y. Li, X. Zhang, K. Su, P. Ma, S. Wan and J. Lang, *Batteries*, 2024, **10**, 54.
107 J. R. Miller and P. Simon, *Science*, 2008, **321**, 651–652.
108 P. Simon and Y. Gogotsi, *Nat. Mater.*, 2008, **7**, 845–854.
109 J. Pedro Aguiar dos Santos, F. Cesar Rufino, J. I. Yutaka Ota, R. C. Fernandes, R. Vicentini, C. J. B. Pagan, L. Morais Da Silva and H. Zanin, *J. Energy Chem.*, 2023, **80**, 265–283.
110 Y. Ge, X. Xie, J. Roscher, R. Holze and Q. Qu, *J. Solid State Electrochem.*, 2020, **24**, 3215–3230.
111 C. Lu, J. Meng, J. Zhang, X. Chen, M. Du, Y. Chen, C. Hou, J. Wang, A. Ju, X. Wang, Y. Qiu, S. Wang and K. Zhang, *ACS Appl. Mater. Interfaces*, 2019, **11**, 25205–25217.
112 T. Khudiyev, J. T. Lee, J. R. Cox, E. Argentieri, G. Loke, R. Yuan, G. H. Noel, R. Tatara, Y. Yu, F. Logan, J. Joannopoulos, Y. Shao-Horn and Y. Fink, *Adv. Mater.*, 2020, **32**, 2004971.
113 S. Seyedin, E. R. S. Yanza and J. M. Razal, *J. Mater. Chem. A*, 2017, **5**, 24076–24082.
114 F. Khan, N. Hossain, F. Hasan, S. M. M. Rahman, S. Khan, A. Z. A. Saifullah and M. A. Chowdhury, *Appl. Eng. Sci.*, 2024, **18**, 100184.
115 Z. Gui, H. Zhu, E. Gillette, X. Han, G. W. Rubloff, L. Hu and S. B. Lee, *ACS Nano*, 2013, **7**, 6037–6046.
116 S. Uzun, S. Seyedin, A. L. Stoltzfus, A. S. Levitt, M. Alhabeb, M. Anayee, C. J. Strobel, J. M. Razal, G. Dion and Y. Gogotsi, *Adv. Funct. Mater.*, 2019, **29**, 1905015.
117 C.-L. Park, B. Goh, E. S. Kim, J. Choi and S. H. Kim, *Carbon*, 2024, **220**, 118775.
118 L. Hu, M. Pasta, F. La Mantia, L. Cui, S. Jeong, H. D. Deshazer, J. W. Choi, S. M. Han and Y. Cui, *Nano Lett.*, 2010, **10**, 708–714.
119 M. Pasta, F. La Mantia, L. Hu, H. D. Deshazer and Y. Cui, *Nano Res.*, 2010, **3**, 452–458.
120 S. Seyedin, M. S. Romano, A. I. Minett and J. M. Razal, *Sci. Rep.*, 2015, **5**, 14946.
121 A. Levitt, S. Seyedin, J. Zhang, X. Wang, J. M. Razal, G. Dion and Y. Gogotsi, *Small*, 2020, **16**, 2002158.
122 Z. Zhang, D. Zhang, H. Lin and Y. Chen, *J. Power Sources*, 2019, **433**, 226711.
123 M. Pal and K. M. Subhedar, *Carbon*, 2024, **229**, 119552.
124 K. Jost, C. R. Perez, J. K. McDonough, V. Presser, M. Heon, G. Dion and Y. Gogotsi, *Energy Environ. Sci.*, 2011, **4**, 5060–5067.
125 M. Firew Adamu, T. Tesfaye, B. Berhanu and A. Simegnaw, *Textil. Prog.*, 2025, **57**, 1–71.
126 S. Seyedin, M. S. Romano, A. I. Minett and J. M. Razal, *Sci. Rep.*, 2015, **5**, 14946.
127 L. Feng, Y. Chang, J. Zhong and D.-C. Jia, *Sci. Rep.*, 2018, **8**, 10803.
128 Z. Xia, H. Dai, J. Chang, J. Yang, H. Wang, Y. Wang, Z. Hui, R. Wang and G. Sun, *Small*, 2023, **19**, 2304687.
129 J. Garcia-Torres, A. J. Roberts, R. C. T. Slade and C. Crean, *Electrochim. Acta*, 2019, **296**, 481–490.
130 H. Shen, T. Sun and J. Zhou, *Macromol. Mater. Eng.*, 2023, **308**, 2300089.
131 L. Cao, L. Zhang, Z. Zhao, S. Wang, Z. Li, D. Jing and S. Zhang, *Polymers*, 2025, **17**, 2504.
132 S. Seyedin, S. Moradi, C. Singh and J. M. Razal, *Appl. Mater. Today*, 2018, **11**, 255–263.
133 S. Seyedin, S. Moradi, C. Singh and J. M. Razal, *Data Brief*, 2018, **18**, 1765–1772.
134 A. Ahmadian, A. Shafiee, N. Aliahmad and M. Agarwal, *Textiles*, 2021, **1**, 206–226.
135 Y. Cho, J. W. Baek, M. Sagong, S. Ahn, J. S. Nam and I.-D. Kim, *Adv. Mater.*, 2025, **37**, 2500162.
136 W. Wang, H. Wang, H. Wang, X. Jin, J. Li and Z. Zhu, *RSC Adv.*, 2018, **8**, 28480–28486.
137 M. Kim, Y. Kim, K. M. Lee, S. Y. Jeong, E. Lee, S. H. Baeck and S. E. Shim, *Carbon*, 2016, **99**, 607–618.
138 Y. Wang, Y. Song, C. Ye and L. Xu, *Beilstein J. Nanotechnol.*, 2020, **11**, 1280–1290.
139 Y. Liu, Z. Zeng, B. Bloom, D. H. Waldeck and J. Wei, *Small*, 2018, **14**, 1703237.

140 Z. Wang, D. Zhang, Y. Guo, H. Jiang, D. Wang, J. Cheng, P. K. Chu, H. Yan and Y. Luo, *Chem. Commun.*, 2023, **59**, 14309–14312.
141 A. Malara, *Sci. Rep.*, 2024, **14**, 8293.
142 X. Mu, V. Fitzpatrick and D. L. Kaplan, *Adv. Healthcare Mater.*, 2020, **9**, 1901552.
143 B. Li, M. Yu, Z. Li, C. Yu, H. Wang and Q. Li, *Adv. Funct. Mater.*, 2022, **32**, 2201166.
144 A. Schwab, R. Levato, M. D'Este, S. Piluso, D. Eglin and J. Malda, *Chem. Rev.*, 2020, **120**, 11028–11055.
145 H. Tetik, Y. Wang, X. Sun, D. Cao, N. Shah, H. Zhu, F. Qian and D. Lin, *Adv. Funct. Mater.*, 2021, **31**, 2103410.
146 S. Nouseen and M. Pumera, *Adv. Funct. Mater.*, 2025, **35**, 2421987.
147 Y. Jiang, Z. Xu, T. Huang, Y. Liu, F. Guo, J. Xi, W. Gao and C. Gao, *Adv. Funct. Mater.*, 2018, **28**, 1707024.
148 W. Yang, J. Yang, J. J. Byun, F. P. Moissinac, J. Xu, S. J. Haigh, M. Domingos, M. A. Bissett, R. A. W. Dryfe and S. Barg, *Adv. Mater.*, 2019, **31**, 1902725.
149 S. S. Nath and P. Sundriyal, *Sustain. Energy Fuels*, 2025, **9**, 5367–5382.
150 M. M. Ovhal, H. B. Lee, V. V. Satale, B. Tyagi, S. Chowdhury and J.-W. Kang, *Adv. Energy Mater.*, 2024, **14**, 2303053.
151 S. Strauß, B. Schroth and J. Hubbuch, *Front. Bioeng. Biotechnol.*, 2022, **10**, 2022.
152 R. Xu, J. Wei, F. Guo, X. Cui, T. Zhang, H. Zhu, K. Wang and D. Wu, *RSC Adv.*, 2015, **5**, 22015–22021.
153 C. Choi, K. M. Kim, K. J. Kim, X. Lepró, G. M. Spinks, R. H. Baughman and S. J. Kim, *Nat. Commun.*, 2016, **7**, 13811.
154 L. Liu, Y. Yu, C. Yan, K. Li and Z. Zheng, *Nat. Commun.*, 2015, **6**, 7260.
155 J. A. Lee, M. K. Shin, S. H. Kim, H. U. Cho, G. M. Spinks, G. G. Wallace, M. D. Lima, X. Lepró, M. E. Kozlov, R. H. Baughman and S. J. Kim, *Nat. Commun.*, 2013, **4**, 1970.
156 F. Shao, N. Hu, Y. Su, L. Yao, B. Li, C. Zou, G. Li, C. Zhang, H. Li, Z. Yang and Y. Zhang, *Chem. Eng. J.*, 2020, **392**, 123692.
157 Y. J. Kang, Y. Yoo and W. Kim, *ACS Appl. Mater. Interfaces*, 2016, **8**, 13909–13917.
158 M. Duan, Y. Ren, X. Sun, X. Zhu, X. Wang, L. Sheng and J. Liu, *ACS Omega*, 2021, **6**, 24444–24449.
159 S. Wang, Y. Li, L. Wei, J. Zhu, Q. Zhang, L. Lan, L. Tang, F. Wang, Z. Zhang, L. Wang and J. Mao, *ACS Nano*, 2025, **19**, 6357–6370.
160 X. Pu, L. Li, M. Liu, C. Jiang, C. Du, Z. Zhao, W. Hu and Z. L. Wang, *Adv. Mater.*, 2015, **28**, 98–105.
161 G. S. Rama Raju, S. Kondrat, N. R. Chodankar, S.-K. Hwang, J. H. Lee, T. Long, E. Pavitra, S. J. Patil, K. S. Ranjith, M. V. B. Rao, P. Wu, K. C. Roh, Y. S. Huh and Y.-K. Han, *J. Mater. Chem. A*, 2023, **11**, 15540–15552.
162 X. Xiao, T. Li, P. Yang, Y. Gao, H. Jin, W. Ni, W. Zhan, X. Zhang, Y. Cao, J. Zhong, L. Gong, W.-C. Yen, W. Mai, J. Chen, K. Huo, Y.-L. Chueh, Z. L. Wang and J. Zhou, *ACS Nano*, 2012, **6**, 9200–9206.
163 L. Kou, T. Huang, B. Zheng, Y. Han, X. Zhao, K. Gopalsamy, H. Sun and C. Gao, *Nat. Commun.*, 2014, **5**, 3754.
164 J. Sun, Y. Huang, Y. N. Sze Sea, Q. Xue, Z. Wang, M. Zhu, H. Li, X. Tao, C. Zhi and H. Hu, *Mater. Today Energy*, 2017, **5**, 1–14.
165 Z. Guo, Z. Lu, Y. Li and W. Liu, *Adv. Mater. Interfaces*, 2022, **9**, 2101977.
166 F. Ma, L. Li, C. Jia, X. He, Q. Li, J. Sun, R. Jiang, Z. Lei and Z.-H. Liu, *J. Colloid Interface Sci.*, 2023, **643**, 92–101.
167 Q. Zhang, J. Sun, Z. Pan, J. Zhang, J. Zhao, X. Wang, C. Zhang, Y. Yao, W. Lu, Q. Li, Y. Zhang and Z. Zhang, *Nano Energy*, 2017, **39**, 219–228.
168 K. M. Joseph, H. J. Kasparian and V. Shanov, *Energies*, 2022, **15**, 6506.
169 M. S. Arsha and B. V, *Energy Fuels*, 2024, **38**, 19076–19087.
170 S. V. Sadavar, S.-Y. Lee and S.-J. Park, *Adv. Sci.*, 2024, **11**, 2403172.
171 G. S. Rama Raju, E. Pavitra, G. Nagaraju, N. R. Chodankar, S. K. Vishwanath, J. Y. Park, Y. S. Huh and Y.-K. Han, *J. Mater. Chem. A*, 2019, **7**, 26893–26904.
172 X. Dong, J. Liang, H. Li, Z. Wu, L. Zhang, Y. Deng, H. Yu, Y. Tao and Q.-H. Yang, *Nano Energy*, 2021, **80**, 105523.
173 X. Cheng, J. Zhang, J. Ren, N. Liu, P. Chen, Y. Zhang, J. Deng, Y. Wang and H. Peng, *J. Phys. Chem. C*, 2016, **120**, 9685–9691.
174 H. Yuan, G. Wang, Y. Zhao, Y. Liu, Y. Wu and Y. Zhang, *Nano Res.*, 2020, **13**, 1686–1692.
175 Z. Pan, J. Zhong, Q. Zhang, J. Yang, Y. Qiu, X. Ding, K. Nie, H. Yuan, K. Feng, X. Wang, G. Xu, W. Li, Y. Yao, Q. Li, M. Liu and Y. Zhang, *Adv. Energy Mater.*, 2018, **8**, 1702946.
176 W. Cai, T. Lai, J. Lai, H. Xie, L. Ouyang, J. Ye and C. Yu, *Sci. Rep.*, 2016, **6**, 26890.
177 P. Sundriyal and S. Bhattacharya, *Sci. Rep.*, 2020, **10**, 13259.
178 X. Wang, J. Sun, J. Zhao, Z. Zhou, Q. Zhang, C.-p. Wong and Y. Yao, *J. Phys. Chem. C*, 2019, **123**, 985–993.
179 J. Kim, Y. Kim, S. Ramasamy and S.-K. Kim, *J. Power Sources*, 2024, **606**, 234570.
180 P. K. Adusei, K. Johnson, S. N. Kanakaraj, G. Zhang, Y. Fang, Y.-Y. Hsieh, M. Khosravifar, S. Gbordzoe, M. Nichols and V. Shanov, *C*, 2021, **7**, 62.
181 H. He, X. Yang, L. Wang, X. Zhang, X. Li and W. Lü, *Chem.–Eur. J.*, 2020, **26**, 17212.
182 S. Shahrokhian, L. Naderi and R. Mohammadi, *ACS Sustain. Chem. Eng.*, 2018, **6**, 14574–14588.
183 T. Cen, L. Chen, X. Zhang, Y. Tian and X. Fan, *Electrochim. Acta*, 2021, **367**, 137488.
184 Q. Zhang, W. Xu, J. Sun, Z. Pan, J. Zhao, X. Wang, J. Zhang, P. Man, J. Guo, Z. Zhou, B. He, Z. Zhang, Q. Li, Y. Zhang, L. Xu and Y. Yao, *Nano Lett.*, 2017, **17**, 7552–7560.
185 G. Shao, C. Su, J. Li, Y. Huang, Q. Yu, T. Fu, H. Shao, J. Jiang, M. Ye, N. Chen, R. Yu and X. Y. Liu, *Cell Rep. Phys. Sci.*, 2021, 2.
186 G. Wu, X. Yang, C. Hou, Y. Li, Q. Zhang and H. Wang, *Chemelectrochem*, 2020, **7**, 4641–4648.
187 X. Lu, Y. Bai, R. Wang and J. Sun, *J. Mater. Chem. A*, 2016, **4**, 18164–18173.
188 M. Liu, Z. Cong, X. Pu, W. Guo, T. Liu, M. Li, Y. Zhang, W. Hu and Z. L. Wang, *Adv. Funct. Mater.*, 2019, **29**, 1806298.

189 B. Saravanakumar, S. Sivabalan Jayaseelan, M.-K. Seo, H.-Y. Kim and B.-S. Kim, *Nanoscale*, 2017, **9**, 18819–18834.
190 D. D. Khumujam, T. Kshetri, T. I. Singh, N. H. Kim and J. H. Lee, *Chem. Eng. J.*, 2022, **449**, 137732.
191 Q. Zhang, X. Wang, Z. Pan, J. Sun, J. Zhao, J. Zhang, C. Zhang, L. Tang, J. Luo, B. Song, Z. Zhang, W. Lu, Q. Li, Y. Zhang and Y. Yao, *Nano Lett.*, 2017, **17**, 2719–2726.
192 J. Tang, X. Zheng, B. Ding, L. Zou, P. Wang, C. Li, X. Hong and Z. Wang, *Mater. Lett.*, 2024, **355**, 135494.
193 H. Rao Goli, M. V. Basaveswara Rao, N. Purushotham Reddy, M. Reddy Pallavolu, P. Wu, Y.-K. Han, G. Seeta Rama Raju and P. A. Alvi, *Chem. Eng. J.*, 2022, **446**, 137347.
194 N. He, J. Song, J. Liao, F. Zhao and W. Gao, *npj Flexible Electron.*, 2022, **6**, 19.
195 J. Yu, W. Lu, J. P. Smith, K. S. Booksh, L. Meng, Y. Huang, Q. Li, J.-H. Byun, Y. Oh, Y. Yan and T.-W. Chou, *Adv. Energy Mater.*, 2017, **7**, 1600976.
196 B. Saravanakumar, S. S. Jayaseelan, M.-K. Seo, H.-Y. Kim and B.-S. Kim, *Nanoscale*, 2017, **9**, 18819–18834.
197 J. Kim, J. Yin, X. Xuan and J. Y. Park, *Micro Nano Syst. Lett.*, 2019, **7**, 4.
198 X. Gong, S. Li and P. S. Lee, *Nanoscale*, 2017, **9**, 10794–10801.
199 K. Guo, X. Wang, L. Hu, T. Zhai, H. Li and N. Yu, *ACS Appl. Mater. Interfaces*, 2018, **10**, 19820–19827.
200 H. Cai, Z. Liu, M. Xu, L. Chen, X. Chen, L. Cheng, Z. Li and F. Dai, *Electrochim. Acta*, 2021, **390**, 138895.
201 S. Lee, H. W. Choi, C. L. Figueiredo, D.-W. Shin, F. M. Moncunill, K. Ullrich, S. Sinopoli, P. Jovančić, J. Yang, H. Lee, M. Eisenreich, U. Emanuele, S. Nicotera, A. Santos, R. Igreja, A. Marrani, R. Momentè, J. Gomes, S.-M. Jung, S. D. Han, S. Y. Bang, S. Zhan, W. Harden-Chaters, Y.-H. Suh, X.-B. Fan, T. H. Lee, J.-W. Jo, Y. Kim, A. Costantino, V. G. Candel, N. Durães, S. Meyer, C.-H. Kim, M. Lucassen, A. Nejim, D. Jiménez, M. Springer, Y.-W. Lee, G.-H. An, Y. Choi, J. I. Sohn, S. Cha, M. Chhowalla, G. A. J. Amaratunga, L. G. Occhipinti, P. Barquinha, E. Fortunato, R. Martins and J. M. Kim, *Sci. Adv.*, 2023, **9**, eadf4049.
202 B. K. Dejene, *Energy Rep.*, 2025, **14**, 898–943.
203 M. Liu, Z. Cong, X. Pu, W. Guo, T. Liu, M. Li, Y. Zhang, W. Hu and Z. L. Wang, *Adv. Funct. Mater.*, 2019, **29**, 1806298.
204 C. Su, X. Yang, J. Li, Q. Yu, Y. Huang, H. Shao, G. Shao, J. Jiang and N. Chen, *ACS Appl. Energy Mater.*, 2022, **5**, 8472–8482.
205 Y. A. Kumar, S. Vignesh, T. Ramachandran, A. M. Fouda, H. Hegazy, M. Moniruzzaman and T. H. Oh, *J. Ind. Eng. Chem.*, 2025, **145**, 191–215.
206 Y. Wang and W. H. Zhong, *Chemelectrochem*, 2015, **2**, 22–36.
207 F. Su and M. Miao, *Nanotechnology*, 2014, **25**, 135401.
208 M. R. Pallavolu, S. Panugamti, V. Hiremath, B. Akkinepally, G. Nagaraju, J. Shim and S. W. Joo, *J. Mater. Chem. A*, 2025, **13**, 13354–13367.
209 M. A. A. Mohd Abdah, N. H. N. Azman, S. Kulandaivalu and Y. Sulaiman, *Sci. Rep.*, 2019, **9**, 16782.
210 M. Serrapede, A. Rafique, M. Fontana, A. Zine, P. Rivolo, S. Bianco, L. Chetibi, E. Tresso and A. Lamberti, *Carbon*, 2019, **144**, 91–100.
211 M. Ma, Z. Shi, Y. Li, Y. Yang, Y. Zhang, Y. Wu, H. Zhao and E. Xie, *J. Mater. Chem. A*, 2020, **8**, 4827–4835.
212 L. Antony, E. Pavitra, K. S. Ranjith, G. S. R. Raju, Y. S. Huh and Y.-K. Han, *Adv. Fiber Mater.*, 2024, **6**, 529–542.
213 C. Ye, Q. Yang, M. Xu, H. Qiu, X. Zhang, J. Ma, H. Gao, X. Feng and Y. Li, *Nanomaterials*, 2025, **15**, 1350.
214 B. Shi, L. Li, A. Chen, T.-C. Jen, X. Liu and G. Shen, *Nano-Micro Lett.*, 2021, **14**, 34.
215 R. Zhang, X. Wang, S. Cai, K. Tao and Y. Xu, *Polymers*, 2023, **15**, 1627.
216 C. Choi, J. W. Park, K. J. Kim, D. W. Lee, M. J. de Andrade, S. H. Kim, S. Gambhir, G. M. Spinks, R. H. Baughman and S. J. Kim, *RSC Adv.*, 2018, **8**, 13112–13120.
217 G. Huang, Y. Zhang, L. Wang, P. Sheng and H. Peng, *Carbon*, 2017, **125**, 595–604.
218 B. Patil, S. Ahn, S. Yu, H. Song, Y. Jeong, J. H. Kim and H. Ahn, *Carbon*, 2018, **134**, 366–375.
219 M. Barazandeh, S. H. Kazemi, F. Roohi, D. S. Haydar and I. Odnevall, *ACS Omega*, 2025, **10**, 47973–47984.
220 B. Cheng, R. Cheng, F. Tan, X. Liu, J. Huo and G. Yue, *Nanoscale Res. Lett.*, 2019, **14**, 66.
221 W. Ma, S. Chen, S. Yang, W. Chen, W. Weng, Y. Cheng and M. Zhu, *Carbon*, 2017, **113**, 151–158.
222 C. Wessells, R. A. Huggins and Y. Cui, *J. Power Sources*, 2011, **196**, 2884–2888.
223 C. Zhao and W. Zheng, *Front. Energy Res.*, 2015, **3**, 2015.
224 G. S. R. Raju, L. Antony, P. B. Bhargav, S. Yi, A. Mohammadi, K. S. Ranjith, E. Pavitra, J. S. Yu, Y. S. Huh and Y.-K. Han, *Adv. Compos. Hybrid Mater.*, 2025, **8**, 421.
225 D. Ji and J. Kim, *Nano-Micro Lett.*, 2023, **16**, 2.
226 D. Chao, W. Zhou, F. Xie, C. Ye, H. Li, M. Jaroniec and S.-Z. Qiao, *Sci. Adv.*, 2020, **6**, eaba4098.
227 X. Tian, Q. Zhu and B. Xu, *ChemSusChem*, 2021, **14**, 2501–2515.
228 D. Gomez Vazquez, J. Ingenmey, K. Trapp, D. Ciliak, M. Salanne and M. R. Lukatskaya, *J. Am. Chem. Soc.*, 2025, **147**, 35953–35961.
229 A. M. Patil, N. Kitiphatpiboon, X. An, X. Hao, S. Li, X. Hao, A. Abudula and G. Guan, *ACS Appl. Mater. Interfaces*, 2020, **12**, 52749–52762.
230 A. I. Ribeiro, C. Alves, M. Fernandes, J. Abreu, F. Pedroso de Lima, J. Padrão and A. Zille, *Gels*, 2025, **11**, 392.
231 G. S. R. Raju, L. Antony, H.-J. Kim, A. Mohammadi, K. S. Ranjith, J.-H. Lee, M. V. B. Rao, E. Pavitra, Y. S. Huh and Y.-K. Han, *Chem. Eng. J.*, 2025, **520**, 165726.
232 H. Dai, G. Zhang, D. Rawach, C. Fu, C. Wang, X. Liu, M. Dubois, C. Lai and S. Sun, *Energy Storage Mater.*, 2021, **34**, 320–355.
233 R. Jamil and D. S. Silvester, *Curr. Opin. Electrochem.*, 2022, **35**, 101046.
234 S. Alipoori, S. Mazinani, S. H. Aboutalebi and F. Sharif, *J. Energy Storage*, 2020, **27**, 101072.

235 W. G. Moon, G.-P. Kim, M. Lee, H. D. Song and J. Yi, *ACS Appl. Mater. Interfaces*, 2015, **7**, 3503–3511.
236 N. A. Choudhury, S. Sampath and A. Shukla, *J. Electrochem. Soc.*, 2007, **155**, A74.
237 T. K. L. Nguyen and T.-N. Pham-Truong, *Polymers*, 2024, **16**, 2506.
238 P. K. Adusei, K. Johnson, S. N. Kanakaraj, G. Zhang, Y. Fang, Y.-Y. Hsieh, M. Khosravifar, S. Gbordzoe, M. Nichols and V. Shanov, *C*, 2021, **7**, 62.
239 X. Wu, X. Yu, Z. Zhang, H. Liu, S. Ling, X. Liu, C. Lian and J. Xu, *Adv. Funct. Mater.*, 2023, **33**, 2300329.
240 J. Lu, J. Zhang, X. Wang, J. Zhang, Z. Tian, E. Zhu, L. Yang, X. Guan, H. Ren, J. Wu, X. Li and G. Wang, *J. Energy Storage*, 2024, **103**, 114338.
241 G. Jin, Z. Duan, Z. Dong and Q. Zhou, *J. Phys.: Conf. Ser.*, 2024, **2855**, 012009.
242 V. Kumaravel, J. Bartlett and S. C. Pillai, *Adv. Energy Mater.*, 2021, **11**, 2002869.
243 V. S. Bhat, J. M. Shivanna, A. Shetty, V. Molahalli, S. G. Krishnan, S. Sahoo, R. K. Pai, T. M. Aminabhavi and G. Hegde, *Energy Fuels*, 2025, **39**, 16737–16767.
244 T. Feng, X. Li, G. Li, X. Luo, X. Liu, K. Zhang, X. Jia, Y. Wang, W. Sun and K. Wang, *J. Energy Storage*, 2024, **102**, 114131.
245 W. Liu, Z. Li, F. Pan, Q. He and Q. Zhang, *RSC Adv.*, 2023, **13**, 34652–34659.
246 Y. Yang, T. Zhu, C. Chi, L. Liu, J. Zheng and X. Gong, *ACS Appl. Electron. Mater.*, 2020, **2**, 3906–3914.
247 C. Choi, K. Robert, G. Whang, P. Roussel, C. Lethien and B. Dunn, *Joule*, 2021, **5**, 2466–2478.
248 Y. H. Song, T. Kim and U. H. Choi, *Chem. Mater.*, 2020, **32**, 3879–3892.
249 N. Shirshova, A. Bismarck, E. S. Greenhalgh, P. Johansson, G. Kalinka, M. J. Marczewski, M. S. P. Shaffer and M. Wienrich, *J. Phys. Chem. C*, 2014, **118**, 28377–28387.
250 X. Chen and R. Holze, *Polymers*, 2024, **16**, 3164.
251 A. Dalvi, *RSC Adv.*, 2025, **15**, 6518–6530.
252 M. D. Singh, G. Kaur, S. Sharma and A. Dalvi, *J. Energy Storage*, 2021, **41**, 102984.
253 G. Liao, T. Mahrholz, S. Geier, P. Wierach and M. Wiedemann, *J. Solid State Electrochem.*, 2018, **22**, 1055–1061.
254 X. Hu, Y. Chen, Z. Hu, Y. Li and Z. Ling, *J. Electrochem. Soc.*, 2018, **165**, A1269.
255 Z. Zhang, X. Chen, P. Chen, G. Guan, L. Qiu, H. Lin, Z. Yang, W. Bai, Y. Luo and H. Peng, *Adv. Mater.*, 2014, **26**, 466–470.
256 T. Chen, L. Qiu, Z. Yang, Z. Cai, J. Ren, H. Li, H. Lin, X. Sun and H. Peng, *Angew. Chem., Int. Ed.*, 2012, **51**, 11977–11980.
257 H. Sun, X. You, J. Deng, X. Chen, Z. Yang, P. Chen, X. Fang and H. Peng, *Angew. Chem., Int. Ed.*, 2014, **53**, 6664–6668.
258 Y. Cho, S. Pak, Y.-G. Lee, J. S. Hwang, P. Giraud, G.-H. An and S. Cha, *Adv. Funct. Mater.*, 2020, **30**, 1908479.
259 J. Bae, Y. J. Park, M. Lee, S. N. Cha, Y. J. Choi, C. S. Lee, J. M. Kim and Z. L. Wang, *Adv. Mater.*, 2011, **23**, 3446–3449.
260 Z. Wen, M.-H. Yeh, H. Guo, J. Wang, Y. Zi, W. Xu, J. Deng, L. Zhu, X. Wang, C. Hu, L. Zhu, X. Sun and Z. L. Wang, *Sci. Adv.*, 2016, **2**, e1600097.
261 E. Xie, Q. Xiao, W. Fan, H. Jamshaid, L. Guo and W. Wang, *ACS Omega*, 2025, **10**, 13218–13227.
262 G. Wu, Z. Yang, Z. Zhang, B. Ji, C. Hou, Y. Li, W. Jia, Q. Zhang and H. Wang, *Electrochim. Acta*, 2021, **395**, 139141.
263 C. Choi, S. H. Kim, H. J. Sim, J. A. Lee, A. Y. Choi, Y. T. Kim, X. Lepró, G. M. Spinks, R. H. Baughman and S. J. Kim, *Sci. Rep.*, 2015, **5**, 9387.
264 Z. Pan, J. Yang, L. Li, X. Gao, L. Kang, Y. Zhang, Q. Zhang, Z. Kou, T. Zhang, L. Wei, Y. Yao and J. Wang, *Energy Storage Mater.*, 2020, **25**, 124–130.
265 H.-J. Kil, S.-R. Kim and J.-W. Park, *ACS Appl. Mater. Interfaces*, 2022, **14**, 3838–3848.
266 Y. Zhou, Y. Cai, T. Tu, S. Zhang, T. Li, L. Fang, D. Wang, Y. Liang, Z. Wang, Y. Jiang, C. Zhou and B. Liang, *ACS Appl. Mater. Interfaces*, 2023, **15**, 41839–41849.
267 T. Sun, L. Shen, Y. Jiang, J. Ma, F. Lv, H. Ma, D. Chen and N. Zhu, *ACS Appl. Mater. Interfaces*, 2020, **12**, 21779–21787.
268 S. He, Y. Hu, J. Wan, Q. Gao, Y. Wang, S. Xie, L. Qiu, C. Wang, G. Zheng, B. Wang and H. Peng, *Carbon*, 2017, **122**, 162–167.
269 Z. Qian, Y. Yang, L. Wang, J. Wang, Y. Guo, Z. Liu, J. Li, H. Zhang, X. Sun and H. Peng, *Angew. Chem., Int. Ed.*, 2023, **62**, e202303268.
270 Y. Jang, T. Park, E. Kim, J. W. Park, D. Y. Lee and S. J. Kim, *Angew. Chem., Int. Ed.*, 2021, **60**, 10563–10567.
271 Q. Tang, Y. Zhang, X. Zhu, Y. Wang, Z. Man, C. Yang, J. Xu, G. Wu and W. Lu, *Adv. Funct. Mater.*, 2024, **34**, 2410005.
272 H. S. Mulla, D. S. Sawant, S. V. Gaikwad, A. V. Fulari, R. K. Nimat, D. P. Dubal and G. M. Lohar, *ChemSusChem*, 2025, 2402559.
273 M. Ahmad, A. S. Almalki, W. Sajjad, F. Zafar, H. M. Asif, M. A. Khan, N. Akhtar, M. Sohail, G. A. Mersal and M. M. Ibrahim, *J. Electroanal. Chem.*, 2025, 119282.
274 S. Jha, S. Bandyopadhyay, S. Mehta, M. Yen, T. Chagouri, E. Palmer and H. Liang, *Energy Fuels*, 2021, **36**, 1052–1062.
275 L. Xu, S. Liu, D. Hu, J. Liu, Y. Zhang, Z. Li, Z. Su and D. Liang, *Gels*, 2025, **11**, 464.
276 T. H. Nguyen, J. Lee, D. Lee, M. C. Nguyen and J. Kim, *Chem. Eng. J.*, 2025, **505**, 159375.
277 S. Krishna and A. Mir, *Energy Adv.*, 2024, **3**, 2986–2998.
278 T. Dongale, P. Jadhav, G. Navathe, J. Kim, M. Karanjkar and P. Patil, *Mater. Sci. Semicond. Process.*, 2015, **36**, 43–48.
279 A. Dave, J. Mitchell, S. Burke, H. Lin, J. Whitacre and V. Viswanathan, *Nat. Commun.*, 2022, **13**, 5454.
280 V. Raj, M. R. Nair, N. I. Soaid and M. S. M. Saheed, *Diamond Relat. Mater.*, 2026, **161**, 113085.
281 Y. Yao, X. Rui, R. Bai, Y. Ouyang, G. Li, Y. Zhao, Y.-H. Zhu, M. Zhao, B.-Q. Li, X. Zhang, Z. Li, F. Ling, C. Ma, J. Ma, F. Zhou, Z. Ren, X. Shi, Z. Zhao, Y. Lu, B.-E. Jia, N. Wu, Z. Wang, W. Yao, S. Bi, K. Chen, J.-Y. Li, J.-Y. Wu, J.-X. Li, W.-B. Tu, J. Guan, X.-L. Wu, X.-D. Zhang, K. Wang, Y. Ma, C. Zhu, F. Wan, D. Xie, B. Lu, J.-J. Xu, C. Li, Z. Niu, Y. Tang, Q. Yan, Z. Wen, C. Zhang, X. Li, Z.-S. Wu, J.-Q. Huang, Q. Zhang, S. Xin, Y.-G. Guo and Y. Yu, *ACS Nano*, 2025, **19**, 30568–30687.

282 C. V. V. Muralee Gopi, S. Alzahmi, V. Narayanaswamy, R. Vinodh, B. Issa and I. M. Obaidat, *J. Energy Storage*, 2025, **114**, 115729.
283 L. Luo, Y. Lan, Q. Zhang, J. Deng, L. Luo, Q. Zeng, H. Gao and W. Zhao, *J. Energy Storage*, 2022, **55**, 105839.
284 N. Choudhary, A. Tomar, S. Bhardwaj, J. Ćwiertnia, D. Just, D. Janas, R. Chandra and P. K. Maji, *J. Mater. Chem. A*, 2025, **13**, 4012–4042.
285 W. Xu, B. Mu and A. Wang, *J. Mater. Sci.*, 2018, **53**, 11659–11670.
286 K. Chaitra, R. T. Vinny, P. Sivaraman, N. Reddy, C. Hu, K. Venkatesh, C. S. Vivek, N. Nagaraju and N. Kathyayini, *J. Energy Chem.*, 2017, **26**, 56–62.
287 X. Liu, N. Ostrovsky-Snider, M. Lo Presti, T. Kim, G. Guidetti and F. G. Omenetto, *ACS Biomater. Sci. Eng.*, 2024, **10**, 5390–5398.
288 L. Xia, X. Li, Y. Wu, S. Hu, Y. Liao, L. Huang, Y. Qing and X. Lu, *Chem. Eng. J.*, 2020, **379**, 122325.
289 L. Manjakkal, F. F. Franco, A. Pullanchiyodan, M. González-Jiménez and R. Dahiya, *Adv. Sustain. Syst.*, 2021, **5**, 2000286.
290 N. M. Badawi, N. Agrawal, S. F. Adil, S. Ramesh, K. Ramesh and S. Bashir, *N. Carbon Mater.*, 2023, **38**, 211–225.
291 S. Tan, J. Li, L. Zhou, P. Chen, D. Xu and Z. Xu, *J. Mater. Sci.*, 2018, **53**, 11648–11658.
292 F. Bahmei, A. S. de Buruaga, S. P. Bautista, J. Olarte, J. Ajuria, A. Varzi and M. Weil, *ChemSusChem*, 2025, **18**, e202500583.
293 Z. Jiang, Y. Zou, Y. Li, F. Kong and D. Yang, *Biochar*, 2021, **3**, 701–714.
294 M. Dadashi Firouzjaei, S. K. Nemani, M. Sadrzadeh, E. K. Wujcik, M. Elliott and B. Anasori, *Adv. Mater.*, 2023, **35**, 2300422.
295 C. Lekakou, O. Moudam, F. Markoulidis, T. Andrews, J. F. Watts and G. T. Reed, *J. Nanotechnol.*, 2011, **2011**, 409382.
296 K. Keum, G. Lee, H. Lee, J. Yun, H. Park, S. Y. Hong, C. Song, J. W. Kim and J. S. Ha, *ACS Appl. Mater. Interfaces*, 2018, **10**, 26248–26257.
297 P. Kumar, P. Sephra, M. Gupta, V. Jeoti, C. Tharini and G. M. Stojanović, *J. Energy Storage*, 2026, **141**, 119173.
298 G. K. Yogesh, D. Nandi, R. Yeetsorn, W. Wanchan, C. Devi, R. P. Singh, A. Vasistha, M. Kumar, P. Koinkar and K. Yadav, *Energy Adv.*, 2025, **4**, 119–139.
299 A. Emad-Eldeen, M. A. Azim, M. Abdelsattar and A. AbdelMoety, *J. Energy Storage*, 2024, **100**, 113556.
300 S. Huang, X. Zhu, S. Sarkar and Y. Zhao, *APL Mater.*, 2019, **7**, 100901.
301 Z. Ma, Q. Huang, N. Zhou, Q. Zhuang, S.-W. Ng and Z. Zheng, *Cell Rep. Phys. Sci.*, 2023, **4**, 101300.
302 S.-J. Shin, J. W. Gittins, C. J. Balhatchet, A. Walsh and A. C. Forse, *Adv. Funct. Mater.*, 2024, **34**, 2308497.
303 Z. Wang, L. Wang, W. Jiang, X. Jian and F. Hu, *Sci. China Mater.*, 2023, **66**, 3129–3138.
304 X. Bu, Y. Ge, L. Wang, L. Wu, X. Ma and D. Lu, *Polym. Eng. Sci.*, 2021, **61**, 154–166.
305 J. Huang, Y. Hu, J. Li, H. Wang, T. Wang, H. Wu, Y. Li, M. Wang and J. Zhang, *ACS Energy Lett.*, 2023, **8**, 2316–2324.
306 W. Sun, J. Yang, X. Ji, H. Jiang, L. Gai, X. Li and L. Liu, *Sustain. Mater. Technol.*, 2022, **32**, e00437.
307 S. V. Bhosale and S. V. Bhosale, *Chem. Sci.*, 2025, **16**, 10159–10227.